Eomes-Dependent Loss of the Co-activating Receptor CD226 Restrains CD8+ T Cell Anti-tumor Functions and Limits the Efficacy of Cancer Immunotherapy

Marianne Weulersse, Assia Asrir, Andrea C Pichler, Lea Lemaitre, Matthias Braun, Nadège Carrié, Marie-Véronique Joubert, Marie Le Moine, Laura Do Souto, Guillaume Gaud, et al.

Eomes-dependent loss of the co-activating receptor CD226 restrains CD8+ T cell anti-tumor functions and limits the efficacy of cancer Immunotherapy

Marianne Weulersse[1,8], Assia Asrir[1,8], Andrea C Pichler[1,8], Lea Lemaitre[1], Matthias Braun[2], Nadège Carrié[1], Marie-Véronique Joubert[1,3], Marie Le Moine[4], Laura Do Souto[1,3], Guillaume Gaud[5], Indrajit Das[2], Elisa Brauns[4], Clara M. Scarlata[1,3], Elena Morandi[5], Ashmitha Sundarrajan[2], Marine Cuisinier[1,3], Laure Buisson[1,3], Sabrina Maheo[1,3], Sahar Kassem[1], Arantxa Agesta[5], Michaël Pérès[1,3], Els Verhoeyen[6,7], Alejandra Martinez[1,3], Julien Mazière[1,3], Loic Dupré[5], Camille Guillerey[2], Maha Ayyoub[1,3], Anne Dejean[5], Abdelhadi Saoudi[5], Stanislas Goriely[4], Hervé Avet-Loiseau[1,3], Tobias Bald[2] , Mark J. Smyth[2] and Ludovic Martinet[1,3*].

[1]Cancer Research Center of Toulouse (CRCT), Institut National de la Santé et de la Recherche Médicale (INSERM) UMR 1037, Centre National de la Recherche Scientifique (CNRS), Université Paul Sabatier (UPS), Toulouse, France.

[2]QIMR Berghofer Medical Research Institute, Herston, Queensland, Australia.

[3]Institut Universitaire du Cancer, CHU Toulouse, Toulouse France.

[4]Université Libre de Bruxelles, Institute for Medical Immunology (IMI), Gosselies, 6041 Belgium and UCR-I (ULB Centre for Research in Immunology)

[5]Centre de physiopathologie de Toulouse Purpan (CPTP), Institut National de la Santé et de la Recherche Médicale (INSERM) UMR 1043, Centre National de la Recherche Scientifique (CNRS) UMR 5282, Université Paul Sabatier (UPS), Toulouse, France.

[6]Université Côte d'Azur, INSERM, C3M, Nice, France.

[7]CIRI, Université de Lyon, INSERM U1111, ENS de Lyon, CNRS UMR 5308, Lyon, France

[8]These authors contributed equally

[*]Lead contact

Full correspondence

Lead contact: Dr Ludovic Martinet, INSERM UMR 1037, Cancer Research Center of Toulouse, 2 av Hubert Curien, 31037 Toulouse, France. E-mail address: ludovic.martinet@inserm.fr; Phone: +33-5-8274-1757

8 Figures, 8 Supplementary Figures, 96 References.

Key words: $CD8^+$ T lymphocytes, TCR signaling, Co-stimulation, CD226 (DNAM-1), tumor immune escape, T cell exhaustion, Immunotherapy, immune checkpoint blockade.

IN BRIEF

Through complementary approaches, involving cancer patients' samples and relevant mouse tumor models, this study reveals that the Eomes-dependent loss of the activating receptor CD226 (DNAM-1) represents a critical determinant of tumor infiltrating $CD8^+$ T cell dysfunction potentially affecting immune checkpoint blockade efficacy.

GRAPHICAL ABSTRACT

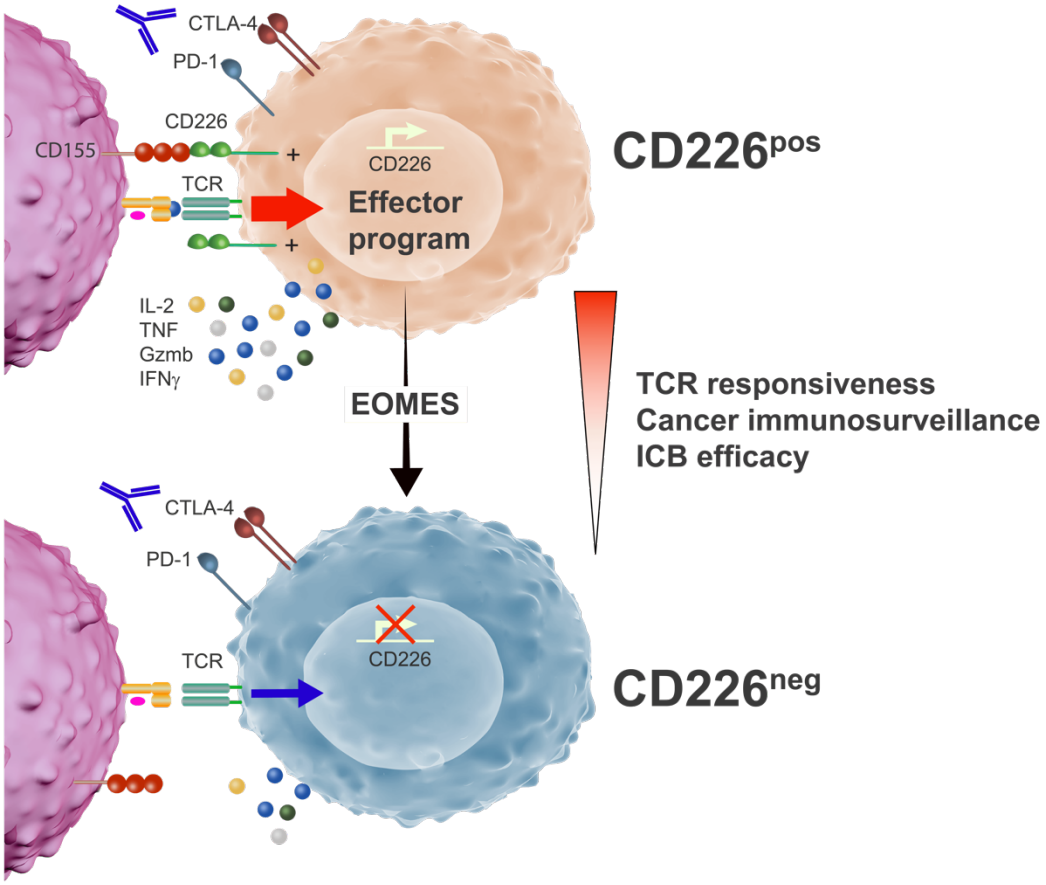

HIGHLIGHTS

- The absence of CD226 impedes TCR signaling and effector program of $CD8^+$ T cells.
- Dysfunctional CD226-negative $CD8^+$ T cells accumulate in tumors.
- Tumor-induced CD226-loss depends on Eomes transcription factor.
- CD226 loss limits $CD8^+$ T cell response to Immune checkpoint blockade.

ABSTRACT

Although anti-PD-1 and anti-CTLA-4 based immune checkpoint blockade (ICB) has represented a turning point in cancer care, clinical responses are observed only in a fraction of cancer patients. Most research focuses on the identification of additional inhibitory receptors restraining the anti-tumor functions of $CD8^+$ T cells. By contrast, herein, we found that loss of the activating receptor CD226 (DNAM-1) was a critical mechanism affecting $CD8^+$ T cell responsiveness to TCR stimulation. Using cancer patients' samples and preclinical mouse models, we discovered that dysfunctional CD226-negative $CD8^+$ T cells progressively accumulated in the tumor microenvironment through a mechanism involving the T-box transcription factor Eomesodermin (EOMES). More importantly, we demonstrated that CD226-negative tumor infiltrating lymphocytes had reduced anti-tumor functions and failed to respond to ICB. Altogether, our results revealed that CD226 loss is a critical immune escape mechanism restraining $CD8^+$ T cell function and potentially affecting the therapeutic efficacy of cancer immunotherapy.

INTRODUCTION

$CD8^+$ T lymphocytes play a critical role in limiting tumor progression and represent the most promising therapeutic host immune target against cancer (Schumacher and Schreiber, 2015). $CD8^+$ T cell activation is mainly triggered by TCR recognition of MHC-I-peptide complexes but additional signals provided through a wide array of stimulatory and inhibitory molecules critically influence $CD8^+$ T cell anti-tumor functions (Chen and Flies, 2013). In the past decade, an extensive number of studies demonstrated the key role played by inhibitory receptors such as PD-1 (CD279) and CTLA-4 (CD152) in driving a state of $CD8^+$ T cell hypo-responsiveness called T cell exhaustion, frequently observed in chronic viral infections and cancer (Wherry and Kurachi, 2015). Some previous striking clinical results achieved with monoclonal antibodies (mAbs) blocking these receptors in metastatic melanoma illustrated the therapeutic promise of targeting inhibitory receptors to restore cytotoxic lymphocyte anti-tumor reactivity (Robert et al., 2011; Topalian et al., 2012). Still, clinical responses are observed only in a fraction of cancer patients treated with Immune checkpoint blockers (ICB). While most of the experimental strategies actually focus on the identification of additional inhibitory receptors restraining anti-tumor reactivity of $CD8^+$ T cells, the importance of activating receptors with regards to anti-tumor $CD8^+$ T cell functions and ICB efficacy remains to be better understood.

CD226 (DNAM-1, PTA-1, TLiSA1) is an adhesion molecule initially described for its ability to stimulate NK cell- and $CD8^+$ T cell-mediated cytotoxicity (Martinet and Smyth, 2015; Shibuya et al., 1996). Its ligands, the nectin and nectin-like receptors CD112 and CD155, are often expressed on cancer cells as a consequence of cellular stress (Chan et al., 2014b) and CD226 deficiency was shown to reduce tumor immunosurveillance in a wide number of solid and lymphoid tumor mouse models (Chan et al., 2014a; Gilfillan et al., 2008; Guillerey et al., 2015; Iguchi-Manaka et al., 2008; Tahara-Hanaoka et al., 2006). TIGIT (T cell immunoreceptor with Ig and ITIM domains) and CD96, two inhibitory receptors that compete with CD226 for the same ligands, were recently identified as promising immunotherapeutic targets to restore immune reactivity against tumors (Blake et al., 2016a; Blake et al., 2016b; Chan et al., 2014a; Guillerey et al., 2018; Kurtulus et al., 2015) highlighting the importance of the CD226 axis in the regulation of anti-tumor immune responses. The CD226 pathway may also represent an important determinant of ICB efficacy as evidenced by a recent study demonstrating that the

PD-1/PD-L1 pathway is a negative regulator of CD226 signaling and that PD-1 and GITR (glucocorticoid-induced tumor necrosis factor receptor-related protein) dual blockade fail to promote mouse tumor regression in the absence of CD226 (Wang et al., 2018).

Despite the critical role of CD226 in the T cell-dependent control of malignancies, the underlying mechanisms remain to be further addressed. Indeed, besides the ability of CD226 to regulate target cell adhesion and killing, there is now accumulating evidence indicating that this molecule may influence additional aspects of T cell biology such as terminal maturation of $CD8^+$ thymocytes (Danisch et al., 2013; Qiu et al., 2010), T helper cell differentiation (Gaud et al., 2018; Lozano et al., 2012; Lozano et al., 2013; Shibuya et al., 2003) and Treg suppressive functions (Koyama et al., 2013). In addition, although recent evidence suggests that CD226 contains an intracellular signaling domain that closely resembles CD28 (Zhang et al., 2015), the importance of this molecule in TCR activation remains poorly understood. In this study, we demonstrate, using complementary set of experiments involving human samples and mouse tumor models, that the absence of CD226 identifies a subset of $CD8^+$ T cells with severely impaired effector functions that accumulates in the tumor microenvironment through an Eomes-dependent mechanism. More importantly, we found that CD226-negative tumor infiltrating lymphocytes have altered TCR signaling, reduced anti-tumor functions and fail to respond to anti-PD-1 immunotherapy. Altogether, our results reveal a yet unappreciated mechanism restraining $CD8^+$ T cell functions and ICB efficacy initiated by the loss of the activating receptor CD226.

RESULTS

The absence of CD226 expression identifies hypo-reactive human CD8$^+$ T cells.

Despite the importance of the CD226 pathway in cancer immunosurveillance and its emerging role in autoimmune disorders and infections (Martinet et al., 2015; Martinet and Smyth, 2015), little information was available regarding the expression of this receptor on human CD8$^+$ T cells. Interestingly, we observed in the peripheral blood of healthy donors (HD) the presence of two distinct CD8$^+$ T cell populations based on CD226 expression (**Figure 1A**). CD226$^-$ and CD226$^+$ CD8$^+$ T cell populations expressed comparable levels of most classical CD8$^+$ T cell markers **(Figure S1A)** and had similar TCR V beta repertoires (**Figure 1B).** These subsets were also similarly present across the different CD8$^+$ T cell maturation stages including naïve (Tn, CD62L$^+$CD45RA$^+$); central memory (Tcm, CD62L$^+$CD45RA$^-$); effector memory (Tem, CD62L$^-$ CD45RA$^-$); terminal effector memory (Temra, CD62L$^-$CD45RA$^+$) (**Figure 1C**) and their frequency was independent of the age and gender of the different donors analyzed (**Figure S1B**). The contrasting expression of CD226 on CD8$^+$ T cells with identical phenotype and maturation questioned about the potential functions of these two subsets. To exclude any analytic bias inherent to mixed CD8$^+$ T maturation stages, we first separated CD226$^-$ and CD226$^+$ CD8$^+$ Tn, Tcm and Tem subsets by flow cytometry. Analysis of TCR-induced proliferation using anti-CD2/CD3/CD28 microbeads revealed that CD226$^-$ CD8$^+$ T cells had strikingly lower proliferation capacities than CD226$^+$ CD8$^+$ T cells regardless of the differentiation stage (**Figure 1D**). Lower CD226$^-$ CD8$^+$ T cell proliferation was confirmed in unsorted CD8$^+$ T cell cultures stimulated with more physiological stimuli such as allogeneic monocyte-derived dendritic cells, CMVpp65 peptide pools or TCR-MHCI crosslinking reagent CytoStim (**Figure 1E and Figure S1C**). CD226$^-$ CD8$^+$ Tems also produced a considerably lower amount of IL-2, IFN-γ, TNF-α, GM-CSF, CCL5 and MIP-1α than CD8$^+$ CD226$^+$ Tems upon TCR stimulation (**Figure 1F and Figure S1D**). Similar results were obtained when we assessed the intracellular production of IFN-γ, TNF-α, or CD107a degranulation marker by CD226$^-$ and CD226$^+$ CD8$^+$ T cells upon stimulation with diverse TCR stimuli including CytoStim, anti-CD2/CD3/CD28 microbeads or FcγR$^+$ P815 cell line coated with increasing concentrations of anti-CD3 mAbs (**Figure 1G and Figure S1E-F**). By contrast, CD226$^-$ and CD226$^+$ CD8$^+$ T cells had comparable cytokine production upon stimulation with PMA/ionomycin (**Figure S1G-H**) suggesting that both CD226$^-$ and CD226$^+$ CD8$^+$ T cells have similar intrinsic functional capacities. Altogether, these results demonstrate that CD8$^+$ CD226$^-$ T cells display functional signs of hypo-responsiveness

including defective proliferation, cytokine secretion and degranulation in response to TCR stimulation.

These data suggested that $CD8^+$ T cells lacking CD226 may have an altered TCR signaling. To test this hypothesis, we first monitored the influx of intracellular Ca^{2+} in $CD226^-$ and $CD226^+$ $CD8^+$ T cells, a key event in TCR signaling cascade. We observed that Ca^{2+} influx triggered by anti-CD3 stimulation was reduced in $CD226^-$ $CD8^+$ T cells as compared to $CD226^+$ $CD8^+$ T cells (**Figure 1H**). In concert, we found that proteins implicated in proximal TCR signaling such as SLP76, ZAP70 and LAT were less phosphorylated in purified $CD226^-$ $CD8^+$ Tems as compared to $CD226^+$ cells upon CD3 stimulation (**Figure 1I-J and Figure S1I).** Lower phosphorylation of key TCR downstream signaling proteins, such as mitogen-activated protein kinases ERK1/2 and the PI3K target Akt, was also observed after anti-CD3 stimulation in sorted $CD226^-$ $CD8^+$ Tems as compared to $CD226^+$ $CD8^+$ Tems (**Figure 1K)**. Altogether, these results establish that the absence of CD226 in healthy individuals identifies a subset of $CD8^+$ T cells with reduced TCR signaling.

The absence of CD226 alters the TCR-induced $CD8^+$ T cell transcriptional program.

To better understand the molecular differences between $CD226^-$ and $CD226^+$ $CD8^+$ T cells, we performed a global transcriptional analysis of purified $CD226^+$ and $CD226^-$ $CD8^+$ Tems before and after TCR activation using next generation RNA sequencing. To our surprise, resting $CD226^-$ and $CD226^+$ $CD8^+$ Tems displayed relatively similar gene expression profiles with only 76 genes differentially expressed (*fold change* >2; *Adjp* <0.01) (**Figure 2A-D**). Of note, *CD226* was the most differentially expressed gene between $CD226^-$ and $CD226^+$ $CD8^+$ T cells (*fold change* = 55 *Adjp* = $4.5x10^{-50}$) (**Figure 2C**). Similar results were obtained comparing transcriptomic profiles of resting Tn, Tcm and Temra $CD226^-$ and $CD226^+$ $CD8^+$ T cell subsets (**Figure S2A-B**) thus indicating that CD226 absence on $CD8^+$ T cells was not only due to ligand-induced protein internalization as shown by *Braun et al.* but rather resulted from transcriptional regulation of this gene. Although functional analysis suggested that $CD226^-$ $CD8^+$ T cells were hypo-responsive to TCR stimulation, our global transcriptional analysis revealed that both $CD226^-$ and $CD226^+$ $CD8^+$ Tems displayed signs of activation upon anti-CD2/CD3/CD28 stimulation with respectively 5850 and 6577 genes differentially expressed between the resting and activation states (*fold change* > 2 ; *Adjp* <0.01) (**Figure 2A-B**). Still, non-hierarchical clustering and principal component analysis (PCA) also revealed critical

differences between anti-CD2/CD3/CD28 activated CD226$^+$ and CD226$^-$ CD8$^+$ Tems with 1209 up-regulated and 880 down-regulated genes (*fold change* > 2 ; *Adjp* <0.01) between both subsets (**Figure 2 A-D and Figure S2C**). In line with our previous findings (**Figure 1**), GSEA and Go term analysis confirmed that activated CD226$^+$ CD8$^+$ Tem specific genes were enriched in gene signatures related to cell cycle, protein synthesis, TCR activation, T_{H1} differentiation and IL-2/IL-15 signaling (**Figure 2E-F and Figure S2D**). Conversely, activated CD226$^-$ CD8$^+$ Tem specific genes were enriched in gene signatures related to resting T cells, regulatory T cells and TGF-β signaling (**Figure 2E-F and Figure S2D**) thus validating at the transcriptional level the functional advantage of CD226$^+$ over CD226$^-$ CD8$^+$ T cells upon TCR stimulation.

Mechanisms underlying CD226$^-$ CD8$^+$ T cell hypo-responsiveness.

To establish the link between CD226 expression and TCR induced effector program of CD8$^+$ T cells, we transduced purified CD226$^-$ and CD226$^+$ CD8$^+$ Tems with GFP lentiviral vector encoding or not for CD226 and analyzed their effector functions in response to TCR stimulation. Consistent with our previous results, we found that CD226$^-$ CD8$^+$ Tems cells, transduced or not with GFP control vectors, had a reduced ability to proliferate, to produce pro-inflammatory cytokines such as IFN-γ, TNF-α and poorly expressed the CD107a degranulation marker in response to TCR stimulation as compared to CD226$^+$ CD8$^+$ T cells (**Figure 3A-B and Figure S3A-B)**. By contrast, CD226$^-$ CD8$^+$ Tems that ectopically expressed CD226 (GFP$^+$ cells) underwent several cell divisions and produced significantly higher levels of IFN-γ, TNF-α and CD107a than cells that were not transduced or transduced with a GFP control vector (**Figure 3A-B and Figure S3A-B)**. Altogether, these results highlight the implication of of CD226 loss in the functional impairment of CD8$^+$ T cells in response to TCR stimulation.

We next investigated the molecular mechanisms underlying CD226$^-$ CD8$^+$ T cell functional defects. Given the importance of LFA-1 in T cell adhesion and TCR signaling (Bachmann et al., 1997; Dustin and Springer, 1989) and the tight link between this integrin and CD226 signaling (Shibuya et al., 1999; Shibuya et al., 2003), we hypothesized that CD226 absence might directly impact LFA-1 functions. LFA-1 is maintained in an inactive bent conformation on resting T lymphocytes and its extension and head-opening is required to increase LFA-1 affinity and binding to ICAM-1 (Comrie et al., 2015). These conformational changes of LFA-1 that expose different epitopes were thus evaluated on CD226$^-$ and CD226$^+$ CD8$^+$ T cells. We found that CD226$^+$ and CD226$^-$ CD8$^+$ T cells expressed comparable levels of total LFA-1 regardless of their

activation state (**Figure S3C-D**). By, contrast, CD226$^+$ CD8$^+$ T cells expressed significantly higher levels of "extended open" high affinity LFA-1 than their CD226$^-$ counterparts both in steady state conditions and upon TCR stimulation (**Figure 3C and Figure S3C-D**). These results were further confirmed by confocal microscopy imaging that also revealed important co-localization between CD226 and high affinity LFA-1 at the cellular interface between anti-CD3 activated CD8$^+$T cells (**Figure 3D-E**)**. To directly establish a link between CD226 expression and LFA_1 activation,** we analyzed the TCR induced activation of LFA-1 by CD226$^-$ and CD226$^+$ CD8$^+$ T cells that were transduced with GFP lentiviral vector encoding or not for CD226 (**Figure 3F**). We found that CD226$^-$ CD8$^+$ T cells transduced with CD226 lentiviral vectors had a significantly higher expression of LFA-1 open conformation as compared to CD226$^-$ CD8$^+$ T cells transduced with GFP control vectors (**Figure 3F**). To investiagte the importance of LFA-1 in CD226$^+$ TCR-induced functions, we analyzed cytokine production by CD226$^+$ and CD226$^-$ CD8$^+$ T cells in the presence of blocking antibodies or pharmacological inhibitors of LFA-1 (**Figure 3G and Figure S3F**). Consistent with the well documented role of LFA-1 in efficient TCR signaling (Bianchi et al., 2000; Perez et al., 2003), we found that inhibiting LFA-1 significantly decreased the proliferation and the production of IFN-γ and TNF-α by CD226$^+$ CD8$^+$ Tems (**Figure 3G and Figure S3F)**. Altogether these results imply that alteration in LFA-1 signaling due to CD226 loss might be involved in CD226$^-$ CD8$^+$ T cell dysfunction.

By contrast, we provided several evidences showing that CD226 negative regulators, CD96, TIGIT or PVRIG (CD112R) (Chan et al., 2014a; Johnston et al., 2014; Zhu et al., 2016), may not directly account for CD226$^-$ CD8$^+$ T cell hypo-responsiveness. First, CD96 or TIGIT blockade did not restore TCR-induced proliferation nor IFN-γ secretion by CD226$^-$ CD8$^+$ T cells **(Figure S3G-H)** and PVRIG transcripts were almost undetectable on purified CD226$^+$ and CD226$^-$ CD8$^+$ T cells **(Figure S3I)**. Second, CD226$^+$ Tems had significantly higher proliferation than their CD226$^-$ counterparts upon anti-CD2/CD3/CD28 microbeads stimulation regardless of TIGIT expression (**Figure S3J**). Finally, their common ligands CD112 and CD155 were hardly detectable at the mRNA level in purified CD8$^+$ T cells (**Figure S3I**) and CD112 and CD155 *in vitro* blockade did not reduce CD226$^+$ CD8$^+$ T cell functions induced by TCR stimulation (**Figure S3G-H**)**.** This also implies that CD226 may act independently of its ligands as evidenced by pioneer studies from *Shibuya et al*. showing that CD226 was phosphorylated by TCR or LFA-1 engagement (Shibuya et al., 1999; Shibuya et al., 2003).

CD226 absence identifies dysfunctional human CD8$^+$ tumor infiltrating lymphocytes.

We next addressed the importance of CD226 expression in the tumor context. We first compared CD226 expression on bone marrow (BM) CD8$^+$ isolated from HD and patients newly diagnosed with multiple myeloma (MM; IFM 2009 (Attal et al., 2017)), a frequent yet incurable hematological malignancy (**Figure S4A**). We found that the percentage of BM CD8$^+$ T cells lacking CD226 expression was significantly increased in MM patients as compared to HD (**Figure 4A and Figure S4B-C**). CD226$^-$ percentages were also significantly higher among CD8$^+$ tumor infiltrating lymphocytes (TILs) than PBMCs in MM patients (**Figure 4B**). Of note, we didn't observe any correlation between the age, the gender and the percentages of BM infiltrating CD226$^-$ CD8$^+$ T cells among MM patients and HD (**Figure S4D**). By contrast, the percentage of CD226 expressing CD8$^+$ T cells significantly correlated with myeloma CD8$^+$ T cell infiltration (**Figure S4E**) and *CD226* gene expression was strongly associated with the expression of cytotoxic lymphocyte functional genes including *CD2, CD3E, CD3D, TBX21, CD8B, PRF1, GZMA, and GZMB* in MM patient's samples (**Figure S4F**). These data suggested a relationship between CD226 loss and CD8$^+$ T cell dysfunction in the tumor microenvironment. Functional analysis of myeloma infiltrating CD8$^+$ T cells upon *in vitro* re-stimulation with anti-CD2/CD3/CD28 microbeads confirmed that CD226$^-$ CD8$^+$ T cells had significantly lower TCR-induced proliferation, IFN-γ and TNF-α production and degranulation than CD226$^+$ CD8$^+$ T cells (**Figure 4C-D and Figure S4G-H**). Of note, CD226$^+$ TILs produced significantly higher cytokine levels than their CD226$^-$ counterparts both in the TIGIT$^-$ and TIGIT$^+$ fractions thus excluding the role for this negative regulator of CD226 in the hypo-responsiveness of CD226$^-$ TILs (**Figure S4I**). Interestingly, for patients with a detectable population of NY-ESO-1 specific TILs, the frequency of CD226$^-$ cells was significantly higher among NY-ESO-1 specific TILs than among polyclonal TILs (**Figure 4E and Figure S4J**). The absence of CD226 expression was again associated with reduced cytokine production by CD8$^+$ T cells upon stimulation with NY-ESO-1 peptide (**Figure 4F**). CD226$^-$ CD8$^+$ T cells with reduced effector functions also represented a significant fraction of TILs isolated from other cancer types including non-small cell lung cancer (NSCLC), breast adenocarcinoma and ovarian carcinoma (**Figure 4G and Figure S4K**). In these tumors, CD226$^-$ percentages were also significantly higher among TILs than CD8$^+$ T cells isolated from healthy distant tissues or PBMCs (**Figure 4G**). In invasive breast cancer (BRCA) cohorts from the TCGA data base, CD226 expression was also associated with significantly

decreased disease-free (DFS) and overall survival (OS) (**Figure 4I and Figure S4L**). Altogether, these results demonstrate that the absence of CD226 expression, (1) identifies TILs with severely impaired functions across diverse malignancies, (2) could impact patient clinical outcome.

Tumor microenvironment drives the differentiation of dysfunctional CD226$^-$ CD8$^+$ T cells.

To understand the link between tumor progression, CD226 loss and CD8$^+$ T cell dysfunction, we explored CD226 expression in well characterized preclinical mouse cancer models. As described previously (Seth et al., 2011), we found that most CD8$^+$ T cells isolated from the spleen C57BL/6 WT mice expressed homogeneous levels of CD226. By contrast, we observed the progressive emergence of a CD226 negative population among CD8$^+$ Tems infiltrating B16F10 melanoma and VK12653 myeloma tumors (**Figure 5A-E and Figure S5A**). In both models, the percentage of CD226$^-$ CD8$^+$ TILs significantly correlated with tumor size (**Figure 5D-E and Figure S5B-C**) confirming the link between CD226 loss and tumor development. As in humans, CD226$^-$ CD8$^+$ T cells accumulating in mouse tumor microenvironment were characterized by significantly decreased proliferation as evidenced by reduced Ki67 staining (**Figure 5F**). Upon *in vitro* re-stimulation with anti-CD3/anti-CD28 mAbs, they also produced significantly less IFN-γ and TNF-α than their CD226$^+$ counterparts (**Figure 5G**). These results confirm that the absence of CD226 in CD8$^+$ T cells marks a dysfunctional population associated with tumor progression.

To address the question of CD226$^-$ TIL antigen specificity, ova-specific OT-1 CD8$^+$ T cells were transferred into WT mice that were subsequently injected with B16F10 expressing or not ova antigen (**Figure 5H**). We detected an accumulation of TCRα2$^+$/Vβ5$^+$ OT-1 CD8$^+$ Tems with a low CD226 expression within B16F10-ova tumors (**Figure 5I**). OT-1 CD8$^+$ Tems were also present in B16F10 tumors, although at lower frequencies (**Figure S5D-E**)**.** Yet, in the absence of their cognate antigen, most of the B16F10 intratumor OT-1 CD8$^+$ Tems retained a high CD226 expression (**Figure 5I**). Of note, CD226$^-$OT-1 CD8$^+$ Tems were also almost undetectable in the spleen of B16F10 and B16F10-ova bearing mice (**Figure 5I**). More importantly, we found that the percentage of CD226$^-$ cells was significantly higher among TCRα2$^+$/Vβ5$^+$ OT-1 cells than among TCRα2$^-$/Vβ5$^-$ T cells in the B16F10-ova model confirming that CD226 loss preferentially occurs in tumor antigen specific TILs than in potential by-stander TILs (**Figure 5J and Figure S5E**). Similar results were obtained when we transferred highly purified naïve CD226$^+$ CD8$^+$ T

cells isolated from the spleen of OT-1 mice into immunodeficient *Rag2*$^{-/-}$*gc*$^{-/-}$ bearing B16F10 or B16F10-ova tumors (**Figure S5F-H**). Taken together these results demonstrate that tumor microenvironment drives the differentiation of CD226^{+} CD8^{+} T cells into CD226^{-} CD8^{+} T cells in a tumor-antigen dependent manner.

Immune checkpoint blockade efficacy relies on CD226.

We analyzed whether the expression of CD226 is implicated in the exhaustion of CD8 T cells. Phenotypic analyses revealed that both CD226^{-} and CD226^{+} CD8^{+} TILs isolated from B16F10 bearing mice had a phenotype consistent with Tex cells characterized by a high expression of PD-1, TIGIT, LAG-3 and CTLA-4 (**Figure 6A and Figure S6A, B**). CD226^{-} and CD226^{+} OT-1 cells infiltrating B16F10-ova tumors upon adoptive transfer into WT mice also expressed similar levels of PD-1 and Tim-3 (**Figure 6B**). These immune-checkpoints were also equally present on CD226^{-} and CD226^{+} TILs isolated from breast and ovarian cancer patients (**Figure 6C and Figure S6C**). Therefore, we hypothesized that CD226 expression might impact CD8^{+} T cell response to immune checkpoint blockade. To test this hypothesis, we analyzed CD226^{-} and CD226^{+} CD8^{+} Tem cell responsiveness to anti-PD-1 blockade using a B16K1 melanoma variant overexpressing MHC-I (Bertrand et al., 2017). Of note, CD226^{-} CD8^{+} TILs that progressively accumulated in this model correlated with tumor size and displayed similar immune checkpoint expression with their CD226^{+} CD8^{+} counterparts (**Figure S6D-E**). As expected (Bertrand et al., 2017), anti-PD-1 mAbs injection led to a significant decrease in tumor growth as compared to control Ig treatment that was abrogated upon monoclonal antibody based depletion of CD8^{+} T cells (**Figure 6D-E**). A concomitant increase in the percentage of tumor infiltrating CD8^{+} T cells and proliferating Ki67^{+} CD8^{+} TILs was also observed (**Figure S6F**). Still, while anti-PD-1 increased the *in vivo* proliferation of CD226^{+} TILs, the proliferation of CD226^{-} CD8^{+} TILs was not significantly affected by this treatment (**Figure 6F**). In addition, unlike their CD226^{+} counterparts, anti-PD-1 treatment failed to increase *ex vivo* IFN-γ production by CD226^{-} CD8^{+} TILs (**Figure 6G**). Altogether, these results suggest that anti-PD-1 treatment may not reverse CD226^{-} CD8^{+} T cells dysfunction suggesting that CD226 expression may be critical for anti-PD-1 efficacy. To confirm this hypothesis, WT or *Cd226*$^{-/-}$ mice bearing B16K1 tumors were treated with anti-PD-1 or control Ig antibodies. PD-1 blockade resulted in significant reduction in tumor growth in WT mice while it only had minor effects in *CD226*$^{-/-}$ mice (**Figure 6H and Figure S6G**). Tumor-bearing WT mice injected with anti-CD226 blocking mAbs also

failed to respond to anti-PD-1 treatment (**Figure 6I and Figure S6H**). Of note, CD226 blockade had quite similar negative impact on anti-PD1 treatment as $CD8^+$ T cell depletion in these experiments (**Figure 6I and Figure S6H**) underlining the critical role of CD226 expressed by $CD8^+$ T cell for anti-PD1 efficacy. Similar results were obtained using MC38 model upon treatment with PD-1 alone or in combination with anti-CTLA-4, thus confirming the importance of CD226 in the efficacy of ICB (**Figure S6I-J**). Altogether, these results highlight that the accumulation of defective $CD226^-$ $CD8^+$ TILs may represent an important parameter limiting the efficacy of ICB.

Tumor-induced $CD226^-$ $CD8^+$ T cells accumulation depends on Eomes expression.

Although RNAseq analysis revealed that human resting $CD226^+$ and $CD226^-$ $CD8^+$ T cells have similar transcriptional program, several genes differed between these two subpopulations (**Figure S2C**). In particular, we found that Eomesodermin (Eomes) transcription factor (TF) mRNA was expressed significantly higher in the $CD226^-$ fraction of both resting and activated human $CD8^+$ T cells (**Figure 7A**). Similar observations were made at the protein level in $CD8^+$ T cells isolated from HD or cancer patient's samples (**Figure 7B**). Together with previous evidence showing that high Eomes expression limits TILs responsiveness to ICB (Blackburn et al., 2008; Paley et al., 2012), these results questioned the role of this TF in the accumulation of dysfunctional $CD226^-$ $CD8^+$ Tems in tumors. To address this point, we analyzed the tumor-induced differentiation of $CD226^-$ $CD8^+$ T cells in *CD4*^{cre}x*Eomes*$^{fl/fl}$ mice (*Eomes*^{KO}) that have T cell specific deletion of *Eomes*. First, we confirmed that $CD226^-$ TILs expressed significantly higher levels of Eomes in both B16F10 (**Figure 7C-D and Figure S7A-C**) and Vk12653 (**Figure S7D-G**) bearing *CD4*^{WT}x*Eomes*$^{fl/fl}$ control mice (*Eomes*^{WT}). More importantly, in both tumor models, the percentage of $CD226^-$ $CD8^+$ TILs was strongly reduced in *Eomes*^{KO} mice as compared to *Eomes*^{WT} mice (**Figure 7C, E and Figure S7G**). Of note, the absence of Eomes did not significantly affect tumor size, nor tumor $CD8^+$ Tem percentage ruling out a potential impact of these parameters in the observed differences between *Eomes*^{KO} and *Eomes*^{WT} mice (**Figure S7A-F**). To confirm the role of Eomes in $CD226^-$ $CD8^+$ T cell development, we next analyzed CD226 expression by $CD8^+$ T cell in mice overexpressing Eomes under the hCD2 promoter (Istaces et al., 2019). As expected, we found that splenic $CD8^+$ T cells isolated from Eomes^{Tg} mice contained significantly higher percentages of $CD226^-$ $CD8^+$ T cells than the $CD8^+$ T cells from control mice (**Figure 7F-G**). These $CD226^-$ $CD8^+$ T cells were also characterized by

higher Eomes expression than their CD226^{+} counterparts confirming the link between Eomes overexpression and CD226 loss (**Figure 7F-G**). In order to determine the mechanisms underlying Eomes regulation of CD226 expression we analyzed ATAC-Seq, Eomes ChIP-Seq and H3K27 histone acetylation profile of *Cd226* locus in CD8^{+} T cells (**Figure S7H**). ChIP-Seq data from ectopic or endogenous Eomes in CD8 T cells (GSE122895; PMID: 30619337 and GSE124914; PMID 31341159) both revealed a clear fixation peak in an accessible intronic region of *Cd226*, indicating that Eomes is able to directly interacts with regulatory elements of the Cd226 gene (**Figure S7H**).

CD226 loss restrains CD8^{+} T cells antitumor functions during CD137 immunotherapy.

Agonist antibodies against CD137 (TNFRSF9, 4-1BB) represent promising immunotherapeutic agents previously shown to induce Eomes up-regulation in T cells (Curran et al., 2013) that could thus affect CD226 expression by CD8^{+} T cells. Indeed, we found that anti-CD137 treatment resulted in the expansion of CD8^{+} T cells with an effector memory phenotype that expressed high levels of Eomes in the different lymphoid organs tested (**Figure 8A-B and Figure S8A**). Remarkably, anti-CD137-induced Eomes over-expression was accompanied by the progressive emergence of CD8^{+} Tems lacking CD226 expression in a dose dependent manner (**Figure 8A-B and Figure S8B-C**). By contrast, agonist mAbs targeting other immunostimulatory members of the TNF receptor family such as GITR or OX40 did not increase Eomes expression nor the frequency of CD226^{-} CD8^{+} T cells (**Figure S8D-E).** Once again, CD226^{-} CD8^{+} T cells were characterized by higher Eomes levels (**Figure 8C**) and Eomes deficiency significantly abrogated CD226 loss induced by anti-CD137 mAb treatment (**Figure S8F**) thus confirming the importance of this TF in the program leading to CD226 loss. Interestingly, CD226 loss induced by anti-CD137 mAb treatment was also abrogated in *CD4*^{cre}x*Eomes*$^{fl/wt}$ (*Eomes*^{het}) mice (**Figure 8D)** that were characterized by lower Eomes level as compared to *Eomes*^{WT} but induced similar effector CD8^{+} T cell expansion upon CD137 treatment (**Figure S8G**). By contrast, anti-CD137 induced CD226^{-} CD8^{+} T cell accumulation was not affected by CD155 deficiency, ruling out any critical role of CD226/CD155 interactions in the emergence of CD8^{+} T cells lacking CD226 expression upon CD137 stimulation (**Figure 8E**).

To confirm whether anti-CD137 agonists promoted the differentiation of CD226$^+$ T cells into CD226$^-$ T cells as shown in the tumor context, we transferred purified CD226$^+$ naïve CD8$^+$ T cells into *Rag2*$^{-/-}$*gc*$^{-/-}$ mice (**Figure S8H**). A few days after cell transfer, most CD8$^+$ T cells had undergone several rounds of division as a result of homeostatic expansion. They had also acquired a CD44^{hi} memory T cell phenotype but remained CD226$^+$ T cells, ruling out that the emergence of CD226$^-$ cells only resulted from CD8$^+$ T cell division or memory T cell differentiation (**Figure S8I**). By contrast, the subsequent injection of anti-CD137 mAbs promoted the accumulation of CD226$^-$ CD8$^+$ Tems confirming that the accumulation of CD226$^-$ CD8$^+$ T cells upon CD137 activation resulted from the CD226$^+$ CD8$^+$ T cell differentiation (**Figure S8J**). The emergence of OT-1 cells lacking CD226 expression was also observed following adoptive transfer of CD226$^+$ OT-1 cells into WT mice upon treatment with anti-CD137 mAbs (**Figure S8K**). Altogether, these results demonstrate that Eomes over-expression induced by CD137 immunotherapy drives the differentiation of CD226$^+$ into CD226$^-$ CD8$^+$ T cells.

Given the overall clinical interest around CD137 agonists as immunotherapeutic agents in cancer, we next analyzed the functions of CD226$^-$ and CD226$^+$ CD8$^+$ Tems induced upon anti-CD137 treatment. We found that purified CD226$^-$ CD8$^+$ Tems from anti-CD137-treated mice divided less and produced lower levels of IFN-γ and TNF-α than their CD226$^+$ counterparts in response to anti-CD3/anti-CD28 stimulation (**Figure 8F-G**). Using OT-1 mice treated with anti-CD137, we confirmed that anti-CD137 induced CD226$^-$ CD8$^+$ OT-1 cells have lower effector functions than their CD226$^+$ counterparts in response to their cognate antigen (**Figure 8H**). It is worth mentioning that CD226$^-$ CD8$^+$ Tems isolated from anti-CD137-treated mice had strongly reduced CD226 mRNA levels as compared to CD226$^+$ CD8$^+$ Tems confirming, as in humans, that CD226 loss process occurs at the transcriptional level (**Figure S8L**).

Finally, to gain clear insight whether CD226 loss may affect the *in vivo* anti-tumor functions of CD8$^+$ T cells that expand upon anti-CD137 immunotherapy, *Pmel-1* transgenic mice, that all harbor CD8$^+$ T cells specific for the B16 gp100 melanoma antigen, were treated with anti-CD137 mAbs. Sorted CD226$^-$ or CD226$^+$ CD8$^+$ Tems were transferred into B16F10 melanoma bearing mice according to previously described adoptive cell transfer (ACT) protocol (Landsberg et al., 2012)(**Figure 8I**). Consistent with their reduced effector capabilities *in vitro*, CD226$^-$ CD8$^+$ T cells only mildly reduced tumor development while the transfer of CD226$^+$ CD8$^+$

T cells resulted in a drastic reduction in tumor growth and significantly prolonged survival of mice (**Figure 8J-K**). These results confirm that Eomes dependent CD226 loss induced by anti-CD137 treatment could limit the anti-tumor efficacy of this treatment *in vivo*.

DISCUSSION

The mechanisms underlying the lack of responsiveness of anti-tumor $CD8^+$ T cells are still poorly understood and finding additional signals that regulate their functions has become a major priority. In the present study, we found that loss of the activating receptor CD226 is a critical mechanism that alters $CD8^+$ T cell responsiveness to TCR stimulation. Pre-clinical tumor mouse model confirmed that tumor development drives the accumulation of dysfunctional $CD8^+$ T cell lacking CD226 expression through an Eomes-dependent mechanism. More importantly, our results demonstrated that $CD8^+$ T cells fail to respond to ICB in the absence of CD226 and that CD226 loss affects anti-CD137 agonist efficacy. Taken together our study suggests that CD226 loss represents an underappreciated determinant of $CD8^+$ T cell dysfunction in the tumor microenvironment that may impact cancer patient response to immunotherapy.

The profound cancer-immunosurveillance defects depicted by our group and others in diverse tumor mouse models (Gilfillan et al., 2008; Guillerey et al., 2015; Iguchi-Manaka et al., 2008) in the absence of CD226 suggested this receptor might exert central functions in T lymphocyte biology. The implication of this receptor in $CD4^+$ T helper cell differentiation (Gaud et al., 2018; Lozano et al., 2012; Lozano et al., 2013) and the association between *CD226* gene single nucleotide polymorphism (SNP) with increased development of autoimmune pathologies (Maiti et al., 2010; Song et al., 2012; Todd et al., 2007) supported this hypothesis. Yet, initial studies using CD226-deficient mice indicated that CD226 is not formally required for antigen-specific $CD8^+$ T cell activation and no striking immune defects were found in the absence of CD226 (Gilfillan et al., 2008). Based on this evidence, this receptor was so far mainly considered as a co-stimulatory receptor increasing cytotoxic T lymphocyte- and NK cell-mediated cytotoxicity against CD112- and CD155-expressing targets (Martinet and Smyth, 2015). Herein, using diverse TCR triggering agents, in the presence or absence of CD28 co-stimulation, we presented compelling evidence that $CD8^+$ T cells that do not express CD226 are hypo-responsive to TCR stimulation and have limited effector functions. These results imply that CD226 plays a more central role than originally thought in $CD8^+$ T cell activation program induced by TCR engagement.

The phenotype of $CD8^+$ T cells expressing CD226 or not were very similar for the different healthy donors and cancer patients analyzed in our study. These results were confirmed by RNAseq analysis of freshly purified peripheral blood $CD226^-$ and $CD226^+$ $CD8^+$ T cells with only 76 genes differentially expressed between both subsets. It is unlikely that these subtle differences at the resting state may be responsible for the divergent functional outcomes observed between $CD226^-$ and $CD226^+$ $CD8^+$ T cells upon TCR stimulation since we found that CD226 forced expression through lentiviral vectors restored $CD226^-$ $CD8^+$ T cells functions in response to TCR stimulation. These results together with the reduced phosphorylation of several key TCR downstream signaling molecules observed upon anti-CD3 stimulation in the absence of CD226 strongly argue for a key role of CD226 in $CD8^+$ T cell TCR signaling. Although $CD226^-$ and $CD226^+$ $CD8^+$ T cells both underwent important transcriptional modifications upon anti-CD2/CD3/CD28 stimulation, archetypal effector T cell-associated genes were only detected in stimulated $CD226^+$ T cells. Such results suggest that the presence of CD226 directly impacts TCR induced $CD8^+$ T cell effector program. Understanding how CD226 modulate TCR signaling in $CD8^+$ T cells may provide new approaches to restore T cells functions especially in tumor context.

Several pieces of evidence indicate that CD226 is implicated in LFA-1 functions (Shibuya et al., 1999; Shirakawa et al., 2005; Shirakawa et al., 2006). LFA-1 binding to ICAM-1 on contacting cells represents a critical early event driving actin-cytoskeleton reorganization, immune synapse formation, and co-stimulation ultimately lowering TCR activation threshold (Bachmann et al., 1997; Bianchi et al., 2000; Perez et al., 2003). We brought significant evidence that LFA-1 functions are affected by the absence of CD226. Indeed, we found that TCR induced LFA-1 activation into its high-affinity conformation (Dustin and Springer, 1989), was greatly reduced in the absence of CD226 in $CD8^+$ T cells and that CD226 forced expression restored these defects. In addition, we observed that LFA-1 inhibition reduced $CD8^+$ T cell activation similar to CD226 loss. Thus, our results suggest that LFA-1 defects owing to CD226 loss may represent an important mechanism of TCR hypo-responsiveness and $CD8^+$T cell dysfunction in tumors. The observations from *Braun et al.* showing actin cytoskeleton reorganization and LFA-1 polarization defects in *Cd226*$^{-/-}$ $CD8^+$ T cells support this hypothesis (Braun et al.). Future work will be needed to better understand how CD226 intrinsic signaling connects with TCR signaling and LFA-1 in $CD8^+$ T cells. CD226 contains at least two

phosphorylation sites on tyrosine residue 322 and on serine residue 329 in its intracellular domain (Martinet and Smyth, 2015; Shibuya et al., 1996). A recent study stressed the importance of the conserved $Y^{322}XN^{324}X$ immunoglobulin tyrosine tail (ITT) motif in the NK cell cytolytic functions of CD226 (Zhang et al., 2015). This typical consensus binding sequence was indeed shown to connect CD226 with Grb2 SH2 domain, subsequently leading to the activation of Vav-1, phospholipase C-γ1 and ERK1,2 (Zhang et al., 2015). CD226 ITT motif could therefore represent a critical relay to amplify TCR downstream signaling. The decreased phosphorylation of ZAP-70, SLP76, LAT and ERK1,2 observed in $CD8^+$ T cells lacking CD226 and the recent evidence that Vav-1 associates with CD226 in $CD4^+$ T cells may support this hypothesis (Gaud et al., 2018). Surprisingly, no immune synapse, nor functional defects were observed by *Braun et al*. in $CD8^+$ T cells isolated from *Cd226*^{Y} mice harboring a point of mutation on the Y319 of CD226 (mouse equivalent Y^{322}) suggesting that this signaling is dispensable for CD226 synergy with LFA-1 and TCR co-stimulation (Braun et al.). Although the importance of Ser 329 phosphorylation in the propagation of CD226 downstream signaling remains a matter of debate (Zhang et al., 2015), this residue could represent a critical link between TCR signaling, CD226 and LFA-1. Indeed, Ser 329 of CD226 was found to be phosphorylated upon CD3/CD28 stimulation and was required for CD226 physical association with LFA-1 in lipid raft (Shibuya et al., 1999; Shirakawa et al., 2005; Shirakawa et al., 2006). Besides, CD226 may also play a critical role in cytoskeleton remodeling, a central process for TCR signaling and LFA-1 conformational activation. This hypothesis is supported by a study from Ralston and colleagues showing that CD226 could bind tightly to the actin cytoskeleton through its interaction with the MAGUK homologue human discs large (hDlg) and the actin-binding protein 4.1G (Ralston et al., 2004).

It is now well established that many human tumors express specific antigens that can elicit $CD8^+$ T cell activation and the accumulation of $CD8^+$ effector T cells in the tumor microenvironment (Schumacher and Schreiber, 2015). Unfortunately, successful eradication of tumor cells by these TILs is often limited by diverse immunosuppressive mechanisms (Thommen and Schumacher, 2018). Among them, the up-regulation of multiple inhibitory receptors such as PD-1, Tim-3, TIGIT, and LAG-3 at the cell surface of TILs has emerged as major mechanisms of T cell dysfunction protecting tumors from immune attack (Thommen and Schumacher, 2018). Our study addressed an additional mechanism of cancer immune

escape other than the classical immune checkpoints through the loss of a critical activation receptor, CD226. We presented considerable new evidence that tumor development favors the accumulation of dysfunctional $CD8^+$ T cells lacking CD226 expression. While almost all mouse $CD8^+$ T cells expressed CD226 in steady-state conditions, we found the progressive accumulation of TILs lacking CD226 with a $CD62L^-CD44^{hi}$ effector memory phenotype in the different tumor mouse models tested. Of note, CD226 loss mainly affected tumor antigen-specific $CD8^+$ T cells since we observed that ova-specific purified $CD226^+$ OT-1 cells only converted into $CD226^-$ effector cells when transferred into ova-tumor bearing mice. Still, the differentiation of $CD8^+$ T cells into hypo-reactive $CD226^-$ $CD8^+$ T cells may occur in other contexts as dysfunctional $CD226^-$ $CD8^+$ T cells were detectable in most healthy donors. Whether this reflects a previous immune history of each individual or whether this represents a mechanism ensuring immune homeostasis by preventing over $CD8^+$ T cell activation remains to be more deeply investigated in the future.

Sustained expression of inhibitory receptors was so far considered as a key parameter allowing the identification of exhausted T cells in chronic infectious disease and cancer (Ahmadzadeh et al., 2009; Blackburn et al., 2009; Thommen et al., 2018). The successful reinvigoration of Tex functions by anti-PD-1 mAbs in chronic viral infections (Barber et al., 2006) and the impressive clinical results obtained by ICB in cancer patients (Robert et al., 2015; Robert et al., 2011; Topalian et al., 2012) support the importance of inhibitory receptors in T cell dysfunctions. Still, recent studies suggest that intratumor $PD\text{-}1^+$ exhausted T cells comprise a large spectrum of dysfunctional states (Bengsch et al., 2018; Thommen et al., 2018). More importantly, it becomes evident that the potential of reinvigoration by ICB differs between $CD8^+$ Tex subpopulations, meaning that additional alterations restrain exhausted T cell functions (Pauken et al., 2016; Philip et al., 2017; Scott et al., 2019). Interestingly, both $CD226^-$ and $CD226^+$ cells were found among tumor infiltrating Tex cells with similar IC expression. Still, $CD226^-$ TILs consistently had lower effector functions and proliferation than their $CD226^+$ counterparts. In addition, anti-PD-1 immunotherapy failed to restore effector functions of TILs lacking CD226 expression. Thus, the absence of CD226 activation receptor might represent a yet underappreciated molecular mechanism limiting intratumor T cell responsiveness and correlating with their exhausted state independently of inhibitory receptors.

Although several predictive factors such as $CD8^+$ T cell infiltration (Tumeh et al., 2014), PD-L1 expression (Larkin et al., 2015) as well as tumor neo-antigen load (Rizvi et al., 2015) were identified in the past, it remains still unclear why some patients respond to ICB therapy while others do not. Thus, understanding the molecular mechanisms underlying effective responses to ICB therapy remains an intense field of investigation. Recently, it was demonstrated that PD-1/PD-L1 signaling suppresses T cell function via inactivation of CD28 signaling rather than TCR signaling (Hui et al., 2017) and that CD28/B7 pathway plays a crucial role in the efficacy of anti-PD-1 treatment (Kamphorst et al., 2017). However, the efficacy of anti-PD-1 may also rely on additional co-stimulatory signals as demonstrated by a recent study showing that PD-1/PD-L1 pathway is a negative regulator of CD226 signaling and that the anti-tumor effect of PD-1 and GITR antibody combination was abrogated in the absence of CD226 (Wang et al., 2018). Our study demonstrating that anti-PD-1 immunotherapy fails to restore effector functions of TILs lacking CD226 expression not only confirms the importance of signals provided by CD226 in anti-PD-1 efficacy but also highlights a novel mechanism of tumor resistance to ICB through the loss of CD226 expression. Thus, the extent of $CD226^-$ $CD8^+$ T cells accumulating in the tumor microenvironment may represent an attractive parameter to consider for predicting anti-PD-1 efficacy in cancer patients especially given the high CD226 variability observed among cancer patients in our study.

A better understanding of the tumor signals involved in CD226 loss is required as they may represent interesting target to restore $CD8^+$ T cell anti-tumor functions and immune checkpoint efficacy. CD226 engagement by its ligands, especially CD155, was previously shown to decrease CD226 density at the cell surface of NK and T cells (Li et al., 2018b). The chronic stimulation of CD226 by tumors that frequently overexpress CD155 may therefore participate in CD226 loss as shown by *Braun et al*. (Braun et al.). Although, ligand induced CD226 recycling may account for CD226 loss, especially in the tumor context, our results suggest the existence of additional mechanisms occurring at the transcriptional level. Interestingly, we found that tumor induced CD226 loss was blunted in the absence of Eomes. Conversely, Eomes overexpression promoted the accumulation of dysfunctional $CD226^-CD8^+$ T cells and once again this phenomenon was blunted in the absence of Eomes. While these results demonstrate the implication of Eomes in CD226 loss, the mechanisms underlying CD226 transcriptional repression remains to be further addressed. Still, the presence of an

Eomes fixation pic in a regulatory region of *Cd226* gene suggest that Eomes may directly repress CD226 expression. Several studies suggested that the level of Eomes expression may distinguish two different T cell exhaustion stages induced by chronic antigen exposure (Blackburn et al., 2008; Buggert et al., 2014; Paley et al., 2012). In chronic viral infections, $Eomes^{hi}$ Tex cells expressed higher levels of inhibitory receptors, had reduced effector functions, and did not respond to anti-PDL1-mediated reinvigoration as compared to $Eomes^{lo}$ Tex cells (Blackburn et al., 2008; Paley et al., 2012). Dissecting the exact role of Eomes in T cell dysfunction was complicated by the function of this TF in effector $CD8^+$ T cell program and memory maintenance (Intlekofer et al., 2005; Kaech and Cui, 2012). Recent evidence suggests that low Eomes expression is required for anti-tumor effector T cell expansion and tumor control, while its overexpression favors T cell exhaustion and tumor outgrowth (Li et al., 2018a). Although Eomes was implicated in the up regulation of several immune checkpoints such as PD-1 and Tim-3, our results suggest that CD226 loss may also participate to the terminal exhaustion program associated with Eomes overexpression.

CD137 agonists was shown to stimulate $CD8^+$ T cell dependent antitumor immune response and promote tumor regression in a variety of mouse tumors (Guillerey et al., 2015; Melero et al., 1997). Still, early clinical trials revealed limited anti-CD137 mAb efficacy until now in cancer patients (Chester et al., 2018) and anti–CD137 agonists were shown to suppress clinical symptoms in several mouse models of autoimmunity (Choi et al., 2006; Kim et al., 2011; Seo et al., 2004; Sun et al., 2002). Some of the beneficial effects of anti-CD137 agonists in autoimmune models were ascribed to the expansion of a regulatory population of $CD8^+$ T cells that express CD11c producing high levels of IFN-γ (Choi et al., 2006; Kim et al., 2011). Our results suggest that CD226 loss induced by Eomes overexpression may also account for the immune regulatory function of CD137 and that preserving CD226 expression may increase the efficacy of this treatment in human cancer patients.

Although immunotherapy has represented a major breakthrough in cancer treatment, clinical responses are observed only in a fraction of treated patients and cancer types. Therefore, one of the major current research challenges now resides in the identification of novel mechanisms restraining anti-tumor immune functions. We and *Braun et al.* have demonstrated that CD226 expression represents a critical rheostat for anti-tumor functions

of $CD8^+$ T cells and that Eomes-dependent and/or CD155-induced CD226 loss represents a major tumor immune escape mechanism.

AUTHOR CONTRIBUTION

Study conception and design: A.C.P., M.W., A.A., S.G., T.B., M.J.S and L.M. Acquisition of data: A.C.P., M.W., A.A., L.L., M.B., N.C, M-V.J., M.L.M, G.G., I.D., E.B, C.M.S., E.M., L.B, S.M., A.S., A.A, M.P., S.K., M.C., C.G., M.J.S and LM. Analysis and interpretation of data: A.C.P., M.W., A.A., M.B., T.B., L.D.S., S.G., M.J.S and L.M. Drafting of manuscript: L.M. Critical revision and editing: A.C.P., M.W., A.A., L.D., L.L., A.D., A.S., T.B., M.J.S and L.M. Provision of key materials: B.C., E.V., A.M., A.D., M.A., J.M., M.P., and H.A.L.

ACKNOWLEDGEMENT

We thank Marie Tosolini, Laetitia Ligat, Liam Town and Brodie Quine and the members from the core facilities at the Cancer Research Center of Toulouse and QIMR Berghofer. We acknowledge the contribution of Gisèle Froment, Didier Nègre and Caroline Costa from lentivectors production facility of SFR Biosciences (UMS3444/CNRS, US8/Inserm, ENS de Lyon, UCBL). We thank Nathalie Rufer for providing PE-labeled NY-ESO-1 multimers and Céline Colacios for breast cancer sample data. We thank Pierre Cordelier and Bettina Couderc for their help on lentiviral vector. The “Genomic and Immunology of myeloma” laboratory at CRCT is supported by the “Fondation ARC pour la Recherche sur le Cancer” Program Grants (ARC PGA1-20160203788 and PGA1-20190208630). This work was supported by grants from the Institut National du Cancer (PLBIO R16100BB), Cancer Research Institute/Bristol-Myers Squibb CLIP Grant, the “Fondation Toulouse cancer santé” IUCT-O translational research program. A.S. and A.D. were supported by “Fondation pour la Recherche Médicale (DEQ20170336727)” and ARSEP. M.W and A.C.P were supported by la Ligue contre le cancer PhD fellowships. T.B. was supported by an EMBO long-term Fellowship (ALT945-2015) and a National Health and Medical Research Council of Australia (NH&MRC) Early Career Fellowship (1124690). M. J. S. was supported by a NH&MRC Senior Principal Research Fellowship (1078671) and Program Grant (1132519) and E.M was supported by a grant from ECTRIMS. S.G, M.L and E.B were supported by Fonds National de la Recherche Scientifique (FRS-FNRS, Belgium) and the European Regional Development Fund (ERDF) of the Walloon Region (Wallonia-Biomed

portfolio, 411132-957270). The results shown here are in part based upon data generated by the TCGA Research Network: https://www.cancer.gov/tcga.

CONFLICT DISCLOSURE

M.J. Smyth has research agreements with Bristol Myers Squibb and Tizona Therapeutics. L.M has research agreements with Bristol Myers Squibb, Sanofi-Aventis and Roche.

FIGURE LEGENDS

Figure 1: The absence of CD226 identifies hypo-responsive human CD8$^+$ T cells.

(**A**) Representative FACS histogram and graph showing the expression of CD226 by healthy donor (HD) peripheral blood CD8$^+$ T cells. n=77 HD. **(B)** Graph showing the relative frequency of the indicated TCRvβ among CD226$^-$ (blue) and CD226$^+$(red) CD8$^+$ T cells. Representative from n=20 HD. **(C)** Representative FACS histograms and graph showing the percentages of CD226$^-$ in the indicated CD8$^+$ T cell subsets. n = 77 HD. **(D)** Representative FACS histograms and graph recapitulating the proliferation of purified CD226$^-$ and CD226$^+$ CD8$^+$ Tn, Tcm and Tems activated by α-CD2/CD3/CD28 microbeads for 6 days. n=7-14 HD. **(E)** Representative FACS plots showing the proliferation of purified CD8$^+$ T cells activated by allogeneic DCs or CMVpp65 peptides for 6 days. n = 3 HD. **(F)** Graph showing the concentrations of the indicated cytokines in the culture supernatants of purified CD226$^-$ and CD226$^+$ CD8$^+$ Tems stimulated with α-CD2/CD3/CD28 microbeads for 48 hrs. From n=5 HD. **(G)** Representative FACS plots showing the expression of CD107a degranulation marker and the intracellular production of IFN-γ and TNF-α by CD226$^-$ and CD226$^+$ CD8$^+$ T cells activated by FcγR$^+$ P815 cell line coated with α-CD3 mAbs (OKT3, 1μg/ml). n=5 HD. **(H)** Representative graph showing calcium influx by CD226$^-$ and CD226$^+$ CD8$^+$ T cells activated with α-CD3 (OKT3, 10μg/ml). Representative from n=4 HD. **(I)** Graph showing the expression of phosphorylated (p) SLP76 by CD226$^-$ or CD226$^+$ CD8$^+$ Tems stimulated with α-CD3 (OKT3, 10μg/ml) for 0, 1 or 5 minutes. n=5 HD. **(J-K)** Purified CD226$^-$ or CD226$^+$ CD8$^+$ Tems were stimulated with α-CD3 (OKT3, 10 μg/ml) for 0, 1 or 5 minutes. Western blots using antibodies directed against the indicated total and phosphorylated (p) proteins are shown. Representative experiment from n=3 HD. Data are presented as mean ± SEM with each symbol representing an individual HD. Statistical differences between multiple groups were determined by one-way ANOVA with Tukey's correction **(C)**. Statistical differences between two groups were determined using Mann-Whitney test **(D)**, unpaired **(F)** or paired T test **(I)**. * $p<0.05$, ** $p<0.01$, *** $p<0.001$.

Figure 2: The absence of CD226 alters TCR-induced effector program of CD8$^+$ T cells.

(A-F) A global transcriptomic analysis of HD resting CD226$^-$ and CD226$^+$ CD8$^+$ Tems (n=6/group) or activated (ACT; n=4/group) by α-CD2/CD3/CD28 for 24 hrs was performed by RNA

sequencing. **(A)** PCA analysis showing different expression gene profiles between $CD226^-$ and $CD226^+$ $CD8^+$ Tem samples activated or not**. (B)** Venn diagram showing the number of genes differentially expressed between the indicated groups of $CD8^+$ Tems ($p<0.01$, FC> 2). **(C)** Volcano plots showing differentially expressed genes between $CD226^-$ and $CD226^+$ $CD8^+$ Tem samples, activated (ACT) or not. **(D)** Log-normalized gene-expression heatmap showing the hierarchical clustering of $CD226^-$ and $CD226^+$ $CD8^+$ Tem samples according to differentially expressed genes between ACT $CD226^-$ and ACT $CD226^+$ $CD8^+$ Tems. **(E)** Graph showing gene set enrichment of ACT $CD226^+$ vs ACT $CD226^-$ $CD8^+$ Tem specific genes analyzed in C7 immune data sets. **(F)** Table showing GO term analysis performed on ACT $CD226^+$ vs ACT $CD226^-$ $CD8^+$ Tem differentially expressed genes. The associated NES and Adjusted *p* value was indicated. NES and FDR were plotted for each comparison.

Figure 3: Mechanisms underlying $CD226^-$ $CD8^+$ T cell dysfunction.

(A-B) $CD226^-$ and $CD226^+$ $CD8^+$ Tems were stimulated with IL-7 (2ng/ml) for 24hrs and transduced with GFP control or CD226-GFP lentiviral vectors (LVs) for 48hrs. **(A)** FACS histograms and graphs showing the expression of CD226, CD107a, IFN-γ and TNF-α in transduced cells (GFP^+) and untransduced cells (GFP^-) after stimulation with α-CD2/CD3/CD28 microbeads. From n=4. **(B)** Representative FACS histograms and graphs showing the expression of CD226 and the proliferation of transduced (GFP^+) and untransduced (GFP^-) $CD226^+$ and $CD226^-$ cells upon stimulation with α-CD2/CD3/CD28 microbeads. From n=4. **(C)** Representative FACS plots and graph recapitulating the percentages of $CD226^-$ and $CD226^+$ $CD8^+$ Tems stained with m24 mAbs against LFA-1 "extended open" high affinity conformation after 2hrs in presence of α-CD2/CD3/CD28 microbeads or not (NS). From n=5 HD. **(D)** Representative confocal microscopy images showing the expression of CD226 and open LFA-1 (m24) by $CD226^-$ and $CD226^+$ $CD8^+$ Tems after 2hrs on α-CD3 (OKT3, 10μg/ml) coated wells. **(E)** Graphs showing the mean fluorescence intensity of the indicated markers by $CD226^-$ and $CD226^+$ $CD8^+$ Tems quantified on 15 representative field from 3 different experiments as in **(D)**. **(F)** $CD226^-$ and $CD226^+$ $CD8^+$ Tems were transduced with GFP control or CD226-GFP LVs for 48hrs as in **(A)**. Representative FACS plot and graphs recapitulating the percentages of transduced $CD226^-$ and $CD226^+$ $CD8^+$ T cells (GFP^+) expressing CD226 and m24 LFA-1 high affinity open conformation upon stimulation with α-CD2/CD3/CD28 microbeads for 2hrs. From n = 5-7 HD. **(G)** Graph recapitulating the intracellular production of IFN-γ and TNF-α by

$CD226^-$ and $CD226^+$ $CD8^+$ Tems cells activated by α-CD3 (OKT3, 10μg/ml) for 6hrs in the presence of control Ig (cIg) or blocking anti-LFA-1 mAbs (α-LFA-1). n=8 HD. Statistical differences between multiple groups were determined by one-way ANOVA with Tukey's post-test analysis. Statistical differences between two groups were determined using Mann Whitney test. * $p<0.05$, ** $p<0.01$, *** $p<0.001$.

Figure 4: CD226 absence identifies dysfunctional $CD8^+$ tumor infiltrating lymphocytes.

(A) Representative FACS histogram and graph showing the percentage of $CD226^-$ $CD8^+$ T cells isolated from the bone marrow (BM) of newly diagnosed multiple myeloma patients (MM; n=177) and healthy donors (HD; n = 20). **(B)** Representative FACS histogram and graph showing the percentage of $CD226^-$ $CD8^+$ T cells by paired BM (TIL) or blood (PBMC) $CD8^+$ T cells isolated from MM patients (n = 10). **(C)** MM patient $CD138^-$ BM cells were stained with CTV and stimulated with α-CD2/CD3/CD28 microbeads for 5 days. Representative histogram and graph recapitulating the proliferation of $CD226^-$ and $CD226^+$ $CD8^+$ TILs. n=20 MM patients. **(D)** Representative FACS plots and graphs recapitulating the expression of CD107a degranulation marker and the intracellular production of IFN-γ and TNF-α by MM patients' $CD226^-$ and $CD226^+$ $CD8^+$ TILs stimulated with α-CD2/CD3/CD28 microbeads for 6 hours. n = 36 MM patients. **(E)** Representative FACS plot and graph showing $CD226^-$ frequency by polyclonal and NY-ESO-1 specific $CD8^+$ TILs among HLA-A*02^+ MM patients with detectable HLA-A*02-NY-ESO-1-PE multimers staining. **(F)** MM patient $CD138^-$ BM cells were stimulated with HLA-A*02-NY-ESO-1 specific peptide (1μg/ml) for 6hrs. Representative FACS plots as well as pooled data from n=5 HLA-$A2^+$ MM patients with positive NY-ESO response are shown. **(G)** Representative histograms and graphs comparing the percentage of $CD8^+$ T cells lacking CD226 expression in the blood, healthy distant tissue and tumor biopsies of patients newly diagnosed with lung cancer (n=3), breast cancer (n = 10) or ovarian cancer (n=7). **(I)** CD226 expression correlates with breast cancer prognosis. Graph showing Kaplan–Meier disease-free (left) and overall (right) survival estimates for CD226high (>median value, n=503) and CD226low (<median value, n=503) Breast Cancer patients. RNA sequencing data involving 1006 invasive breast Cancer (BRCA) patients from the TCGA database. Data are presented as mean ± SEM with each symbol representing an individual cancer patient. Statistical analyses between two groups were performed using a Mann Whitney U test (**A, C, D**) or paired T test (**B, E, F**). Statistical differences between multiple groups were determined by one-way ANOVA with Tukey's post-

test analysis. Differences in survival were evaluated with the Mantel-Cox test. *p<0.05, **p<0.01, ***p<0.001.

Figure 5: Tumor development promotes dysfunctional CD226$^-$ CD8$^+$ T cell accumulation.

(A-G) C57BL/6 WT mice were left untreated or injected with B16F10 melanoma (s.c 5 x 10^5 cells) or VK12653 myeloma cell line (2 x 10^6 cells, i.v). **(A)** Representative FACS histograms showing CD226 expression by CD8$^+$ Tem (CD44^{hi}CD62L$^-$), Tcm (CD44^{hi}CD62L$^+$) and Tn (CD44^{low}CD62L$^+$) cells isolated from the spleen of non-tumor bearing mice or the indicated tumor lesions. Pooled data from at least 4 independent experiments. **(B)** Graph showing the percentages of CD226$^-$ cells among Tn, Tcm and Tem CD8$^+$ TILs isolated from B16F10 tumors 19 days post injection. Pooled data from at least 4 independent experiments. **(C)** Graph showing the percentage of CD226$^-$ CD8$^+$ Tems isolated from the spleen of WT C57BL/6 mice (Naïve spl) or from tumor, draining lymph nodes (DLN), non-DLN (NDLN) and spleen of B16F10 tumor-bearing mice at day 19 post-tumor inoculation. **(D)** Graphs showing the percentage of CD226$^-$ CD8$^+$ TILs 13 and 19 days after B16F10 injection and tumor volumes in mice with a low or high percentage of CD226$^-$ CD8$^+$ TILs. n = 16-30 mice/group. **(E)** Graphs showing the percentage of CD226$^-$ CD8$^+$ Tems in the BM of mice 0, 14, 21 and 35 days after VK12653 MM cell injection and MM cell percentage in mice with a low or high percentage of CD226$^-$ CD8$^+$ TILs. n = 18-33 mice per group. **(F)** Graph recapitulating the percentages of tumor infiltrating CD226$^-$ and CD226$^+$ CD8$^+$ Tems expressing Ki67 proliferation marker 19 days after B16F10 injection. **(G)** Graphs showing the intracellular production of IFN-γ and TNF-α by CD226$^+$ and CD226$^-$ CD8$^+$ TILs isolated from B16F10 bearing mice upon re-stimulation with α-CD3/CD28 for 6hrs. Pooled data from 3 independent experiments n=12. **(H-J)** 10^7 ova-specific OT-1 splenocytes were injected i.v into WT mice that were subsequently injected s.c with B16F10 or B16F10-ova tumors. **(H)** Schematic representation of the experimental design. (**I**) Representative histograms and graph showing CD226 expression by OT-1 CD8$^+$ Tems isolated from the spleen or tumors. (**J**) Representative FACS plots and graph showing CD226 expression by Vα2$^+$Vβ5$^+$ OT-1$^+$ or Vα2$^-$Vβ5$^-$ endogenous polyclonal TILs isolated from B16F10-ova tumors. Pooled data with from 2 experiments. Data are presented as mean ± SEM with each symbol representing an individual mouse. Statistical differences between multiple groups were determined by one-way ANOVA with Tukey's post-test analysis and differences between two

groups were assessed using a Mann Whitney U test (**D, E**) or paired T test **(F, G, J)**. *p<0.05; **p<0.01, ***p<0.001.

Figure 6: Tumor-induced CD226 loss limits immune checkpoint blockade efficacy.

(A) Representative density plots and graphs showing the expression of PD-1, TIGIT, CTLA-4, LAG3 by $CD226^-$ (blue) and $CD226^+$ (red) $CD8^+$ TILs isolated from B16F10 bearing mice after 19 days. **(B)** Representative histograms and graphs showing PD-1 and Tim-3 expression by $CD226^-$ and $CD226^+$ OT-1 $CD8^+$ Tems isolated from the spleen or B16F10-ova tumors as in **Figure 5 H**. **(C)** Graphs comparing the expression of the indicated immune checkpoints on $CD226^-$ and $CD226^+$ $CD8^+$ TILs isolated from ovarian cancer samples (n = 8 patients). **(D-I)** Groups of C57BL/6 wild type (WT) and *Cd226*$^{-/-}$ mice were injected s.c. with B16K1 melanoma cells. Mice were treated on days 6, 9, 12 with cIg (250µg i.p.) or anti-PD-1 (250µg i.p., RMP1-14). Some Groups of WT mice received cIg, anti-CD8β, anti-ASGM1 and/or anti-CD226 (250µg i.p) on days 5, 12, 17 and 24. Tumor diameter was measured every 2-4 days. **(D)** Schematic representation of the experimental design. **(E)** Graph comparing the tumor growth of mice treated or not with anti-PD1 depleted or not of CD8 or NK cells. Data representative of 2 independent experiments with n=5. **(F)** Representative FACS plots and graphs showing the percentages of $Ki67^+$ proliferating $CD226^-$ and $CD226^+$ $CD8^+$ TILs isolated from Ig control (cIg) or anti-PD-1 treated B16K1 bearing mice. Pooled data from 3 independent experiments with n=10-12. **(G)** FACS plots and graph showing the intracellular production of IFN-γ by $CD226^-$ and $CD226^+$ $CD8^+$ TILs isolated from cIg or anti-PD-1 treated B16K1 bearing mice upon in vitro re-stimulation with α-CD3/CD28 mAbs for 6hrs. Pooled data from 3 independent experiments with n=10-12. **(H)** Graph comparing the tumor growth of WT or *Cd226*$^{-/-}$ mice treated or not with anti-PD1. n=8-10 mice/group. **(I)** Graph comparing the tumor growth of cIg or anti-PD-1 treated WT mice injected with cIg, CD226 blocking and/or CD8 depleting antibodies. n=5 mice/group. Data are presented as mean ± SEM with each symbol representing an individual mouse. Statistical differences between two groups were assessed using paired T test and differences between multiple groups were determined by one-way ANOVA with Tukey's post-test analysis. Differences in survival were evaluated with the Mantel-Cox test. *p<0.05; **p<0.01, ***p<0.001.

Figure 7: CD226 loss depends on Eomes expression.

(A) Graph showing normalized Eomes mRNA transcripts of $CD226^-$ and $CD226^+$ $CD8^+$ Tem activated with α-CD2/CD3/CD28 microbeads or not (NS) detected by RNA sequencing depicted in **Figure 2**. **(B)** Representative FACS plots and graphs showing Eomes expression by $CD226^-$ and $CD226^+$ $CD8^+$ T cells from the blood of HD (n = 15) and from the BM of newly diagnosed MM patients (n = 22). **(C-E)** $CD4^{cre}$x $Eomes^{fl/fl}$ ($Eomes^{KO}$) and $CD4^{WT}$x $Eomes^{fl/fl}$ ($Eomes^{WT}$) mice were injected with B16F10 tumor cells. Representative FACS plots **(C)** and graphs **(D)** recapitulating the expression of Eomes among $CD226^+$ and $CD226^-$ tumor infiltrating $CD8^+$ Tems. **(E)** Graph showing the percentages of $CD226^-$ cells among $CD8^+$ TILs isolated from $Eomes^{KO}$ and $Eomes^{WT}$ mice. Data are from 2 pooled experiments with n = 8-10 mice/group. **(F-G)** Representative density plots **(F)** and graphs **(G)** showing CD226 and Eomes expression by $CD8^+$ T cells isolated from the spleen of C57BL/6 wild type (WT) and *CD2-Eomes^{Tg}* mice. From 2 independent experiments with n=3 mice/group. Data are presented as mean ± SEM with each symbol representing an individual mouse. Statistical differences between multiple group were determined by one-way ANOVA with Tukey's post-test analysis and differences between two groups were assessed using paired t test **(B)** or Mann-Whitney **(D, E G).** *p<0.05; **p<0.01, ***p<0.001.

Figure 8: CD226 loss restrains $CD8^+$ T cells antitumor functions.

(A-B) C57BL/6 WT mice were treated with anti-CD137 mAbs (100µg; 3H3, i.p) for the indicated period. **(A-B)** Schematic representation of the experimental design, representative histograms **(A)** and graphs **(B)** showing Eomes and CD226 expression by spleen $CD8^+$ T cells during anti-CD137 treatment. **(C)** Graph comparing the expression of Eomes by the indicated $CD8^+$ T cells isolated from cIg- or anti-CD137-treated mice. n=10 mice/group from 2 pooled experiments. **(D)** FACS plots and graph showing the percentage of $CD226^-CD8^+$ Tems isolated from the blood of $CD4^{cre}$x $Eomes^{fl/fl}$ ($Eomes^{KO}$), $CD4^{WT}$x $Eomes^{fl/fl}$ ($Eomes^{het}$) and $CD4^{WT}$x $Eomes^{fl/fl}$ ($Eomes^{WT}$) mice treated with anti-CD137 mAbs. n = 8-10 mice/group from 2 pooled experiments. **(E)** Graph showing the percentages of $CD226^-CD8^+$ T cells in the spleen of *Cd155$^{-/-}$* and WT mice treated with anti-CD137 mAbs (red) or IgG control (black). **(F-G)** WT mice were treated for 2 weeks with anti-CD137 mAbs (100µg; 3H3, twice a week) and splenic $CD226^+$ and $CD226^-$ $CD8^+$ Tems were sorted by flow cytometry and re-stimulated with α–CD3/CD28 mAbs. **(F)** Representative histogram showing the proliferation of CTV-labeled $CD226^+$ and $CD226^-$ $CD8^+$ Tems after 4 days. **(G)** Graphs showing IFN-γ and TNF-α levels in the supernatant of the

corresponding cultures after 24 Hrs of stimulation. Data are pooled from 5 independent experiments. **(H)** OT-I mice were treated with anti-CD137 mAbs for 2 weeks and splenic $CD8^+$ Tems were purified and activated *in vitro* with α–CD3/CD28 mAbs or ova-peptide for 6hrs. Graphs showing the expression of CD107a and TNF-α by $CD226^+$ and $CD226^-$ $CD8^+$ OT-1 cells. n=7 mice/group from 2 independent experiments. **(I-K)** TCR transgenic *Pmel* mice were stimulated with anti-CD137 mAbs and sorted into $CD226^+$ and $CD226^-$ $CD8^+$ Tems. B16F10 tumor (10-20mm^2) bearing mice were left untreated (control) or injected with the indicated *Pme*l sorted T-cells. Mice pre-conditioned by cyclophosphamide injection were stimulated with a recombinant adenoviral vector vaccine expressing hgp100 and three intratumor injections of TLR ligands CpG and poly(I:C). **(I)** Schematic overview of ACT model, where C= cyclophosphamide, V= Adenovirus encoding hgp100 (=*Pmel*) and TLR= intra-/peri-tumoral injection of CPG and poly(I:C). **(J-K)** Graph showing tumor area **(J)** and Kaplan-Meier survival curves **(K)** of B16F10 bearing mice. Data depicted are representative of two experiments. Data are presented as mean ± SEM with each symbol representing an individual mouse. Statistical differences between multiple group were determined by one-way ANOVA with Tukey's post-test analysis (**B-E, H, J**) and differences between two groups were assessed using Mann-Whitney **(G).** Differences in survival were evaluated with Mantel-Cox log rank **(K)**. *$p<0.05$; **$p<0.01$, ***$p<0.001$.

STAR METHODS

Contact for Reagent and Resource Sharing

Further information and requests for resources and reagents should be directed to and will be fulfilled by the Lead Contact, Ludovic Martinet (ludovic.martinet@inserm.fr)

Human samples

Healthy donors. PBMC obtained from the Etablissement Français du Sang (EFS, Toulouse) were isolated by Ficoll-Hypaque (GE Healthcare) density centrifugation. Unprocessed human bone marrow (BM) aspirates from healthy donors were purchased from Lonza (Switzerland).

Cancer patient's samples. Fresh BM aspirates and peripheral blood from patients with myeloma were collected at the time of diagnosis or relapse in the Institut Universitaire du Cancer de Toulouse-Oncopole (IUCT-O, Toulouse) through the intergroupe francophone du myélome network. BM samples were depleted of malignant plasma cells using anti–CD138-coated magnetic beads (Miltenyi Biotec, France). Samples from newly diagnosed NSCLC, breast or ovarian cancer patients were obtained from surgical resections performed in the IUCT-O (Toulouse, France). Tumor specimens were processed by mechanical dissection and single-cell suspensions were freshly analyzed or cryopreserved. All cancer patients gave written informed consent and collection was approved by French Committee for the Protection of Persons (CPP; DC-2012-1654) as well as by local IUCT-Oncopole review boards.

Flow cytometry

Single cell suspensions were stained according to standard protocols with previously described anti-mouse and human antibodies listed in the STAR*Methods section. Antibodies were purchased from miltenyi biotec, eBioScience, BioLegend, or BD Biosciences. Surface staining was performed with mAbs for 30 min at 4°C in PBS supplemented with 2% FCS and 2 mM EDTA. MM patient $CD8^+$ T cells were stained with PE-labeled HLA-A2/NY–ESO-$1_{157–165}$ (SLLMWITQA) multimers as described previously (Guillerey et al., 2018). For the intracellular staining, cells were fixed and permeabilized using BD Cytofix/Cytoperm permeabilization kit (BD Biosciences) or Transcription Factor Fixation/Permeabilization kit (Thermofisher). Data were collected with LSR II or Fortessa X20 flow cytometers (BD Biosciences) and analyzed with FlowJo software (TreeStar). Dead cells and doublets were excluded by LiveDead staining (Thermofisher).

CD8$^+$ T cell isolation

Primary human tumor biopsies were manually dissociated and digested enzymatically with Tumor Dissociation Kit (Miltenyi Biotec) and then incubated at 37°C for half an hour. After incubation, digested tumors were mashed through 70µm filters and tumor infiltrating lymphocytes were enriched by using CD8 or CD45 microbeads (Miltenyi Biotec). CD8$^+$ T cells were enriched with the appropriate negative selection kits (Miltenyi biotec) from Human PBMCs, MM patient's BM samples, Ovarian and lung cancer biopsies, mouse spleen or tumors and were stained in PBS with 0.5% SVF and 2 mM EDTA containing fluorochrome-conjugated antibodies listed in the listed in STAR*Methods section. The indicated CD8$^+$ T cell subsets were then highly purified based on CD226, CD45RA and CD62L expression (human) or CD226, CD44 and CD62L expression (mouse) using Aria Fusion (BD biosciences) or MoFLo Astrios (Beckman Coulter) cell sorters.

Human T cell functional assays

The indicated CD8$^+$ T cell subsets purified from HD or cancer patients were stimulated with plate bound α-CD3 mAbs (clone OKT3 or UCHT1, Bioxcell), anti-CD2/CD3/CD28 microbeads (T cell expansion kit, Miltenyi Biotec), CytoStim (Miltenyi Biotec), monocyte-derived allogeneic mature dendritic cells, CMVpp65 peptide pools (PepTivator® Miltenyi Biotec) or NY-ESO-1157-165 analog (SLLMWITQA, Peptide 2.0 Inc, 1 µg/ml) in RPMI 1640 medium (ThermoFisher Scientific) supplemented with 10% fetal bovine serum (ThermoFisher Scientific) and L-glutamine (SIGMA Aldrich). Intracellular cytokine staining was performed after 6 hrs in the presence of APC-conjugated α-CD107a (H4A3, BD bioscience) and Golgiplug (BD biosciences). Alternatively, cells were stained with Cell Trace Violet (CTV, Thermo Fisher Scientific) prior to stimulation followed by CTV dilution assessment 5 days later. Cytokine levels were measured in the cell culture supernatants by CBA (BD Biosciences) after 48 hrs. Cytotoxic capacities of CD8$^+$ T cells were assessed in co-cultures with P815 mastocytoma cell line coated with the indicated concentrations of anti-CD3 mAbs at a 2:1 effector: target ratio. Where indicated, mAb against TIGIT (Clone MBSA43, Thermo Fisher scientific), CD96 (Clone NK92.39, Biolegend), CD226 (clone DX11, Abcam), CD112 (clone TX31, Biolegend), CD155 (clone SKII.4, Biolegend) or LFA-1 (Clone TS1/18, BioXcell) or irrelevant IgG1 (clone MG1-45, Biolegend) were added to cultures at a final concentration of 10µg/ml. For the detection of the high-

affinity form of LFA-1, $CD8^+$ T cells were activated for 2 hrs. Previously described m24 mAb (Petit et al., 2016) directed against the extended/open high affinity conformation of LFA-1 (2 μg/ml; clone 24, Biolegend) were added into the culture for the last 30 minutes of the assay.

Monocyte-derived mature dendritic cell

Monocytes were isolated from PBMCs with $CD14^+$ immunomagnetic beads (Miltenyi Biotech) as described by the manufacturer recommendations. Isolated $CD14^+$ cells were cultured in complete RPMI 1640 medium with GM-CSF (100 ng/mL) and IL-4 (50 ng/mL) for 5 days. Mature dendritic cells were obtained by adding TNF-α (50 ng/ml), IL-1β (50 ng/ml) and IL-6 (50 ng/ml) for two additional days and used in functional assays after phenotypic analysis.

Lentiviral vector production

Human tagged CD226 cDNA (NM_006566, Origene) was cloned into PCDH-EF1-copGFP-T2A-Puro vectors kindly provided by Kazuhiro Oka (Addgene plasmid # 72263; http://n2t.net/addgene:72263 ; RRID : Addgene_72263). Lentivirus pseudotyped with a baboon retroviral envelope glycoprotein (BaEV-LVs) and measles virus glycoprotein-displaying LVs (hemagglutinin and fusion protein LVs [H/F-LVs]) that efficiently transduce IL-7 stimulated primary human T lymphocytes were used (Girard-Gagnepain et al., 2014; Levy et al., 2017). Self-inactivating HIV-1–derived vectors encoding CD226 and/or GFP, were generated by transfection of 293T cells as described in detail elsewhere (Levy et al., 2017). Eighteen hours after transfection, the medium was replaced by Opti-MEM supplemented with HEPES (Invitrogen). Viral supernatants were harvested 48 hrs after transfection and filtered. The vectors were concentrated at low speed overnight at 3000g at 4°C. Infectious titers (in transduction units [TU]/ml) were determined by fluorescence-activated cell sorting (FACS) of target cells using serial dilutions of the supernatants added to the 293T cells. Alternatively, highly concentrated CD226 and/or GFP Integrative lentiviral vectors™ that also efficiently transduce IL-7 stimulated primary human T lymphocytes were purchased (Flash Therapeutics) and used to transduce $CD8^+$ T cells in proliferation and LFA-1 functional experiments.

Transductions of human $CD8^+$ T cells

10^5 FACS sorted $CD226^-$ and $CD226^+$ $CD8^+$ Tems were cultured in RPMI complete medium supplemented with IL-7 (1-2 ng/ml) for 24 hr and transduced with either control-GFP or CD226-GFP lentivirus on retronectin-coated 96-well plate at a MOI of 2-10. After 48 hrs, cells were analyzed for GFP expression and tested in functional assays.

TCR signaling analysis

Sorted $CD226^-$ and $CD226^+$ $CD8^+$ Tem cells were stimulated with α-CD3 mAbs (10μg/ml; UCHT-1- Thermo fisher) followed by goat anti-mouse Fab'2 secondary antibody (20μg/mL; Jackson ImmunoResearch) cross-linking or with plate bound α-CD3 (OKT3, eBioscienes, 10μg/ml) for indicated time. Cells were then homogenized in RIPA lysis buffer (Sigma-Aldrich) supplemented with complete protease inhibitor tablet (Roche). Cell extracts were separated by SDS-PAGE and transferred onto PVDF membranes (Bio-Rad). Immunoblots were performed with phospho-specific antibodies (Cell Signaling Technology) to PLC γ1 (Tyr783), ZAP-70 (Tyr319), LAT (Tyr191), ERK1/2 (Thr202 and Tyr204) and AKT (Ser473) followed by appropriate HRP-conjugated secondary antibodies (Cell Signalling technology). The proteins were visualized by ECL-Plus (GE Healthcare) using Pxi (Syngene) or ImageQuant LAS 500 (GE Healthcare Life Sciences) imaging systems. For phospho-specific flow cytometry, purified $CD8^+$ T cells were incubated with biotin-conjugated α-CD3 (10μg/ml; OKT3) for 15 min on ice, washed with ice-cold PBS and incubated with cross-linking anti-biotin secondary antibody on ice for additional 15 minutes. Cells were then stimulated at 37°C for the indicated times. Cells were fixed with pre-warmed Cytofix/Cytoperm solution (BD Biosciences) for 10 min and permeabilized with Perm III solution (BD Biosciences) for 30 min on ice. Cells were washed in FACS buffer solution and stained with anti-SLP76 (Y128) and anti-CD247 (Y142) for 1 hr and phosphoproteins were detected by flow cytometry. Investigation of intracellular calcium flux in $CD8^+$ T cells was performed according to previous protocols (Lee et al., 2012) using Calcium Assay kit (BD Biosciences). Briefly calcium dye-loaded $CD8^+$ T cells were coated with α-CD3 mAbs (10μg/ml; OKT3) for 15 min on ice, washed with ice-cold PBS and activated with goat anti-mouse Fab'2 secondary antibody at 37°C (13 μg/ml) before flow cytometry analysis of calcium influx.

Confocal microscopy.

8-well µ-slides (Ibidi) were coated overnight with poly-L-lysine (Sigma-aldrich) and α-CD3 (clone OKT3, 10 µg/ml). $4x10^4$ $CD226^-$ or $CD226^+$ $CD8^+$ Tems freshly purified by FACS using AF488 conjugated anti-CD226 antibodies (Clone 11A8) were plated in complete medium for 2h at 37°C. LFA-1 open extended conformation m24 antibody labelled with Alexa Fluor™ 647 Antibody Labeling Kit (thermofisher) was added for the last 30 min of the assay. After 3 washes (PBS, BSA 3%, HEPES 1%) cells were fixed in PBS containing 3% PFA for 3 min à 37°C. Nuclear counterstaining was performed with DAPI (1/3000) for 5 minutes à 37°C. Slides were mounted using Fluoromount™ medium (Thermofisher) and analysed under Fast Airyscan LSM880 Confocal microscope (Zeiss) with 60x oil objective. The cell intensity of each fluorochrome was quantified on 15 representative fields by condition using ImageJ software.

Library construction for RNA sequencing.

Total RNA was extracted from freshly FACS purified $CD226^-$ or $CD226^+$ $CD8^+$ Tems or activated for 24 hr with anti-CD2/CD3/CD28 microbeads (T cell expansion kit, Miltenyi Biotec) using RNeasy micro kit (Qiagen) according to the manufacturer's instruction. The quality of the isolated total RNA from each sample was checked on 2200 Tapestation System (Agilent, Santa Clara, USA) using the RNA ScreenTape assay and the quantitation was performed using the NanoVue Plus Spectrophotometer (Biochrom Ltd, Cambridge, UK). 100-300 ng of total RNA per sample with a RNA integrity number >8 were used for library preparation. The RNA-Seq library preparation was performed using TruSeq Stranded mRNA Sample Preparation kit (Illumina, San Diego, Calif) according to the manufacturer's instructions (High Sample Protocol). The RNA-Seq libraries were checked on the 2200 Tapestation System (Agilent) using the High-Sensitivity DNA 1000 ScreenTape assay. Libraries were quantified by qPCR on a LightCycler 480 System (Roche Molecular Diagnostics, Pleasanton, Calif) using KAPA Library Quantification Kit for Illumina platforms (Kapa Biosystems, Boston, Massachusetts). Libraries were then pooled in equal quantities, checked and quantified using same techniques (2200 Tapestation and LightCycler 480). Paired-end sequencing (2 x 150 bps) of these libraries was performed on a NextSeq 500 Illumina sequencing platform (Illumina) by 2 successive runs using NextSeq 500 High Output kit v2 (Illumina) generating in average 20 million pairs of reads per sample. RNA-Sequencing data from the CD138- fractions of 73 newly diagnosed MM patient BM aspirates have already been described (GSE63473; (Nakamura et al., 2018)).

RNA-seq bioinformatic analysis

Fastq files were aligned to the Ensembl GRCh38 human reference genome using STAR (version 2.4.2 (Dobin et al., 2013) and gene expression summary was obtained using the Subread featurecount algorithm (version 1.4.6) (Liao et al., 2014). Read counts were normalized using the DESeq function (Love et al., 2014) retaining only genes expressed (more than 10 aligned reads) in at least 50% of samples. *Principal component analysis* (PCA) was created from normalized reads as described previously (Varet et al., 2016). The R packages Sartools (https://github.com/PF2-pasteur-fr/SARTools) using DESeq2 (Love et al., 2014) was used to perform differential gene expression analysis (Love et al., 2015). Genes differentially expressed with p value <0.01 and FC>2 with Benjamini-Hochberg (BH) multiple testing correction at 1% false-discovery rate (FDR) were considered. To perform the gene set enrichment analysis, R fGSEA package was used to derive the absolute enrichment scores using C7 immunologic signatures (The signatures were generated by manual curation of published studies in human and mouse immunology) of the Molecular Signature Database version 6.0 (Subramanian et al., 2005).

TCGA transcriptomic analysis

Gene expression data (RNA-seq) of TGCA breast cancer cohort (BRCA) was accessed through the cBioportal for Cancer Genomics (http://www.cbioportal.org) using the R-based package CGDS-R and following the TCGA guidelines for the use of TCGA data (https://cancergenome.nih.gov/). For Kaplan-Meier plots, optimal cutoffs were determined with the survival R package and the Log-Rank p values were corrected using the Benjamini-Hochberg method.

Mouse Models

Mouse strains were maintained either in the SPF animal facility of the US006 CREFRE-Inserm/UPS which is accredited by the French Ministry of Agriculture (accreditation number A-31 55508) or in the SPF animal facility of the QIMR Berghofer Medical Research Institute. Tumor experiments used both male and female mice between 6 and 12 weeks of age. Donors and recipients of adoptive T cell transfers were sex matched. Animal experiments were

conducted and approved by the QIMR Berghofer Medical Research Institute Animal Ethics Committee and the Ministère de l'enseignement supérieur, de la recherche et de l'innovation (APAFIS#5614-20 16060815487810 v4) and are in compliance with the French and Australian regulations on care and protection of laboratory animals. For survival analysis, mice were monitored daily according to institutional ethic guidelines, and were euthanized when mice developed signs of reduced mobility including paralysis, hunched posture, or respiratory distress. All mice used in this study were on a C57BL/6 genetic background. WT mice were purchased from Janvier laboratories or from the Walter and Eliza Hall institute for Medical Research. *OT1* (Hogquist et al., 1994), *Pmel-1* (Overwijk et al., 2003), *Cd226*$^{-/-}$ (Gilfillan et al., 2008), *Rag2*$^{-/-}$*Il2rg*$^{-/-}$ (von Scheidt et al., 2014) and *Cd8*$^{-/-}$ (Fung-Leung et al., 1991) have already been described. *Cd155*$^{-/-}$ mice (Kamran et al., 2013) were kindly provided by the Dr Yoshimi Takai (Kobe University, Kobe, Japan). *Eomes*$^{fl/fl}$ *x Cd4*^{CRE} mice (Zhu et al., 2010) were kindly provided by Anne Dejean (CPTP institute, Toulouse, France). Mice overexpressing Eomes under the hCD2 promoter (Istaces et al., 2019) were kindly provided by Stanislas Goriely (IMI, Gosselies, Belgium).

Cell lines, cell culture, plasmids and transduction

Well described MC38 colon cancer cell line, B16F10 melanoma cell line and variants expressing constitutively OVA protein (B16F10-OVA) or stably expressing the MHC-I molecule H-2Kb (B16K1) (Porgador et al., 1989) were used in this study. Cells were cultured in DMEM medium containing 10% heat-inactivated fetal calf serum (FCS). Cells were tested negatively for mycoplasma contamination and maintained in culture for a limited number of passages. Transplantable Vk∗MYC MM cell line (Vk12653) were kindly provided by Bergsagel. L (Mayo clinic, USA). Transplantable MM cell line Vk12653 were generated and expanded as previously described (Chesi et al., 2008; Guillerey et al., 2015). Briefly, these cells were maintained in *Rag2*$^{-/-}$*Il2rg*$^{-/-}$ mice to avoid contamination with host-derived lymphocytes as described previously (Guillerey et al., 2015).

Mouse tumor implantation, tumor digestion and tumor volume measurements

The left flank of mice was shaved and B16F10 (5 x 10^5), B16-OVA cells (5 x 10^5), B16K1 cells (10^6), MC38 (2 x 10^6) were injected subcutaneously (s.c.) in 100 µl of PBS. Tumor volume were estimated by measuring the tumor size in two dimensions using a caliper. The tumor volume

was calculated according the formula (length x width^2 / 2). Tumors were measured three times per week. Mice were sacrificed at the indicated time points or when the estimated tumor volume reached 2 cm^3. TILs were analyzed as previously described. Briefly, solid tumors were excised, manually dissociated and enzymatically digested with Tumor Dissociation Kit (Miltenyi Biotec) and then incubated at 37°C for 30 minutes. After incubation, digested tumors were mashed through 70µm filters and immune cells were enriched using CD45 microbeads (Miltenyi Biotec) before TILs analysis. Vk12653 MM cells (2×10^6) were injected i.v. into tail vein of indicated strains of mice. The percentage of monoclonal Ig in the serum was quantified by serum protein electrophoresis (Sebia Hydrasys system). The phenotype, percentage and number of BM B220$^-$CD138$^+$CD155$^+$PCs and CD8$^+$ TILs were analyzed by flow cytometry at the indicated time points as described previously (Guillerey et al., 2015).

Mouse T-cell functional assays

For cytokine production assays, total splenocytes, TILs or freshly isolated CD8$^+$ T cells were stimulated with plate-bound α-CD3 (3µg/ml; 145-2C11, BioLegend) and α-CD28 (1 µg/ml; 37.51, BioLegend), ova-peptide (Sigma, 10 µg/mL) or with Phorbol myristate acetate (PMA; 50ng/ml, Sigma) and ionomycin (1µg/ml, Sigma) in the presence of Golgi Plug (BD biosciences) and/or Golgi Stop (BD Biosciences) for 5 hrs. Intracellular cytokine staining was performed as described above. For T cell proliferation assay, freshly sorted CD8$^+$ T cells were loaded with CTV (Thermofisher) according to manufacturer's instructions prior to stimulation. CTV dilution was analyzed after 4 days. Cytokine levels were measured in the corresponding cell culture supernatants by Cytometric Bead Array (CBA from BD Biosciences) after 24-48 hrs.

Immune checkpoint blockade treatment

Immune checkpoint blockade treatment (ICB treatment) was started on palpable B16K1 tumors (25-50 mm^3 volume). Briefly, groups of C57BL/6 wild type (WT) or *Cd226*$^{-/-}$ mice were injected s.c. with B16K1 melanoma cells. Mice were treated on days 6, 9, 12 (relative to tumor inoculation) with cIg (250µg i.p; Mac4, BioXCell) or anti-PD-1 (250µg i.p., RMP1-14). Some groups of WT mice received cIg (250µg i.p), anti-CD8β (250µg i.p), anti-ASGM1 (250µg i.p) and/or anti-CD226 (250µg i.p., 480.1) on days 5, 12, 17 and 24. TILs phenotypic and functional analysis was performed one week after the end of the ICB treatment. Alternatively, MC38 (1×10^5) were s.c. injected into the indicated strains of mice in a final volume of 200µl (day 0).

Mice were treated on days 10, 14, 18 and 22 (relative to tumor inoculation) with cIg (250µg i.p; Mac4, BioXCell), anti-PD-1 (250µg i.p., RMP1-14, BioXCell) or anti-CTLA4 (100µg i.p., 9D9 IgG2a, BMS). Some groups of mice received cIg (250µg i.p.) or anti-DNAM-1 (250µg i.p., 480.1) on days 9, 10, 14, 17, 20, 24 and 28. Digital callipers were used to measure the perpendicular diameters of each individual tumor every 2-4 days.

TNFR agonist treatment.

C57BL/6 *WT*, *Eomes* $^{fl/fl}$ *x Cd4*^{CRE}, *OT-1* or *Pmel-1* mice were treated by i.p. injection with anti-CD137 mAbs (100µg; 3H3,BioXcell, twice a week), anti-mouse OX40 (200µg; OX-86,BioXcell, twice a week), anti-mouse GITR (200µg; DTA-1–,BioXcell, twice a week) or with control IgG (HRPN,BioXcell). After 2-3 weeks, lymphoid organs were isolated for $CD8^+$ T cell phenotypic analysis and functional assays. For dose-response experiments, C57BL/6 mice were treated with 1, 10 or 100µg of anti-CD137 mAbs twice a week for 2 weeks.

Adoptive T cell Transfer experiments

For tumor adoptive transfer experiments, 10^7 OT-1 splenocytes were injected i.v into WT mice that were subsequently injected s.c with B16F10 or B16F10-ova tumors (5 x 10^5; s.c). After 19 days when the estimated tumor volume reached 1-2 cm^3, $CD8^+$ T cells were isolated from the spleen and tumors and analyzed for CD226 expression as described above. Alternatively, naïve $CD226^+$ $CD8^+$ T cells were isolated from the spleen of OT-1 using mouse $CD8^+$ T cell isolation kit (Miltenyi Biotec) and FACSaria™ Fusion (BD biosciences). 10^6 OT-1 cells were adoptively transferred by tail vein injection into *Rag2*$^{-/-}$*Il2rg*$^{-/-}$ mice bearing B16F10 or B16F10-OVA tumors for 6 days (5 x 10^5; s.c). One week later, $CD8^+$ T cells were isolated from the spleen and tumors and analyzed for CD226 expression as described above.

For CD137 treatment adoptive transfer experiments, either 10^6 naïve $CD226^+$ $CD8^+$ T cells or 10^7 OT-1 splenocytes were transferred by tail vein injection into WT or *Rag2*$^{-/-}$*Il2rg*$^{-/-}$ mice respectively. The blood was collected by retro-orbital puncture under isoflurane anesthesia 7 days later and $CD8^+$ T cell phenotype was analyzed by flow cytometry. Mice were then treated with 3 injections of anti-CD137 mAbs (100µg; 3H3 – BioXcell; i.p) or control IgG (HRPN – BioXcell) and lymphoid organs were collected for subsequent $CD8^+$ T cells analysis by flow cytometry.

Adoptive Cell Transfer (ACT) Therapy

ACT immunotherapy was performed as previously described (Glodde et al., 2017). Briefly, when s.c. transplanted B16F10 melanomas reached a size of > 5mm in diameter mice were preconditioned by a single i.p. injection of 2mg (~100mg/kg) cyclophosphamide in 100 µl PBS followed by intravenous delivery of 1 x 10^6 hgp100-specific $CD226^+$ or $CD226^-$ $CD8^+$ *Pmel*-1 T cells (in 200µl PBS) the next day. $CD226^+$ or $CD226^-$ *Pmel*-1 T-cells were isolated by FACS from spleens from anti-CD137 mAbs treated mice as described above. 50µg of CpG 1826 (MWG Biotech) and 50µg of polyinosinic:polycytidylic acid (poly(I:C), Invivogen) in 100 µl PBS were injected peritumorally 3, 6, and 9 days after adoptive *Pmel*-1 T cell transfer and tumor growth and survival monitored.

Statistical Analysis

Statistical analyses were performed using GraphPad Prism 7 Software. Mann-Whitney U test or paired and unpaired student t test were used for single comparisons between two groups. For comparison of three or more groups, one-way ANOVA with Tukey's multiple comparison test, Holm-Sidak multiple test correction, or non-parametric Kruskal-Wallis test with Dunn's multiple comparison post-test were used. Differences in survival were evaluated with the Mantel-Cox test. $P < 0.05$ was considered statistically significant ($P<0.05$ = *; $P<0.01$ = **; $P<0.001$ = ***).

REFERENCES

Ahmadzadeh, M., Johnson, L.A., Heemskerk, B., Wunderlich, J.R., Dudley, M.E., White, D.E., and Rosenberg, S.A. (2009). Tumor antigen-specific CD8 T cells infiltrating the tumor express high levels of PD-1 and are functionally impaired. Blood *114*, 1537-1544.

Attal, M., Lauwers-Cances, V., Hulin, C., Leleu, X., Caillot, D., Escoffre, M., Arnulf, B., Macro, M., Belhadj, K., Garderet, L*., et al.* (2017). Lenalidomide, Bortezomib, and Dexamethasone with Transplantation for Myeloma. N Engl J Med *376*, 1311-1320.

Bachmann, M.F., McKall-Faienza, K., Schmits, R., Bouchard, D., Beach, J., Speiser, D.E., Mak, T.W., and Ohashi, P.S. (1997). Distinct roles for LFA-1 and CD28 during activation of naive T cells: adhesion versus costimulation. Immunity *7*, 549-557.

Barber, D.L., Wherry, E.J., Masopust, D., Zhu, B., Allison, J.P., Sharpe, A.H., Freeman, G.J., and Ahmed, R. (2006). Restoring function in exhausted CD8 T cells during chronic viral infection. Nature *439*, 682-687.

Bengsch, B., Ohtani, T., Khan, O., Setty, M., Manne, S., O'Brien, S., Gherardini, P.F., Herati, R.S., Huang, A.C., Chang, K.M*., et al.* (2018). Epigenomic-Guided Mass Cytometry Profiling Reveals Disease-Specific Features of Exhausted CD8 T Cells. Immunity *48*, 1029-1045 e1025.

Bertrand, F., Montfort, A., Marcheteau, E., Imbert, C., Gilhodes, J., Filleron, T., Rochaix, P., Andrieu-Abadie, N., Levade, T., Meyer, N*., et al.* (2017). TNFalpha blockade overcomes resistance to anti-PD-1 in experimental melanoma. Nat Commun *8*, 2256.

Bianchi, E., Denti, S., Granata, A., Bossi, G., Geginat, J., Villa, A., Rogge, L., and Pardi, R. (2000). Integrin LFA-1 interacts with the transcriptional co-activator JAB1 to modulate AP-1 activity. Nature *404*, 617-621.

Blackburn, S.D., Shin, H., Freeman, G.J., and Wherry, E.J. (2008). Selective expansion of a subset of exhausted CD8 T cells by alphaPD-L1 blockade. Proc Natl Acad Sci U S A *105*, 15016-15021.

Blackburn, S.D., Shin, H., Haining, W.N., Zou, T., Workman, C.J., Polley, A., Betts, M.R., Freeman, G.J., Vignali, D.A., and Wherry, E.J. (2009). Coregulation of CD8+ T cell exhaustion by multiple inhibitory receptors during chronic viral infection. Nat Immunol *10*, 29-37.

Blake, S.J., Dougall, W.C., Miles, J.J., Teng, M.W., and Smyth, M.J. (2016a). Molecular Pathways: Targeting CD96 and TIGIT for Cancer Immunotherapy. Clin Cancer Res *22*, 5183-5188.

Blake, S.J., Stannard, K., Liu, J., Allen, S., Yong, M.C., Mittal, D., Aguilera, A.R., Miles, J.J., Lutzky, V.P., de Andrade, L.F*., et al.* (2016b). Suppression of Metastases Using a New Lymphocyte Checkpoint Target for Cancer Immunotherapy. Cancer Discov *6*, 446-459.

Buggert, M., Tauriainen, J., Yamamoto, T., Frederiksen, J., Ivarsson, M.A., Michaelsson, J., Lund, O., Hejdeman, B., Jansson, M., Sonnerborg, A*., et al.* (2014). T-bet and Eomes are differentially linked to the exhausted phenotype of CD8+ T cells in HIV infection. PLoS Pathog *10*, e1004251.

Chan, C.J., Martinet, L., Gilfillan, S., Souza-Fonseca-Guimaraes, F., Chow, M.T., Town, L., Ritchie, D.S., Colonna, M., Andrews, D.M., and Smyth, M.J. (2014a). The receptors CD96 and CD226 oppose each other in the regulation of natural killer cell functions. Nat Immunol *15*, 431-438.

Chan, C.J., Smyth, M.J., and Martinet, L. (2014b). Molecular mechanisms of natural killer cell activation in response to cellular stress. Cell Death Differ *21*, 5-14.

Chen, L., and Flies, D.B. (2013). Molecular mechanisms of T cell co-stimulation and co-inhibition. Nat Rev Immunol *13*, 227-242.

Chesi, M., Robbiani, D.F., Sebag, M., Chng, W.J., Affer, M., Tiedemann, R., Valdez, R., Palmer, S.E., Haas, S.S., Stewart, A.K*., et al.* (2008). AID-dependent activation of a MYC transgene induces multiple myeloma in a conditional mouse model of post-germinal center malignancies. Cancer Cell *13*, 167-180.
Chester, C., Sanmamed, M.F., Wang, J., and Melero, I. (2018). Immunotherapy targeting 4-1BB: mechanistic rationale, clinical results, and future strategies. Blood *131*, 49-57.
Choi, B.K., Asai, T., Vinay, D.S., Kim, Y.H., and Kwon, B.S. (2006). 4-1BB-mediated amelioration of experimental autoimmune uveoretinitis is caused by indoleamine 2,3-dioxygenase-dependent mechanisms. Cytokine *34*, 233-242.
Comrie, W.A., Babich, A., and Burkhardt, J.K. (2015). F-actin flow drives affinity maturation and spatial organization of LFA-1 at the immunological synapse. J Cell Biol *208*, 475-491.
Curran, M.A., Geiger, T.L., Montalvo, W., Kim, M., Reiner, S.L., Al-Shamkhani, A., Sun, J.C., and Allison, J.P. (2013). Systemic 4-1BB activation induces a novel T cell phenotype driven by high expression of Eomesodermin. J Exp Med *210*, 743-755.
Danisch, S., Qiu, Q., Seth, S., Ravens, I., Dorsch, M., Shibuya, A., Shibuya, K., Forster, R., and Bernhardt, G. (2013). CD226 interaction with CD155 impacts on retention and negative selection of CD8 positive thymocytes as well as T cell differentiation to follicular helper cells in Peyer's Patches. Immunobiology *218*, 152-158.
Dobin, A., Davis, C.A., Schlesinger, F., Drenkow, J., Zaleski, C., Jha, S., Batut, P., Chaisson, M., and Gingeras, T.R. (2013). STAR: ultrafast universal RNA-seq aligner. Bioinformatics *29*, 15-21.
Dustin, M.L., and Springer, T.A. (1989). T-cell receptor cross-linking transiently stimulates adhesiveness through LFA-1. Nature *341*, 619-624.
Fung-Leung, W.P., Schilham, M.W., Rahemtulla, A., Kundig, T.M., Vollenweider, M., Potter, J., van Ewijk, W., and Mak, T.W. (1991). CD8 is needed for development of cytotoxic T cells but not helper T cells. Cell *65*, 443-449.
Gaud, G., Roncagalli, R., Chaoui, K., Bernard, I., Familiades, J., Colacios, C., Kassem, S., Monsarrat, B., Burlet-Schiltz, O., de Peredo, A.G*., et al.* (2018). The costimulatory molecule CD226 signals through VAV1 to amplify TCR signals and promote IL-17 production by CD4(+) T cells. Sci Signal *11*.
Gilfillan, S., Chan, C.J., Cella, M., Haynes, N.M., Rapaport, A.S., Boles, K.S., Andrews, D.M., Smyth, M.J., and Colonna, M. (2008). DNAM-1 promotes activation of cytotoxic lymphocytes by nonprofessional antigen-presenting cells and tumors. J Exp Med *205*, 2965-2973.
Girard-Gagnepain, A., Amirache, F., Costa, C., Levy, C., Frecha, C., Fusil, F., Negre, D., Lavillette, D., Cosset, F.L., and Verhoeyen, E. (2014). Baboon envelope pseudotyped LVs outperform VSV-G-LVs for gene transfer into early-cytokine-stimulated and resting HSCs. Blood *124*, 1221-1231.
Glodde, N., Bald, T., van den Boorn-Konijnenberg, D., Nakamura, K., O'Donnell, J.S., Szczepanski, S., Brandes, M., Eickhoff, S., Das, I., Shridhar, N*., et al.* (2017). Reactive Neutrophil Responses Dependent on the Receptor Tyrosine Kinase c-MET Limit Cancer Immunotherapy. Immunity *47*, 789-802 e789.
Guillerey, C., Ferrari de Andrade, L., Vuckovic, S., Miles, K., Ngiow, S.F., Yong, M.C., Teng, M.W., Colonna, M., Ritchie, D.S., Chesi, M*., et al.* (2015). Immunosurveillance and therapy of multiple myeloma are CD226 dependent. J Clin Invest *125*, 2077-2089.
Guillerey, C., Harjunpaa, H., Carrie, N., Kassem, S., Teo, T., Miles, K., Krumeich, S., Weulersse, M., Cuisinier, M., Stannard, K*., et al.* (2018). TIGIT immune checkpoint blockade restores CD8(+) T cell immunity against multiple myeloma. Blood.

Hogquist, K.A., Jameson, S.C., Heath, W.R., Howard, J.L., Bevan, M.J., and Carbone, F.R. (1994). T cell receptor antagonist peptides induce positive selection. Cell *76*, 17-27.
Hui, E., Cheung, J., Zhu, J., Su, X., Taylor, M.J., Wallweber, H.A., Sasmal, D.K., Huang, J., Kim, J.M., Mellman, I., and Vale, R.D. (2017). T cell costimulatory receptor CD28 is a primary target for PD-1-mediated inhibition. Science *355*, 1428-1433.
Iguchi-Manaka, A., Kai, H., Yamashita, Y., Shibata, K., Tahara-Hanaoka, S., Honda, S., Yasui, T., Kikutani, H., Shibuya, K., and Shibuya, A. (2008). Accelerated tumor growth in mice deficient in DNAM-1 receptor. J Exp Med *205*, 2959-2964.
Intlekofer, A.M., Takemoto, N., Wherry, E.J., Longworth, S.A., Northrup, J.T., Palanivel, V.R., Mullen, A.C., Gasink, C.R., Kaech, S.M., Miller, J.D.*, et al.* (2005). Effector and memory CD8+ T cell fate coupled by T-bet and eomesodermin. Nat Immunol *6*, 1236-1244.
Istaces, N., Splittgerber, M., Lima Silva, V., Nguyen, M., Thomas, S., Le, A., Achouri, Y., Calonne, E., Defrance, M., Fuks, F.*, et al.* (2019). EOMES interacts with RUNX3 and BRG1 to promote innate memory cell formation through epigenetic reprogramming. Nat Commun *10*, 3306.
Johnston, R.J., Comps-Agrar, L., Hackney, J., Yu, X., Huseni, M., Yang, Y., Park, S., Javinal, V., Chiu, H., Irving, B.*, et al.* (2014). The Immunoreceptor TIGIT Regulates Antitumor and Antiviral CD8(+) T Cell Effector Function. Cancer Cell *26*, 923-937.
Kaech, S.M., and Cui, W. (2012). Transcriptional control of effector and memory CD8+ T cell differentiation. Nat Rev Immunol *12*, 749-761.
Kamphorst, A.O., Wieland, A., Nasti, T., Yang, S., Zhang, R., Barber, D.L., Konieczny, B.T., Daugherty, C.Z., Koenig, L., Yu, K.*, et al.* (2017). Rescue of exhausted CD8 T cells by PD-1-targeted therapies is CD28-dependent. Science *355*, 1423-1427.
Kamran, N., Takai, Y., Miyoshi, J., Biswas, S.K., Wong, J.S., and Gasser, S. (2013). Toll-like receptor ligands induce expression of the costimulatory molecule CD155 on antigen-presenting cells. PLoS One *8*, e54406.
Kim, Y.H., Choi, B.K., Shin, S.M., Kim, C.H., Oh, H.S., Park, S.H., Lee, D.G., Lee, M.J., Kim, K.H., Vinay, D.S., and Kwon, B.S. (2011). 4-1BB triggering ameliorates experimental autoimmune encephalomyelitis by modulating the balance between Th17 and regulatory T cells. J Immunol *187*, 1120-1128.
Koyama, M., Kuns, R.D., Olver, S.D., Lineburg, K.E., Lor, M., Teal, B.E., Raffelt, N.C., Leveque, L., Chan, C.J., Robb, R.J.*, et al.* (2013). Promoting regulation via the inhibition of DNAM-1 after transplantation. Blood *121*, 3511-3520.
Kurtulus, S., Sakuishi, K., Ngiow, S.F., Joller, N., Tan, D.J., Teng, M.W., Smyth, M.J., Kuchroo, V.K., and Anderson, A.C. (2015). TIGIT predominantly regulates the immune response via regulatory T cells. J Clin Invest *125*, 4053-4062.
Landsberg, J., Kohlmeyer, J., Renn, M., Bald, T., Rogava, M., Cron, M., Fatho, M., Lennerz, V., Wolfel, T., Holzel, M., and Tuting, T. (2012). Melanomas resist T-cell therapy through inflammation-induced reversible dedifferentiation. Nature.
Larkin, J., Chiarion-Sileni, V., Gonzalez, R., Grob, J.J., Cowey, C.L., Lao, C.D., Schadendorf, D., Dummer, R., Smylie, M., Rutkowski, P.*, et al.* (2015). Combined Nivolumab and Ipilimumab or Monotherapy in Untreated Melanoma. N Engl J Med *373*, 23-34.
Lee, S.H., Toth, Z., Wong, L.Y., Brulois, K., Nguyen, J., Lee, J.Y., Zandi, E., and Jung, J.U. (2012). Novel Phosphorylations of IKKgamma/NEMO. mBio *3*, e00411-00412.
Levy, C., Amirache, F., Girard-Gagnepain, A., Frecha, C., Roman-Rodriguez, F.J., Bernadin, O., Costa, C., Negre, D., Gutierrez-Guerrero, A., Vranckx, L.S.*, et al.* (2017). Measles virus envelope pseudotyped lentiviral vectors transduce quiescent human HSCs at an efficiency without precedent. Blood Adv *1*, 2088-2104.

Li, J., He, Y., Hao, J., Ni, L., and Dong, C. (2018a). High Levels of Eomes Promote Exhaustion of Anti-tumor CD8(+) T Cells. Front Immunol *9*, 2981.
Li, X.Y., Das, I., Lepletier, A., Addala, V., Bald, T., Stannard, K., Barkauskas, D., Liu, J., Aguilera, A.R., Takeda, K.*, et al.* (2018b). CD155 loss enhances tumor suppression via combined host and tumor-intrinsic mechanisms. J Clin Invest *128*, 2613-2625.
Liao, Y., Smyth, G.K., and Shi, W. (2014). featureCounts: an efficient general purpose program for assigning sequence reads to genomic features. Bioinformatics *30*, 923-930.
Love, M.I., Anders, S., Kim, V., and Huber, W. (2015). RNA-Seq workflow: gene-level exploratory analysis and differential expression. F1000Res *4*, 1070.
Love, M.I., Huber, W., and Anders, S. (2014). Moderated estimation of fold change and dispersion for RNA-seq data with DESeq2. Genome Biol *15*, 550.
Lozano, E., Dominguez-Villar, M., Kuchroo, V., and Hafler, D.A. (2012). The TIGIT/CD226 axis regulates human T cell function. J Immunol *188*, 3869-3875.
Lozano, E., Joller, N., Cao, Y., Kuchroo, V.K., and Hafler, D.A. (2013). The CD226/CD155 interaction regulates the proinflammatory (Th1/Th17)/anti-inflammatory (Th2) balance in humans. Journal of immunology *191*, 3673-3680.
Maiti, A.K., Kim-Howard, X., Viswanathan, P., Guillen, L., Qian, X., Rojas-Villarraga, A., Sun, C., Canas, C., Tobon, G.J., Matsuda, K.*, et al.* (2010). Non-synonymous variant (Gly307Ser) in CD226 is associated with susceptibility to multiple autoimmune diseases. Rheumatology *49*, 1239-1244.
Martinet, L., Ferrari De Andrade, L., Guillerey, C., Lee, J.S., Liu, J., Souza-Fonseca-Guimaraes, F., Hutchinson, D.S., Kolesnik, T.B., Nicholson, S.E., Huntington, N.D., and Smyth, M.J. (2015). DNAM-1 Expression Marks an Alternative Program of NK Cell Maturation. Cell reports *11*, 85-97.
Martinet, L., and Smyth, M.J. (2015). Balancing natural killer cell activation through paired receptors. Nat Rev Immunol *15*, 243-254.
Melero, I., Shuford, W.W., Newby, S.A., Aruffo, A., Ledbetter, J.A., Hellstrom, K.E., Mittler, R.S., and Chen, L. (1997). Monoclonal antibodies against the 4-1BB T-cell activation molecule eradicate established tumors. Nat Med *3*, 682-685.
Nakamura, K., Kassem, S., Cleynen, A., Chretien, M.L., Guillerey, C., Putz, E.M., Bald, T., Forster, I., Vuckovic, S., Hill, G.R.*, et al.* (2018). Dysregulated IL-18 Is a Key Driver of Immunosuppression and a Possible Therapeutic Target in the Multiple Myeloma Microenvironment. Cancer Cell *33*, 634-648 e635.
Overwijk, W.W., Theoret, M.R., Finkelstein, S.E., Surman, D.R., de Jong, L.A., Vyth-Dreese, F.A., Dellemijn, T.A., Antony, P.A., Spiess, P.J., Palmer, D.C.*, et al.* (2003). Tumor regression and autoimmunity after reversal of a functionally tolerant state of self-reactive CD8+ T cells. J Exp Med *198*, 569-580.
Paley, M.A., Kroy, D.C., Odorizzi, P.M., Johnnidis, J.B., Dolfi, D.V., Barnett, B.E., Bikoff, E.K., Robertson, E.J., Lauer, G.M., Reiner, S.L., and Wherry, E.J. (2012). Progenitor and terminal subsets of CD8+ T cells cooperate to contain chronic viral infection. Science *338*, 1220-1225.
Pauken, K.E., Sammons, M.A., Odorizzi, P.M., Manne, S., Godec, J., Khan, O., Drake, A.M., Chen, Z., Sen, D.R., Kurachi, M.*, et al.* (2016). Epigenetic stability of exhausted T cells limits durability of reinvigoration by PD-1 blockade. Science *354*, 1160-1165.
Perez, O.D., Mitchell, D., Jager, G.C., South, S., Murriel, C., McBride, J., Herzenberg, L.A., Kinoshita, S., and Nolan, G.P. (2003). Leukocyte functional antigen 1 lowers T cell activation thresholds and signaling through cytohesin-1 and Jun-activating binding protein 1. Nat Immunol *4*, 1083-1092.

Petit, A.E., Demotte, N., Scheid, B., Wildmann, C., Bigirimana, R., Gordon-Alonso, M., Carrasco, J., Valitutti, S., Godelaine, D., and van der Bruggen, P. (2016). A major secretory defect of tumour-infiltrating T lymphocytes due to galectin impairing LFA-1-mediated synapse completion. Nat Commun *7*, 12242.
Philip, M., Fairchild, L., Sun, L., Horste, E.L., Camara, S., Shakiba, M., Scott, A.C., Viale, A., Lauer, P., Merghoub, T.*, et al.* (2017). Chromatin states define tumour-specific T cell dysfunction and reprogramming. Nature *545*, 452-456.
Porgador, A., Feldman, M., and Eisenbach, L. (1989). H-2Kb transfection of B16 melanoma cells results in reduced tumourigenicity and metastatic competence. J Immunogenet *16*, 291-303.
Qiu, Q., Ravens, I., Seth, S., Rathinasamy, A., Maier, M.K., Davalos-Misslitz, A., Forster, R., and Bernhardt, G. (2010). CD155 is involved in negative selection and is required to retain terminally maturing CD8 T cells in thymus. J Immunol *184*, 1681-1689.
Ralston, K.J., Hird, S.L., Zhang, X., Scott, J.L., Jin, B., Thorne, R.F., Berndt, M.C., Boyd, A.W., and Burns, G.F. (2004). The LFA-1-associated molecule PTA-1 (CD226) on T cells forms a dynamic molecular complex with protein 4.1G and human discs large. J Biol Chem *279*, 33816-33828.
Rizvi, N.A., Hellmann, M.D., Snyder, A., Kvistborg, P., Makarov, V., Havel, J.J., Lee, W., Yuan, J., Wong, P., Ho, T.S.*, et al.* (2015). Cancer immunology. Mutational landscape determines sensitivity to PD-1 blockade in non-small cell lung cancer. Science *348*, 124-128.
Robert, C., Long, G.V., Brady, B., Dutriaux, C., Maio, M., Mortier, L., Hassel, J.C., Rutkowski, P., McNeil, C., Kalinka-Warzocha, E.*, et al.* (2015). Nivolumab in previously untreated melanoma without BRAF mutation. N Engl J Med *372*, 320-330.
Robert, C., Thomas, L., Bondarenko, I., O'Day, S., M, D.J., Garbe, C., Lebbe, C., Baurain, J.F., Testori, A., Grob, J.J.*, et al.* (2011). Ipilimumab plus dacarbazine for previously untreated metastatic melanoma. N Engl J Med *364*, 2517-2526.
Schumacher, T.N., and Schreiber, R.D. (2015). Neoantigens in cancer immunotherapy. Science *348*, 69-74.
Scott, A.C., Dundar, F., Zumbo, P., Chandran, S.S., Klebanoff, C.A., Shakiba, M., Trivedi, P., Menocal, L., Appleby, H., Camara, S.*, et al.* (2019). TOX is a critical regulator of tumour-specific T cell differentiation. Nature *571*, 270-274.
Seo, S.K., Choi, J.H., Kim, Y.H., Kang, W.J., Park, H.Y., Suh, J.H., Choi, B.K., Vinay, D.S., and Kwon, B.S. (2004). 4-1BB-mediated immunotherapy of rheumatoid arthritis. Nat Med *10*, 1088-1094.
Seth, S., Qiu, Q., Danisch, S., Maier, M.K., Braun, A., Ravens, I., Czeloth, N., Hyde, R., Dittrich-Breiholz, O., Forster, R., and Bernhardt, G. (2011). Intranodal interaction with dendritic cells dynamically regulates surface expression of the co-stimulatory receptor CD226 protein on murine T cells. J Biol Chem *286*, 39153-39163.
Shibuya, A., Campbell, D., Hannum, C., Yssel, H., Franz-Bacon, K., McClanahan, T., Kitamura, T., Nicholl, J., Sutherland, G.R., Lanier, L.L., and Phillips, J.H. (1996). DNAM-1, a novel adhesion molecule involved in the cytolytic function of T lymphocytes. Immunity *4*, 573-581.
Shibuya, K., Lanier, L.L., Phillips, J.H., Ochs, H.D., Shimizu, K., Nakayama, E., Nakauchi, H., and Shibuya, A. (1999). Physical and functional association of LFA-1 with DNAM-1 adhesion molecule. Immunity *11*, 615-623.
Shibuya, K., Shirakawa, J., Kameyama, T., Honda, S., Tahara-Hanaoka, S., Miyamoto, A., Onodera, M., Sumida, T., Nakauchi, H., Miyoshi, H., and Shibuya, A. (2003). CD226 (DNAM-1) is involved in lymphocyte function-associated antigen 1 costimulatory signal for naive T cell differentiation and proliferation. J Exp Med *198*, 1829-1839.
Shirakawa, J., Shibuya, K., and Shibuya, A. (2005). Requirement of the serine at residue 329 for lipid raft recruitment of DNAM-1 (CD226). Int Immunol *17*, 217-223.

Shirakawa, J., Wang, Y., Tahara-Hanaoka, S., Honda, S., Shibuya, K., and Shibuya, A. (2006). LFA-1-dependent lipid raft recruitment of DNAM-1 (CD226) in CD4+ T cell. Int Immunol *18*, 951-957.
Song, G., Bae, S.C., Choi, S., Ji, J., and Lee, Y. (2012). Association between the CD226 rs763361 polymorphism and susceptibility to autoimmune diseases: a meta-analysis. Lupus *21*, 1522-1530.
Subramanian, A., Tamayo, P., Mootha, V.K., Mukherjee, S., Ebert, B.L., Gillette, M.A., Paulovich, A., Pomeroy, S.L., Golub, T.R., Lander, E.S., and Mesirov, J.P. (2005). Gene set enrichment analysis: a knowledge-based approach for interpreting genome-wide expression profiles. Proc Natl Acad Sci U S A *102*, 15545-15550.
Sun, Y., Lin, X., Chen, H.M., Wu, Q., Subudhi, S.K., Chen, L., and Fu, Y.X. (2002). Administration of agonistic anti-4-1BB monoclonal antibody leads to the amelioration of experimental autoimmune encephalomyelitis. J Immunol *168*, 1457-1465.
Tahara-Hanaoka, S., Shibuya, K., Kai, H., Miyamoto, A., Morikawa, Y., Ohkochi, N., Honda, S., and Shibuya, A. (2006). Tumor rejection by the poliovirus receptor family ligands of the DNAM-1 (CD226) receptor. Blood *107*, 1491-1496.
Thommen, D.S., Koelzer, V.H., Herzig, P., Roller, A., Trefny, M., Dimeloe, S., Kiialainen, A., Hanhart, J., Schill, C., Hess, C*., et al.* (2018). A transcriptionally and functionally distinct PD-1(+) CD8(+) T cell pool with predictive potential in non-small-cell lung cancer treated with PD-1 blockade. Nat Med *24*, 994-1004.
Thommen, D.S., and Schumacher, T.N. (2018). T Cell Dysfunction in Cancer. Cancer Cell *33*, 547-562.
Todd, J.A., Walker, N.M., Cooper, J.D., Smyth, D.J., Downes, K., Plagnol, V., Bailey, R., Nejentsev, S., Field, S.F., Payne, F*., et al.* (2007). Robust associations of four new chromosome regions from genome-wide analyses of type 1 diabetes. Nat Genet *39*, 857-864.
Topalian, S.L., Hodi, F.S., Brahmer, J.R., Gettinger, S.N., Smith, D.C., McDermott, D.F., Powderly, J.D., Carvajal, R.D., Sosman, J.A., Atkins, M.B*., et al.* (2012). Safety, activity, and immune correlates of anti-PD-1 antibody in cancer. N Engl J Med *366*, 2443-2454.
Tumeh, P.C., Harview, C.L., Yearley, J.H., Shintaku, I.P., Taylor, E.J., Robert, L., Chmielowski, B., Spasic, M., Henry, G., Ciobanu, V*., et al.* (2014). PD-1 blockade induces responses by inhibiting adaptive immune resistance. Nature *515*, 568-571.
Varet, H., Brillet-Gueguen, L., Coppee, J.Y., and Dillies, M.A. (2016). SARTools: A DESeq2- and EdgeR-Based R Pipeline for Comprehensive Differential Analysis of RNA-Seq Data. PLoS One *11*, e0157022.
von Scheidt, B., Leung, P.S., Yong, M.C., Zhang, Y., Towne, J.E., Smyth, M.J., and Teng, M.W. (2014). Combined anti-CD40 and anti-IL-23 monoclonal antibody therapy effectively suppresses tumor growth and metastases. Cancer Res.
Wang, B., Zhang, W., Jankovic, V., Golubov, J., Poon, P., Oswald, E.M., Gurer, C., Wei, J., Ramos, I., Wu, Q*., et al.* (2018). Combination cancer immunotherapy targeting PD-1 and GITR can rescue CD8(+) T cell dysfunction and maintain memory phenotype. Sci Immunol *3*.
Wherry, E.J. (2011). T cell exhaustion. Nat Immunol *12*, 492-499.
Wherry, E.J., and Kurachi, M. (2015). Molecular and cellular insights into T cell exhaustion. Nature reviews. Immunology *15*, 486-499.
Zhang, Z., Wu, N., Lu, Y., Davidson, D., Colonna, M., and Veillette, A. (2015). DNAM-1 controls NK cell activation via an ITT-like motif. J Exp Med *212*, 2165-2182.

Zhu, Y., Ju, S., Chen, E., Dai, S., Li, C., Morel, P., Liu, L., Zhang, X., and Lu, B. (2010). T-bet and eomesodermin are required for T cell-mediated antitumor immune responses. J Immunol *185*, 3174-3183.
Zhu, Y., Paniccia, A., Schulick, A.C., Chen, W., Koenig, M.R., Byers, J.T., Yao, S., Bevers, S., and Edil, B.H. (2016). Identification of CD112R as a novel checkpoint for human T cells. J Exp Med *213*, 167-176.

Figure 1

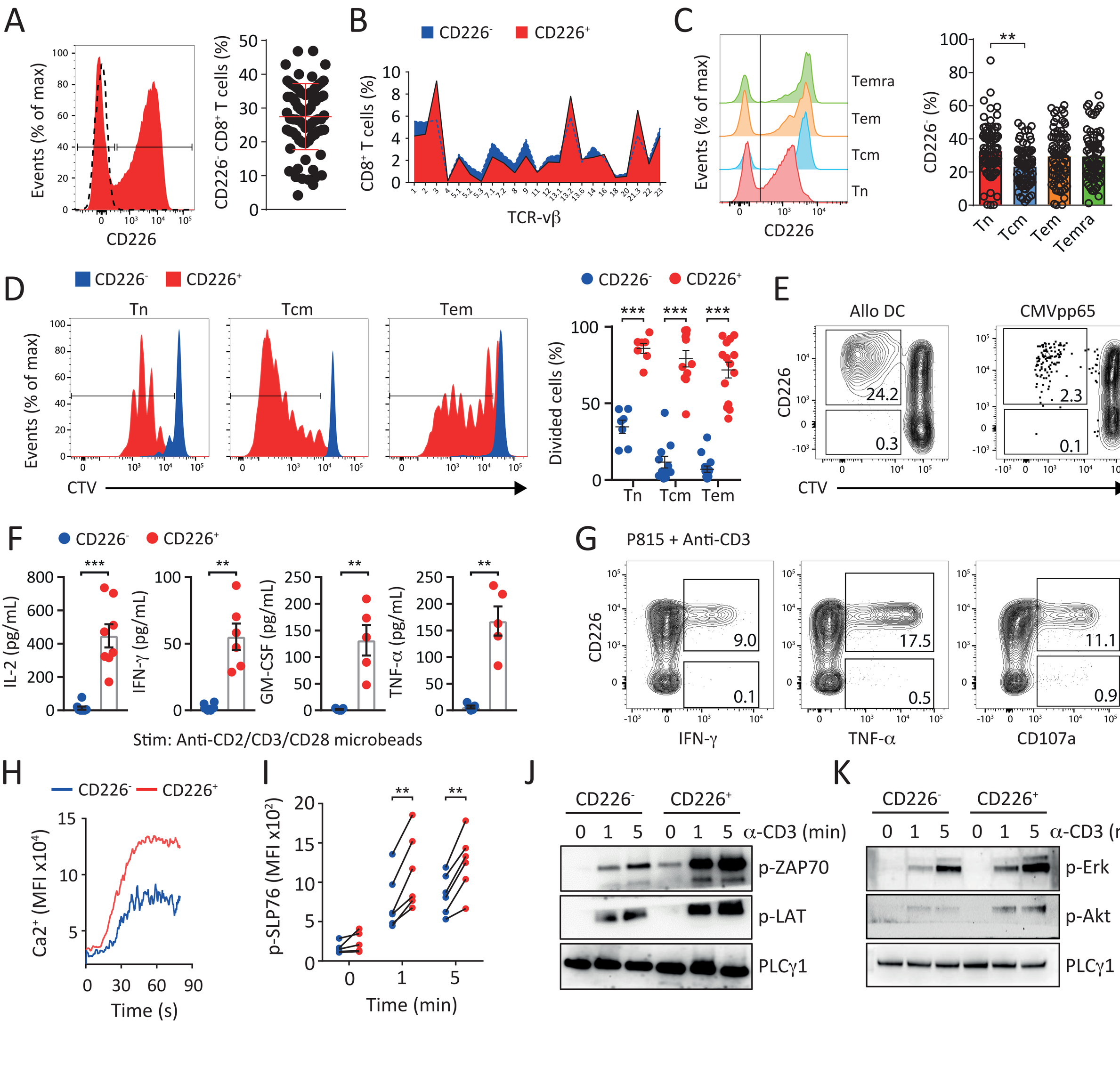
A
Events (% of max)
CD226
CD226⁻ CD8⁺ T cells (%)
B
CD226⁻
CD226⁺
CD8⁺ T cells (%)
TCR-vβ
C
Events (% of max)
CD226
Temra
Tem
Tcm
Tn
CD226⁻ (%)
Tn
Tcm
Tem
Temra
D
CD226⁻
CD226⁺
Tn
Tcm
Tem
Events (% of max)
CTV
Divided cells (%)
E
Allo DC
CMVpp65
CD226
24.2
0.3
2.3
0.1
CTV
F
CD226⁻
CD226⁺
IL-2 (pg/mL)
IFN-γ (pg/mL)
GM-CSF (pg/mL)
TNF-α (pg/mL)
Stim: Anti-CD2/CD3/CD28 microbeads
G
P815 + Anti-CD3
CD226
9.0
0.1
17.5
0.5
11.1
0.9
IFN-γ
TNF-α
CD107a
H
CD226⁻
CD226⁺
Ca2⁺ (MFI x10⁴)
Time (s)
I
p-SLP76 (MFI x10²)
Time (min)
J
CD226⁻
CD226⁺
0 1 5 0 1 5 α-CD3 (min)
p-ZAP70
p-LAT
PLCγ1
K
CD226⁻
CD226⁺
0 1 5 0 1 5 α-CD3 (min)
p-Erk
p-Akt
PLCγ1

Figure 2

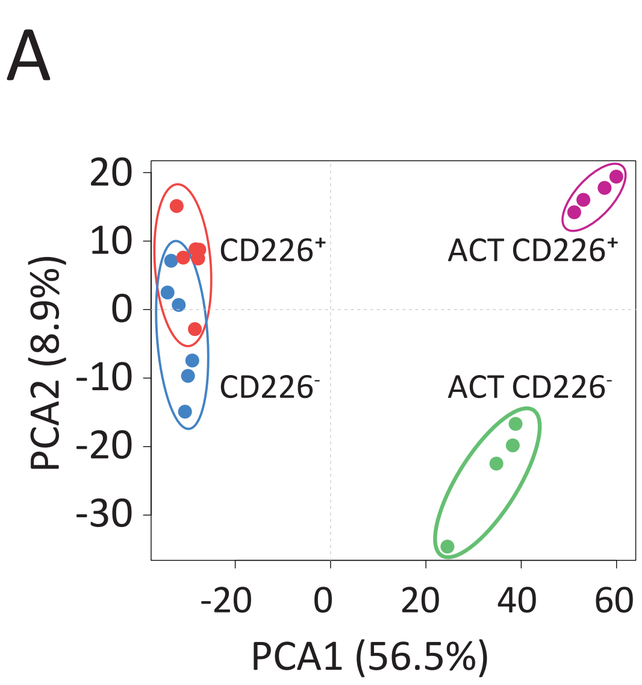

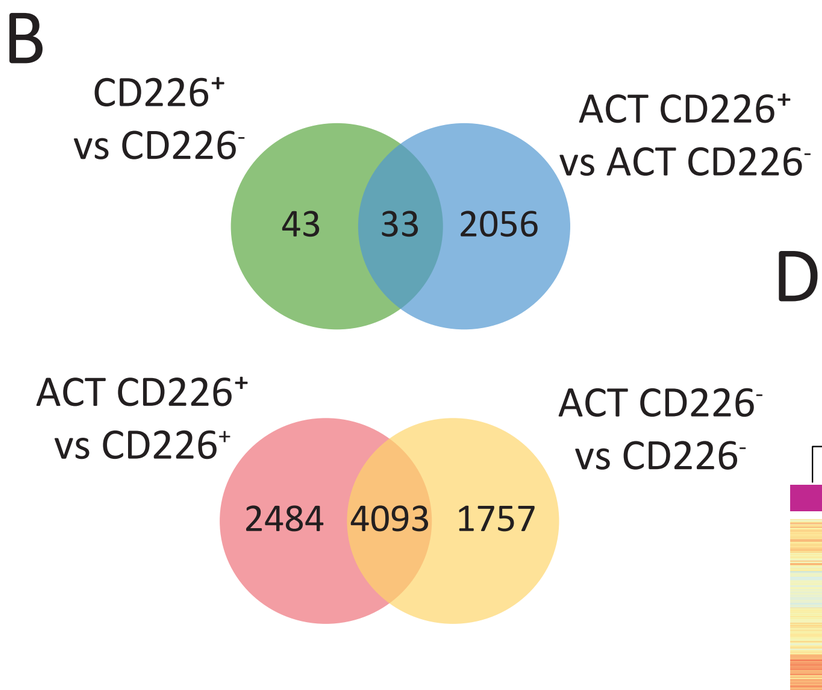

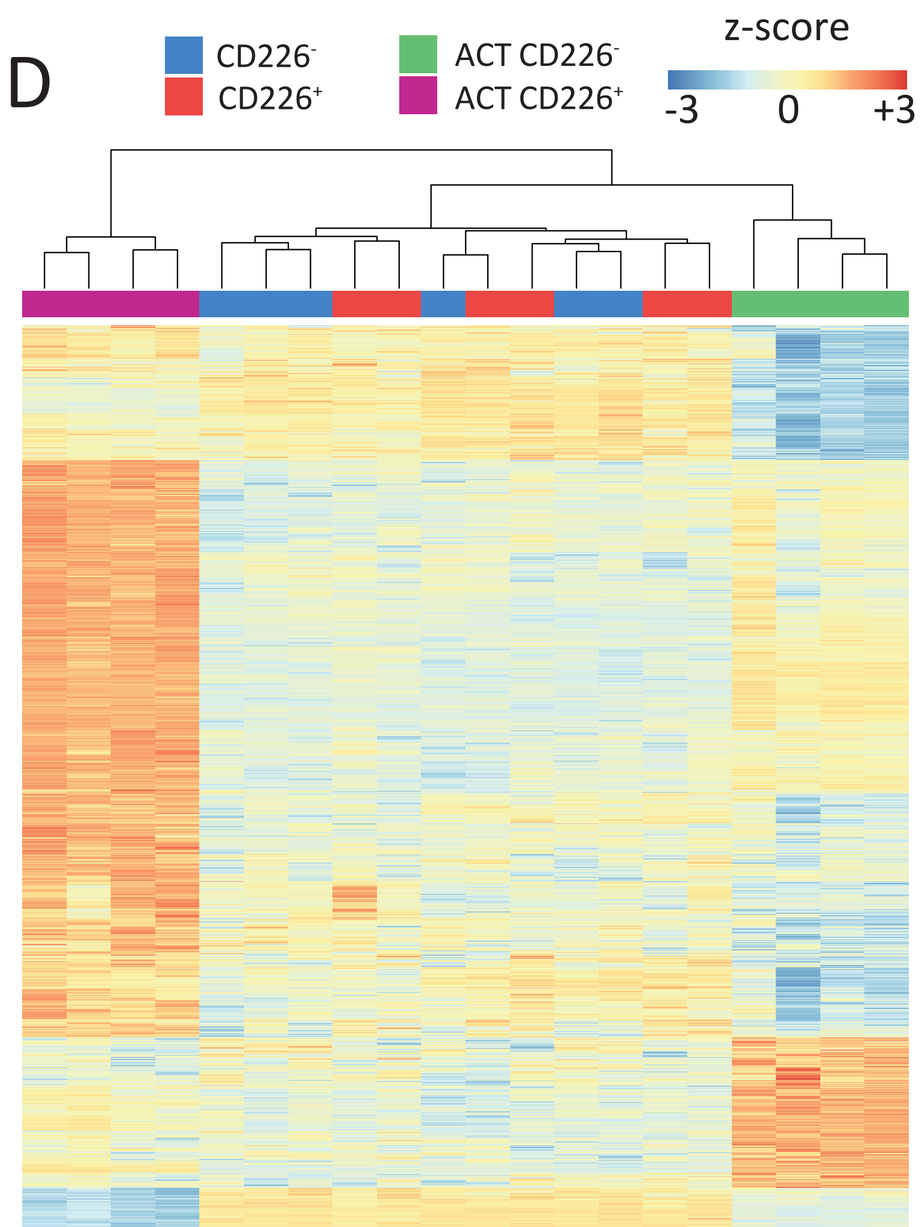

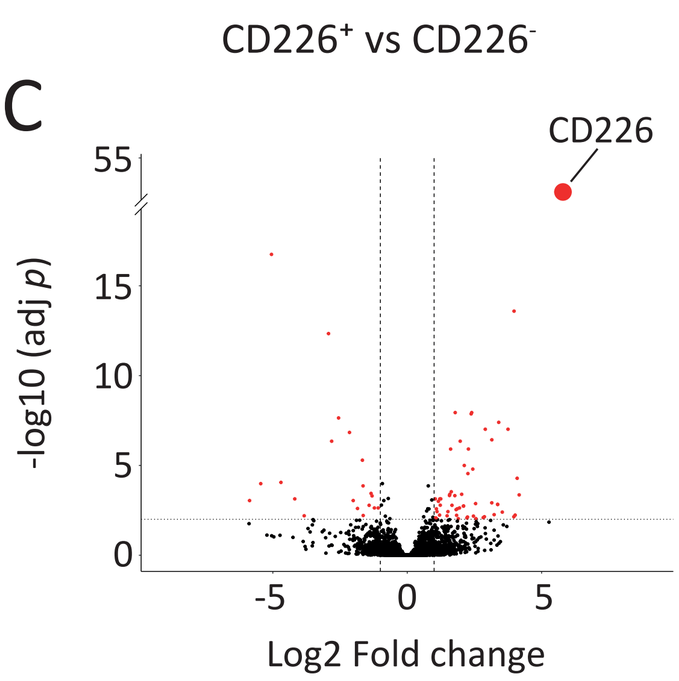

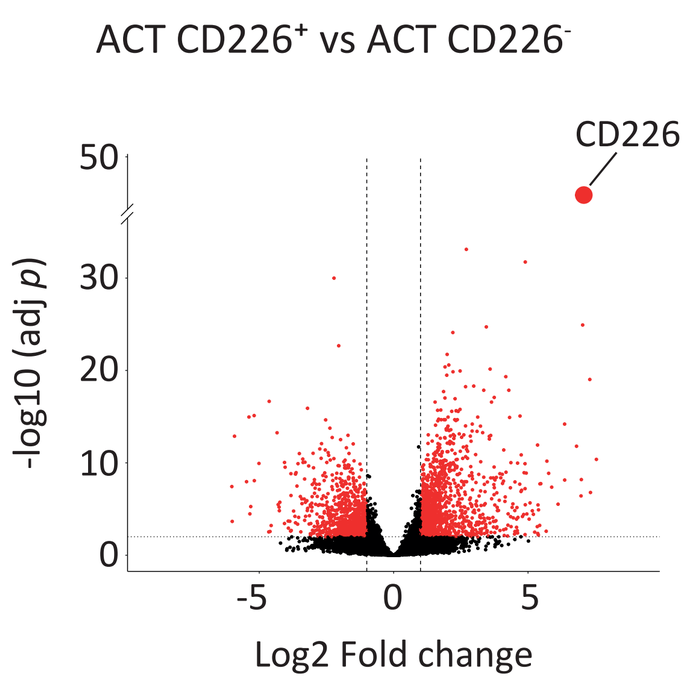

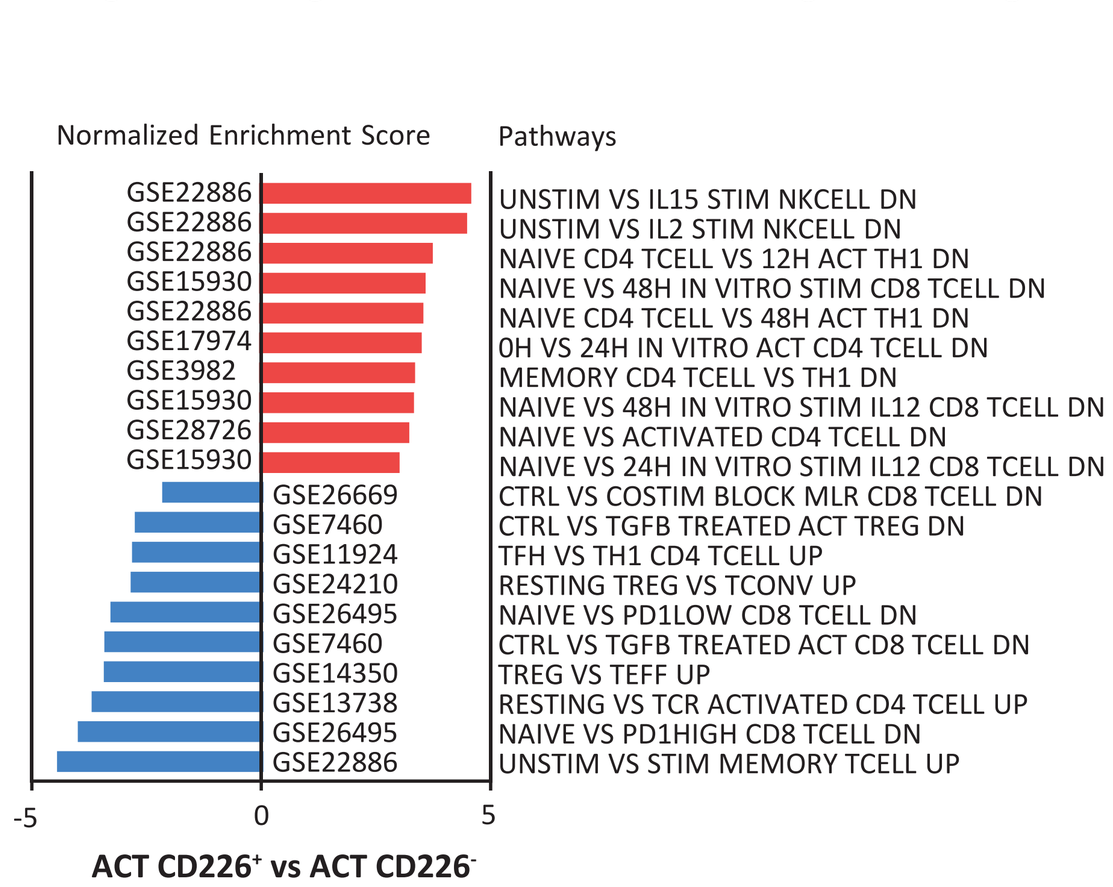

F

Go term : ACT CD226⁺ vs ACT CD226⁻	*Adj P*	*NES*
RNA PROCESSING	0.002	3.4
PEPTIDE METABOLIC PROCESS	0.002	3.1
MITOTIC CELL CYCLE	0.002	2.6
NIK NF KAPPAB SIGNALING	0.009	2.3
T CELL RECEPTOR SIGNALING PATHWAY	0.02	2.2

Figure 3

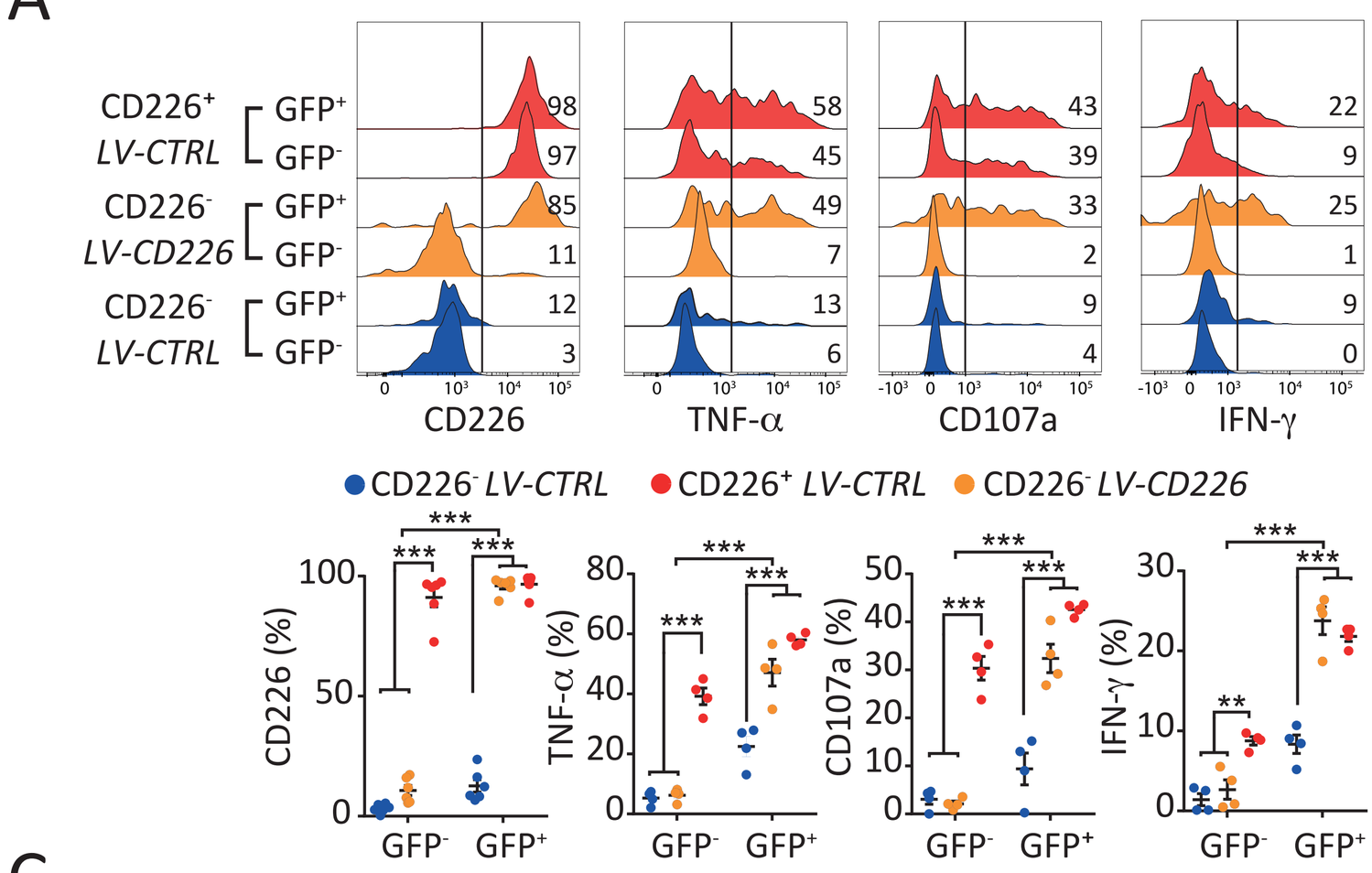
A
CD226+ LV-CTRL
CD226- LV-CTRL
CD226- LV-CD226
GFP+
GFP-
98
97
85
11
12
3
58
45
49
7
13
6
43
39
33
2
9
4
22
9
25
1
9
0
CD226
TNF-α
CD107a
IFN-γ
CD226- LV-CTRL
CD226+ LV-CTRL
CD226- LV-CD226
CD226 (%)
TNF-α (%)
CD107a (%)
IFN-γ (%)
GFP- GFP+
B
CD226
CTV
CD226 (%)
Divided (%)
GFP- GFP+

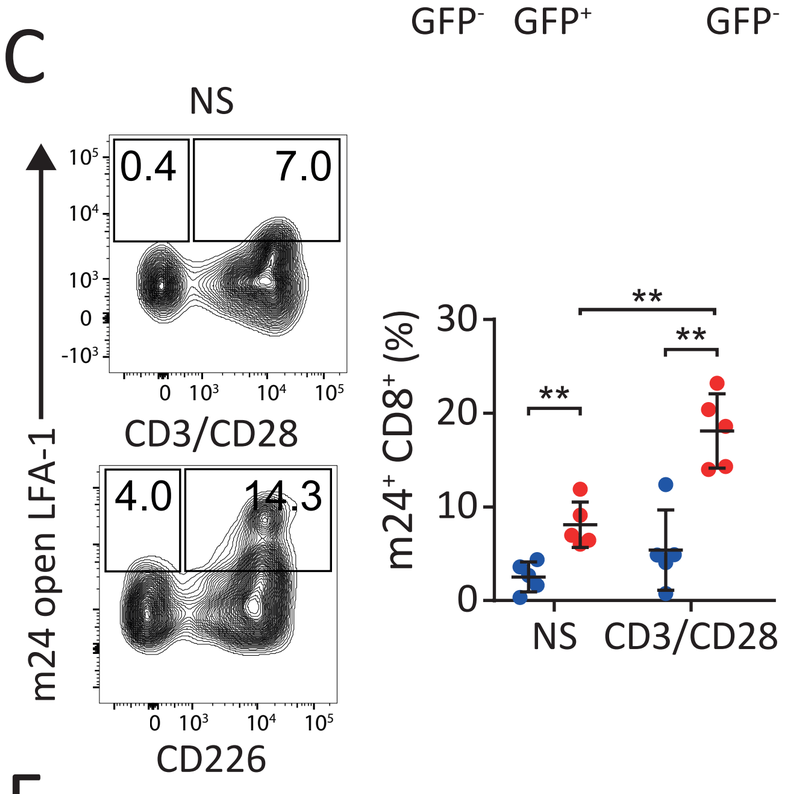
C
NS
0.4
7.0
CD3/CD28
4.0
14.3
m24 open LFA-1
CD226
m24+ CD8+ (%)
NS CD3/CD28

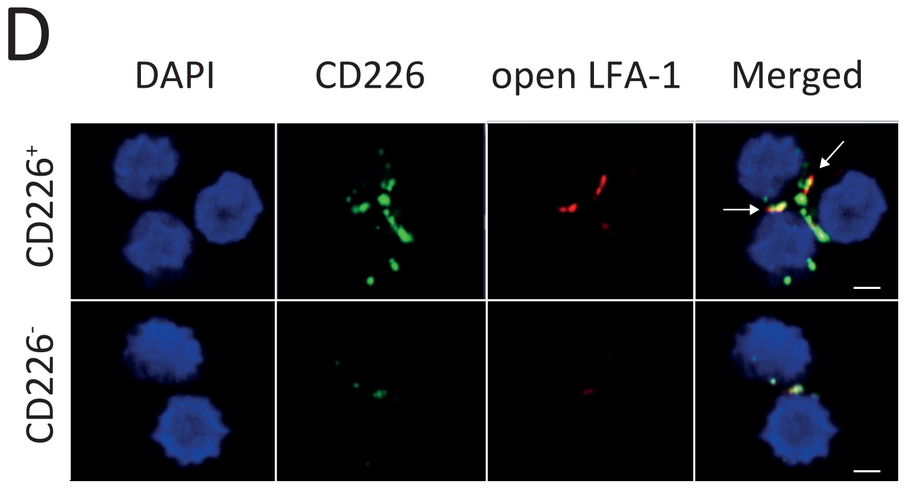
D
DAPI
CD226
open LFA-1
Merged
CD226+
CD226-

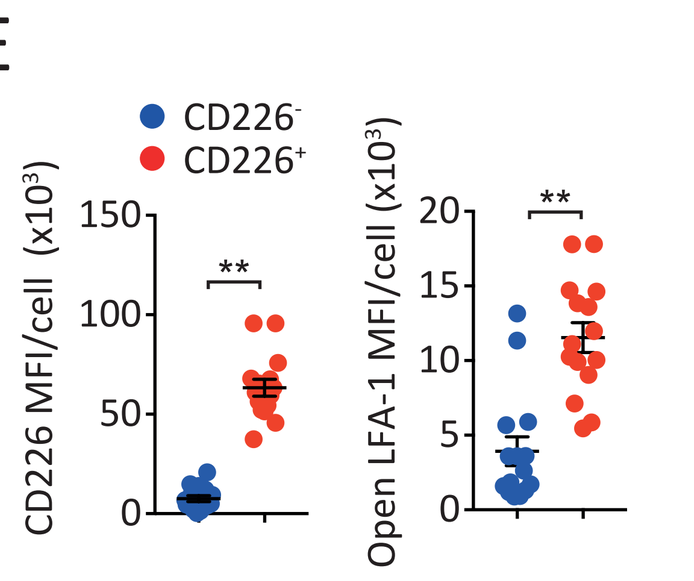
E
CD226-
CD226+
CD226 MFI/cell (x10³)
Open LFA-1 MFI/cell (x10³)

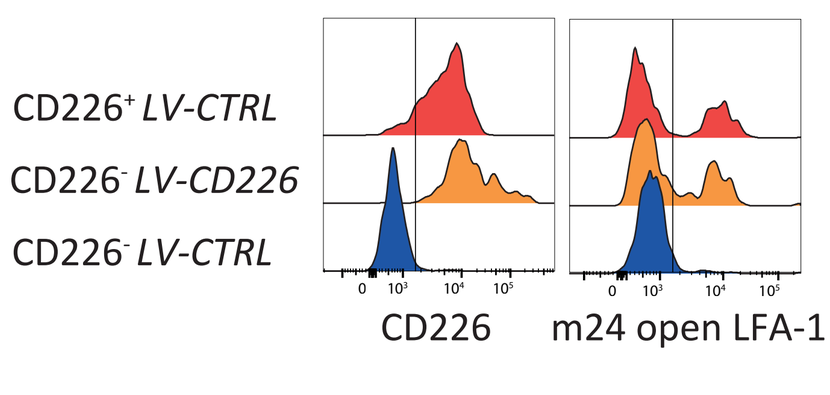
F
CD226+ LV-CTRL
CD226- LV-CD226
CD226- LV-CTRL
CD226
m24 open LFA-1

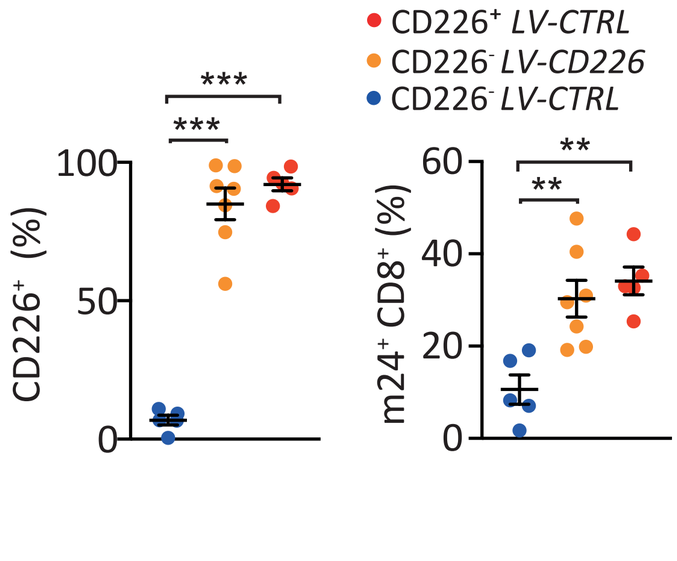
CD226+ LV-CTRL
CD226- LV-CD226
CD226- LV-CTRL
CD226+ (%)
m24+ CD8+ (%)

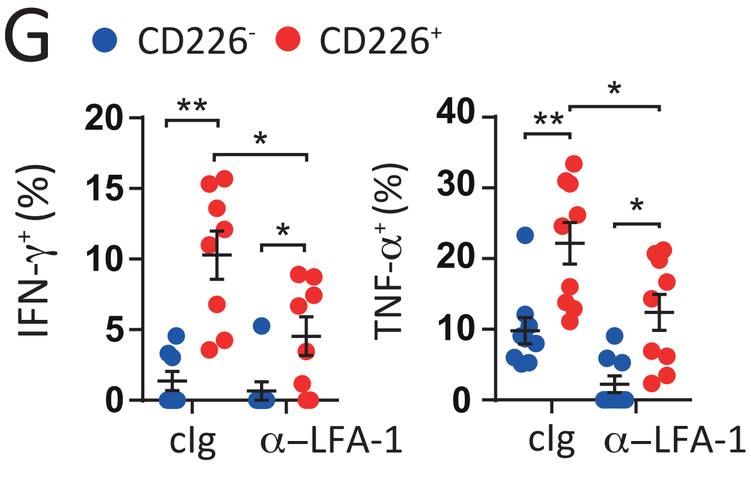
G
CD226-
CD226+
IFN-γ+ (%)
TNF-α+ (%)
cIg
α–LFA-1

Figure 4

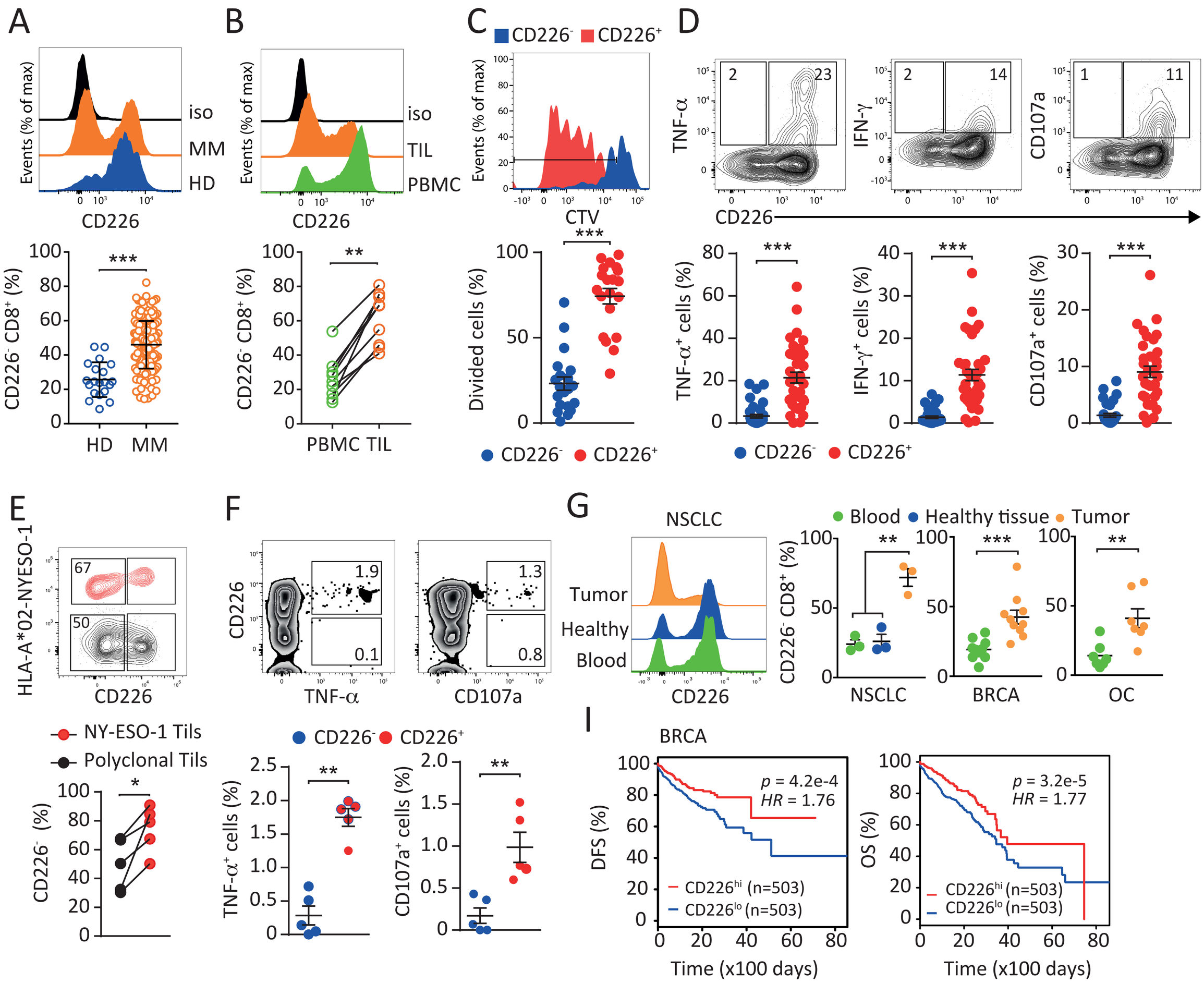
A
Events (% of max)
iso
MM
HD
CD226
CD226⁻ CD8⁺ (%)
***
HD
MM
B
Events (% of max)
iso
TIL
PBMC
CD226
CD226⁻ CD8⁺ (%)
**
PBMC
TIL
C
CD226⁻
CD226⁺
Events (% of max)
CTV
***
Divided cells (%)
CD226⁻
CD226⁺
D
TNF-α
IFN-γ
CD107a
2
23
2
14
1
11
CD226
***
TNF-α⁺ cells (%)
IFN-γ⁺ cells (%)
CD107a⁺ cells (%)
CD226⁻
CD226⁺
E
HLA-A*02-NYESO-1
67
50
CD226
F
CD226
TNF-α
CD107a
1.9
0.1
1.3
0.8
G
NSCLC
Tumor
Healthy
Blood
CD226
Blood
Healthy tissue
Tumor
CD226⁻ CD8⁺ (%)
**
***
**
NSCLC
BRCA
OC
H
NY-ESO-1 Tils
Polyclonal Tils
CD226⁻ (%)
*
CD226⁻
CD226⁺
TNF-α⁺ cells (%)
**
CD107a⁺ cells (%)
**
I
BRCA
DFS (%)
p = 4.2e-4
HR = 1.76
CD226hi (n=503)
CD226lo (n=503)
Time (x100 days)
OS (%)
p = 3.2e-5
HR = 1.77
CD226hi (n=503)
CD226lo (n=503)
Time (x100 days)

Figure 5

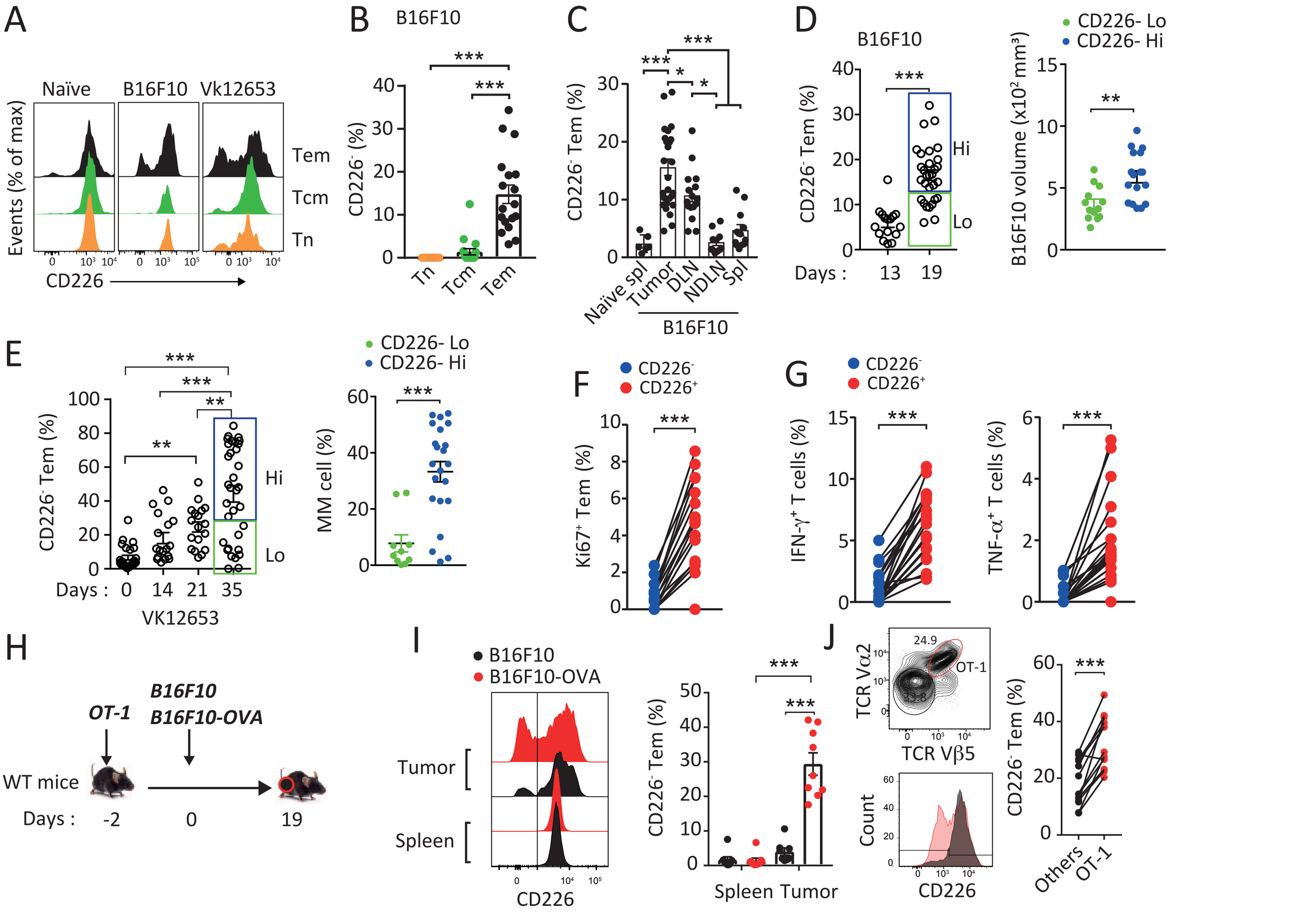
A
Naïve
B16F10
Vk12653
Events (% of max)
Tem
Tcm
Tn
CD226
B
B16F10
CD226⁻ (%)
Tn
Tcm
Tem
C
CD226⁻ Tem (%)
Naïve spl
Tumor
DLN
NDLN
Spl
B16F10
D
B16F10
CD226⁻ Tem (%)
Hi
Lo
Days :
13
19
CD226- Lo
CD226- Hi
B16F10 volume (x10² mm³)
E
CD226⁻ Tem (%)
Hi
Lo
Days :
0
14
21
35
VK12653
CD226- Lo
CD226- Hi
MM cell (%)
F
CD226⁻
CD226⁺
Ki67⁺ Tem (%)
G
CD226⁻
CD226⁺
IFN-γ⁺ T cells (%)
TNF-α⁺ T cells (%)
H
OT-1
B16F10
B16F10-OVA
WT mice
Days :
-2
0
19
I
B16F10
B16F10-OVA
Tumor
Spleen
CD226
CD226⁻ Tem (%)
Spleen
Tumor
J
TCR Vα2
TCR Vβ5
24.9
OT-1
15.8
Count
CD226
CD226⁻ Tem (%)
Others
OT-1

Figure 6

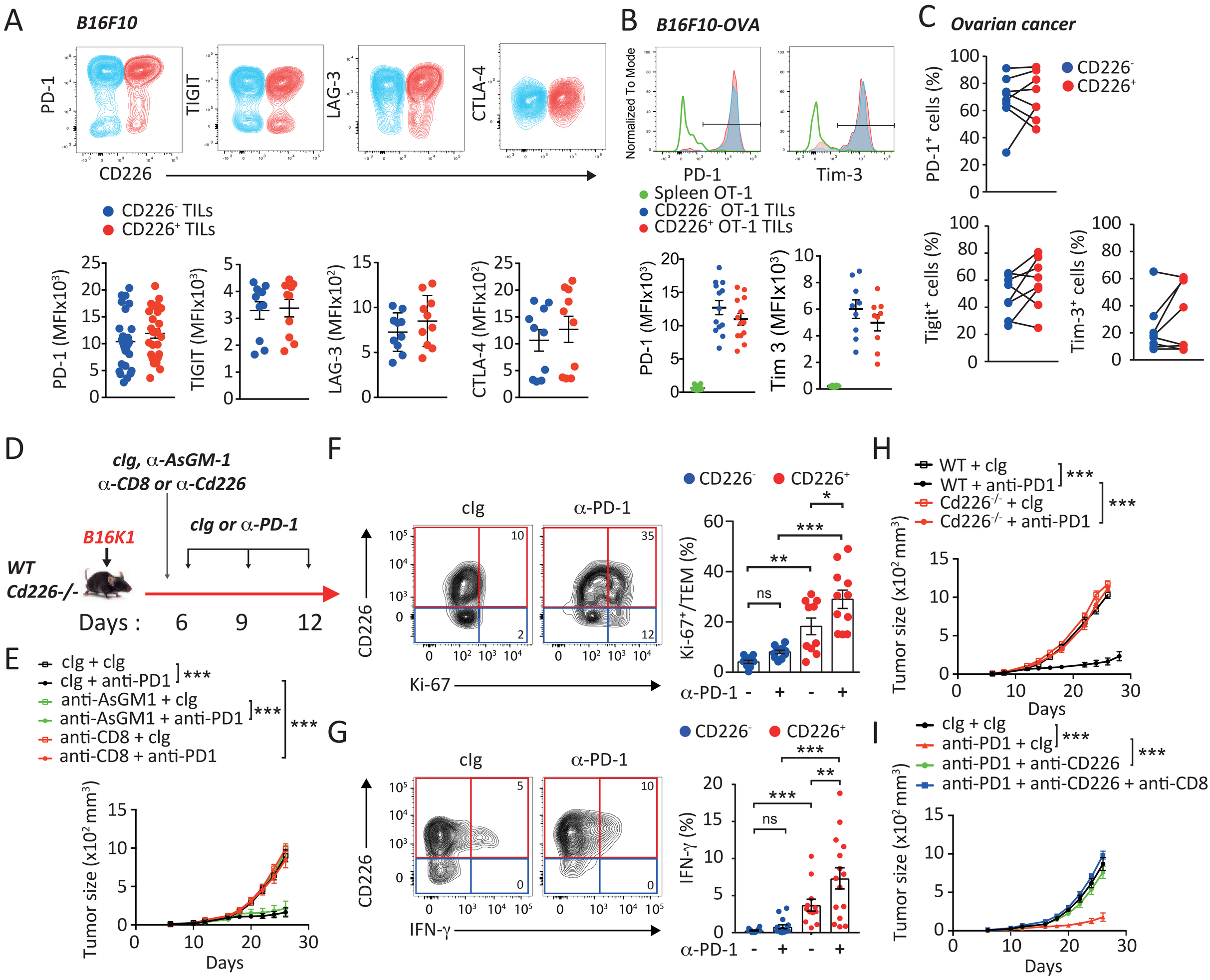
A
B16F10
PD-1
TIGIT
LAG-3
CTLA-4
CD226
CD226- TILs
CD226+ TILs
PD-1 (MFIx10³)
TIGIT (MFIx10³)
LAG-3 (MFIx10²)
CTLA-4 (MFIx10²)
B
B16F10-OVA
Normalized To Mode
PD-1
Tim-3
Spleen OT-1
CD226- OT-1 TILs
CD226+ OT-1 TILs
PD-1 (MFIx10³)
Tim 3 (MFIx10³)
C
Ovarian cancer
PD-1+ cells (%)
CD226-
CD226+
Tigit+ cells (%)
Tim-3+ cells (%)
D
clg, α-AsGM-1
α-CD8 or α-Cd226
clg or α-PD-1
B16K1
WT
Cd226-/-
Days : 6 9 12
E
clg + clg
clg + anti-PD1
anti-AsGM1 + clg
anti-AsGM1 + anti-PD1
anti-CD8 + clg
anti-CD8 + anti-PD1
***
Tumor size (x10² mm³)
Days
F
clg
α-PD-1
CD226
Ki-67
10
2
35
12
CD226-
CD226+
Ki-67+/TEM (%)
ns
**
***
*
α-PD-1 - + - +
G
clg
α-PD-1
CD226
IFN-γ
5
0
10
0
IFN-γ (%)
H
WT + clg
WT + anti-PD1
Cd226-/- + clg
Cd226-/- + anti-PD1
Tumor size (x10² mm³)
Days
I
clg + clg
anti-PD1 + clg
anti-PD1 + anti-CD226
anti-PD1 + anti-CD226 + anti-CD8
Tumor size (x10² mm³)
Days

Figure 7

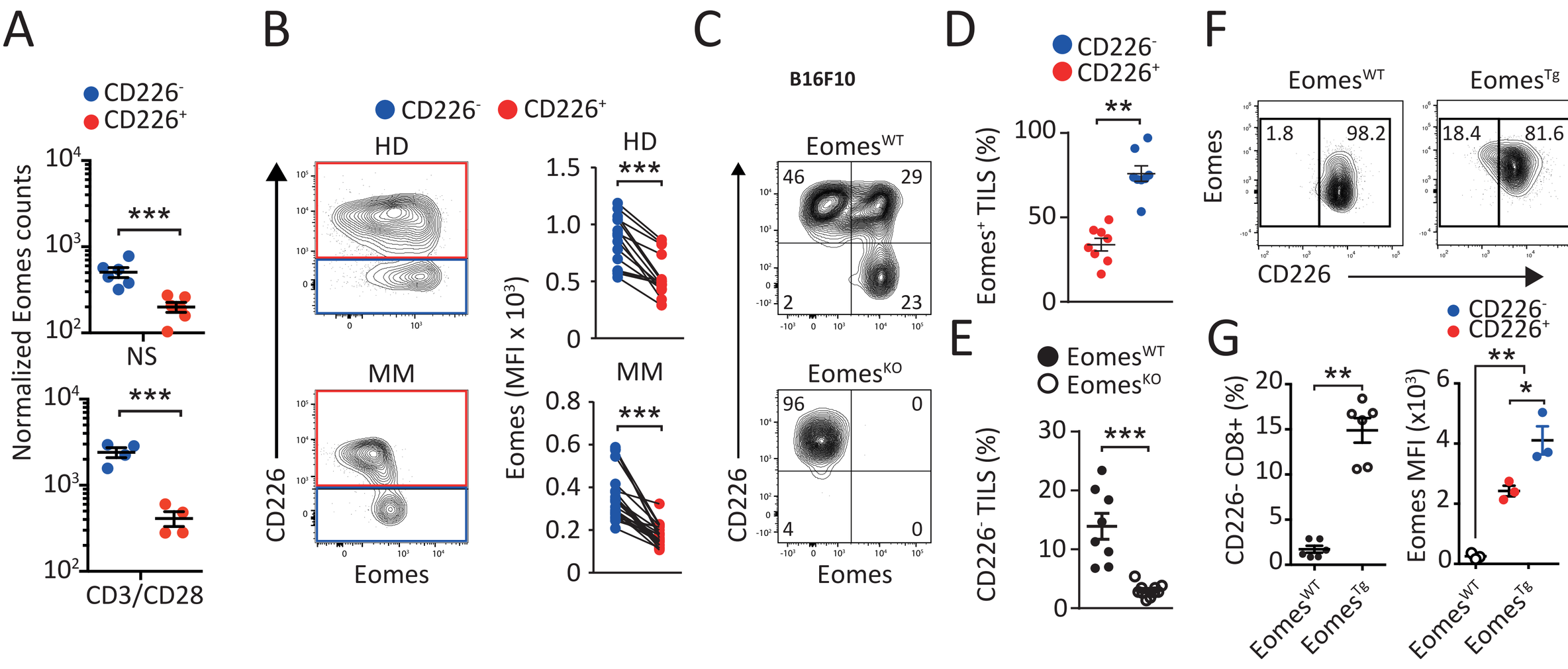
A
CD226-
CD226+
Normalized Eomes counts
NS
***
CD3/CD28
B
HD
MM
CD226
Eomes
Eomes (MFI x 10³)
C
B16F10
Eomes^WT
Eomes^KO
46
29
2
23
96
0
4
0
D
Eomes⁺ TILS (%)
**
E
Eomes^WT
Eomes^KO
CD226⁻ TILS (%)
F
Eomes^WT
Eomes^Tg
1.8
98.2
18.4
81.6
CD226
G
CD226- CD8+ (%)
Eomes MFI (x10³)

Figure 8

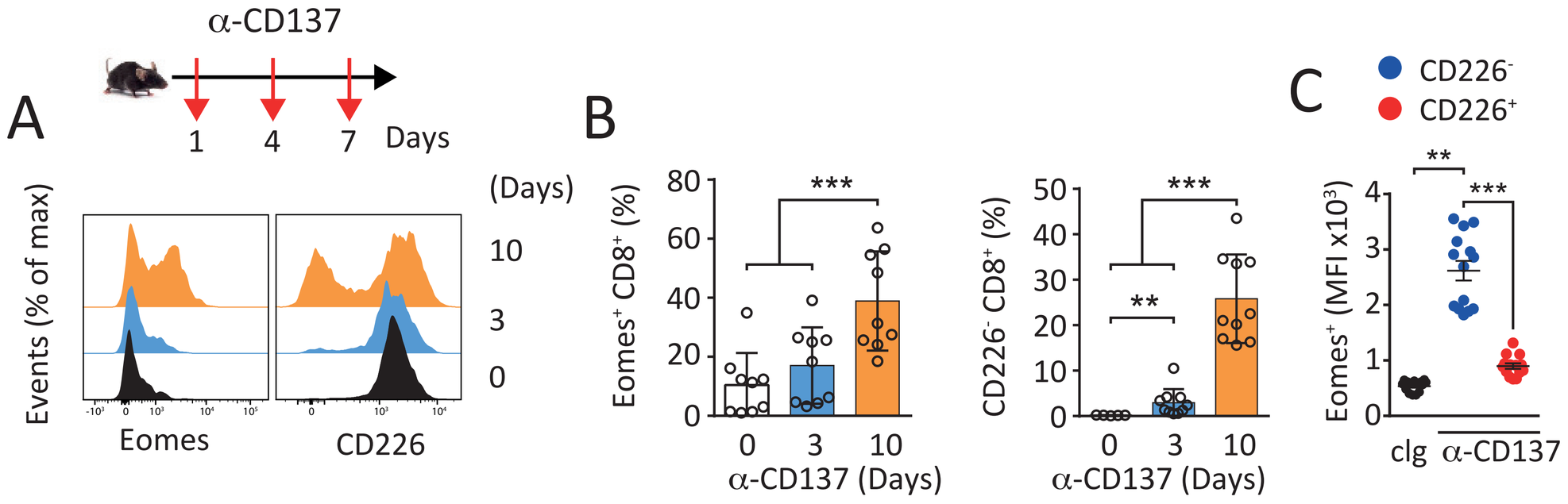
A
α-CD137
1
4
7
Days
Events (% of max)
Eomes
CD226
(Days)
10
3
0
B
Eomes+ CD8+ (%)
***
0
3
10
α-CD137 (Days)
CD226- CD8+ (%)
**
C
CD226-
CD226+
Eomes+ (MFI x10³)
clg
α-CD137
D
Clg
α-CD137
Eomes^WT
Eomes^KO
Eomes^het
Eomes^WT
Eomes
CD226
CD226- Tem (%)
E
clg
α-CD137
CD226- CD8+ (%)
WT
CD155^KO
F
CD226+
CD226-
Events (% of max)
CTV
G
CD226+
CD226-
IFN-γ (ng/mL)
TNF-α (pg/mL)
H
OT-1 CD226-
OT-1 CD226+
CD107a+ (%)
TNF-α+ (%)
CD3
Ova
I
α-CD137
pmel
Sorted :
Tem CD226-
Tem CD226+
B16F10
melanoma
C
V
TLR
C57BL/6
Days : 0 8 9 12 14 16
J
PBS
Pmel CD226-
Pmel CD226+
Tumor area (mm²)
Days after B16F10 injection
K
PBS
Pmel CD226-
Pmel CD226+
Survival (%)
Days after B16F10 injection

Figure S1 related to Figure 1

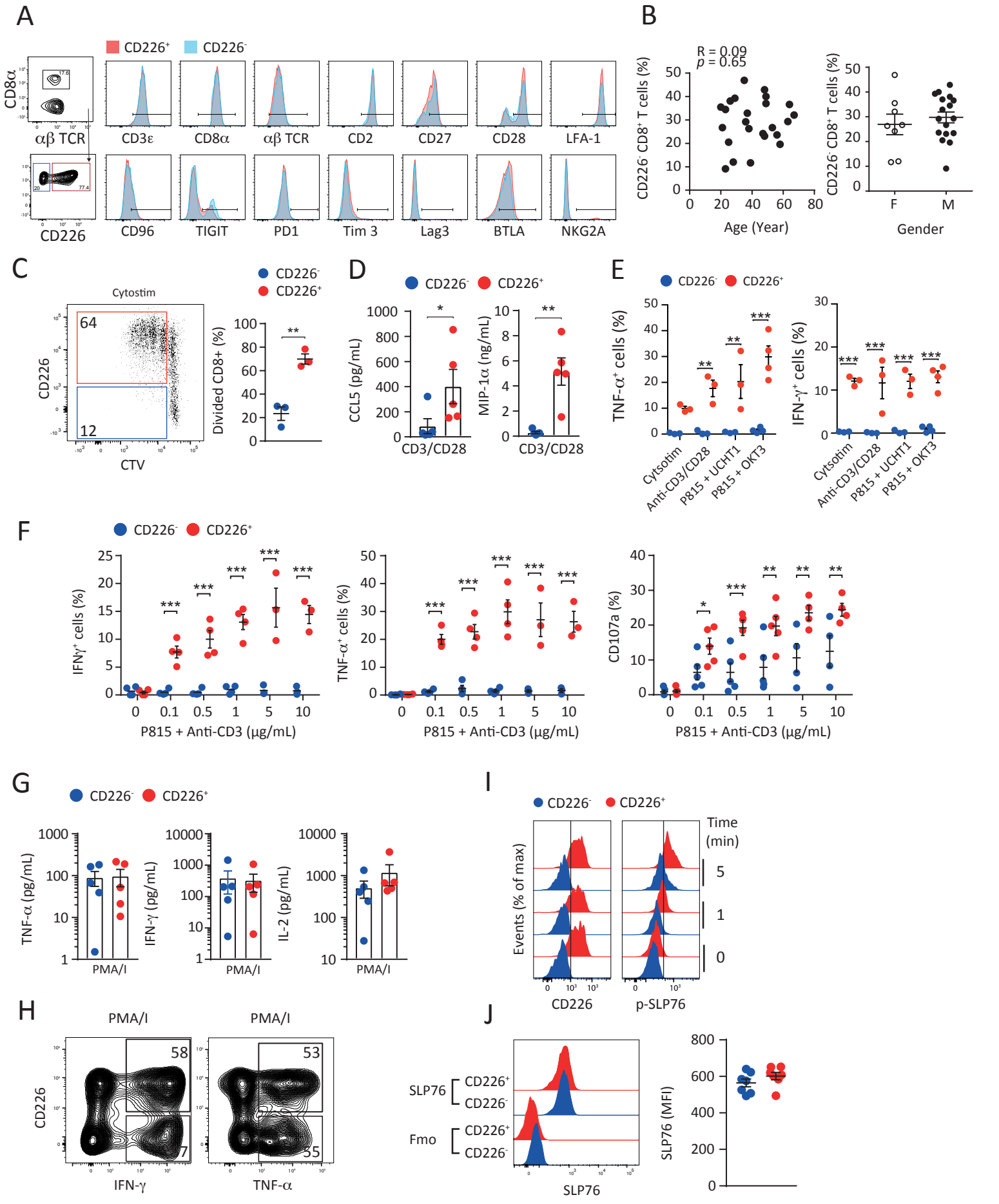

Figure S2 related to Figure 2

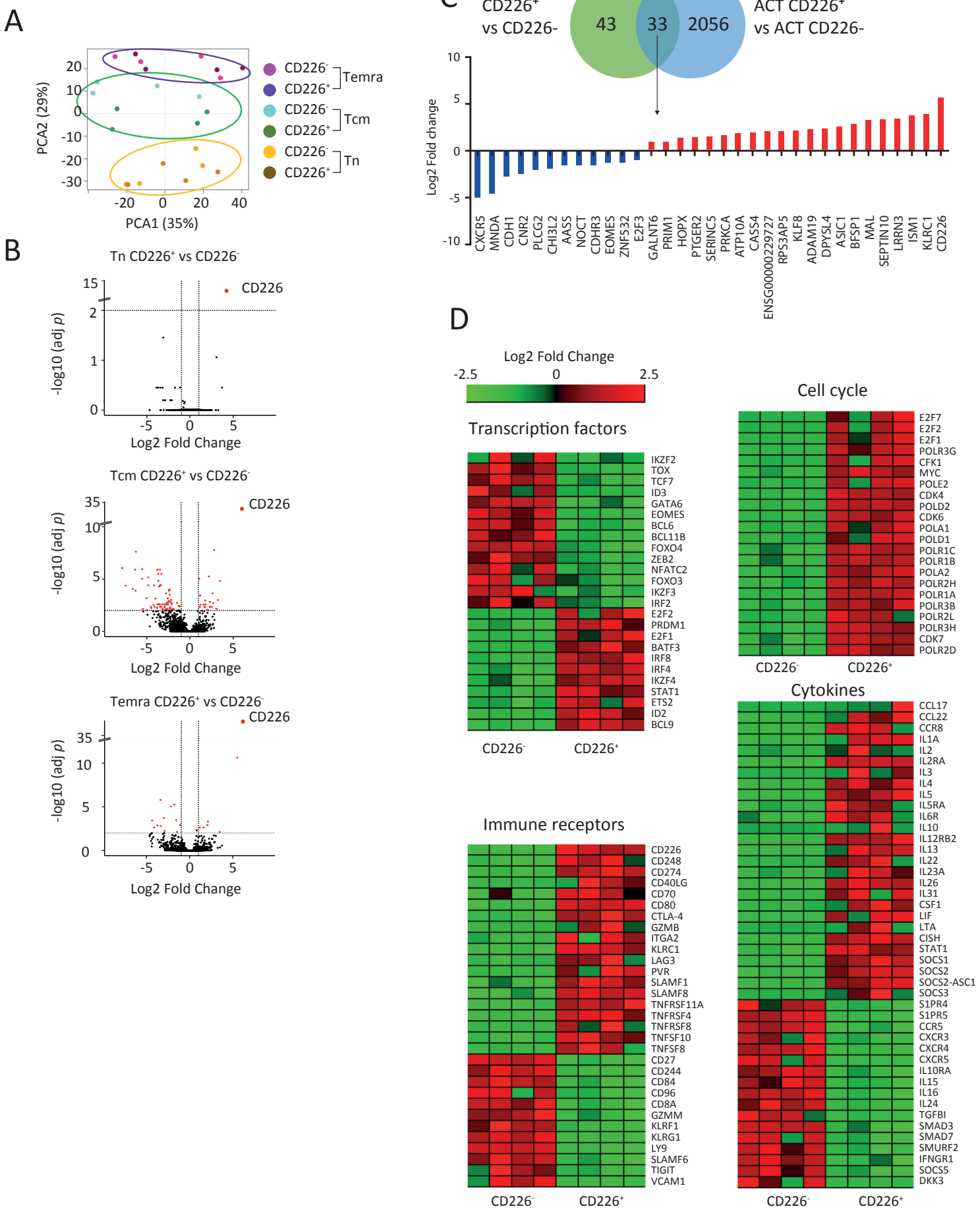

Figure S3 related to Figure 3

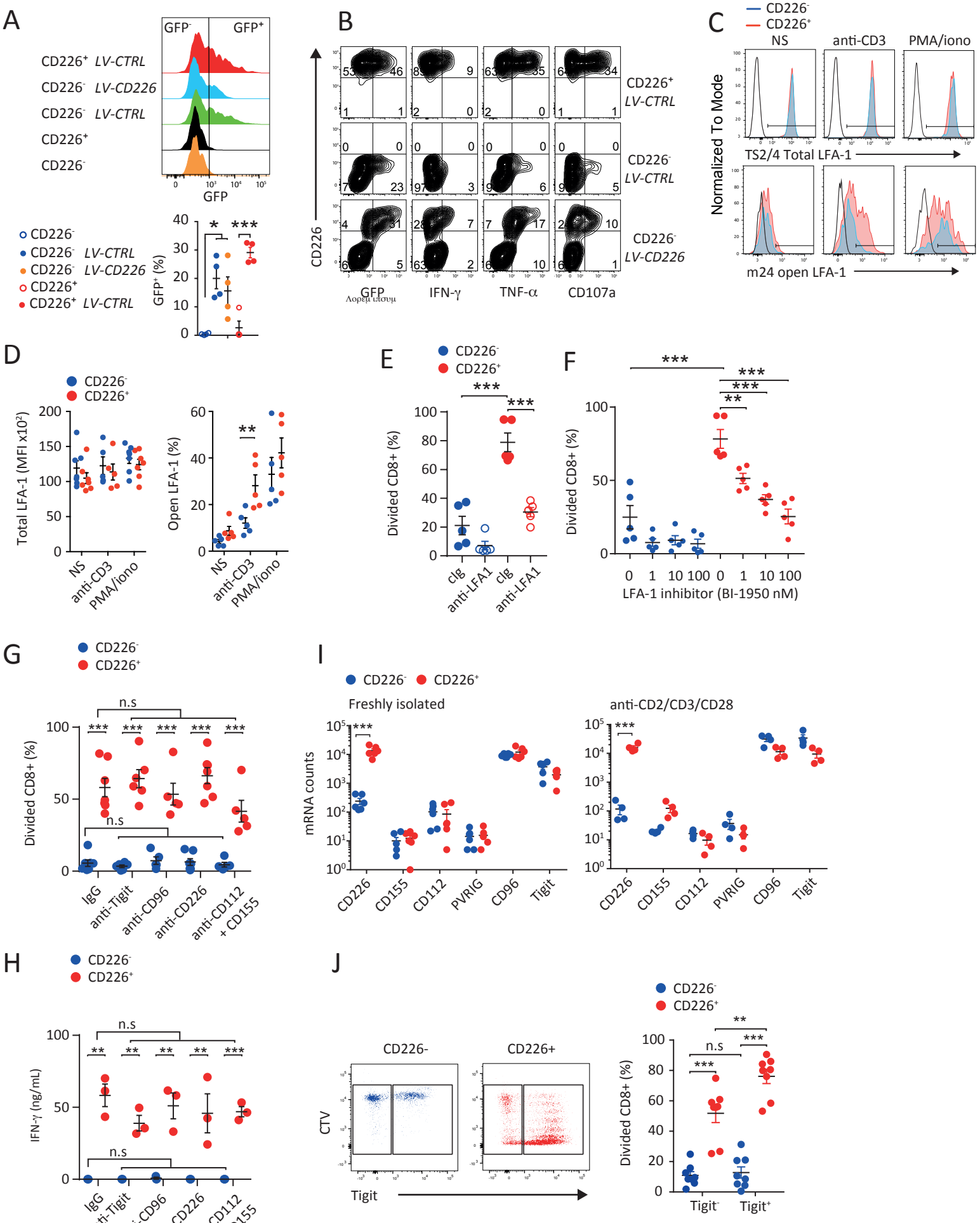

Figure S4 related to Figure 4

A

Variable		N
Age	>60	101
	<60	76
Grade		
	ISS1	59
	ISS2	84
	ISS3	33
	missing	1
Sexe		
	M	111
	F	66
b2m		
	<3.5	92
	3.5 -5.5	53
	>5.5	32
del 17		
	yes	15
	No	146
t(4;14)		
	Yes	13
	No	148

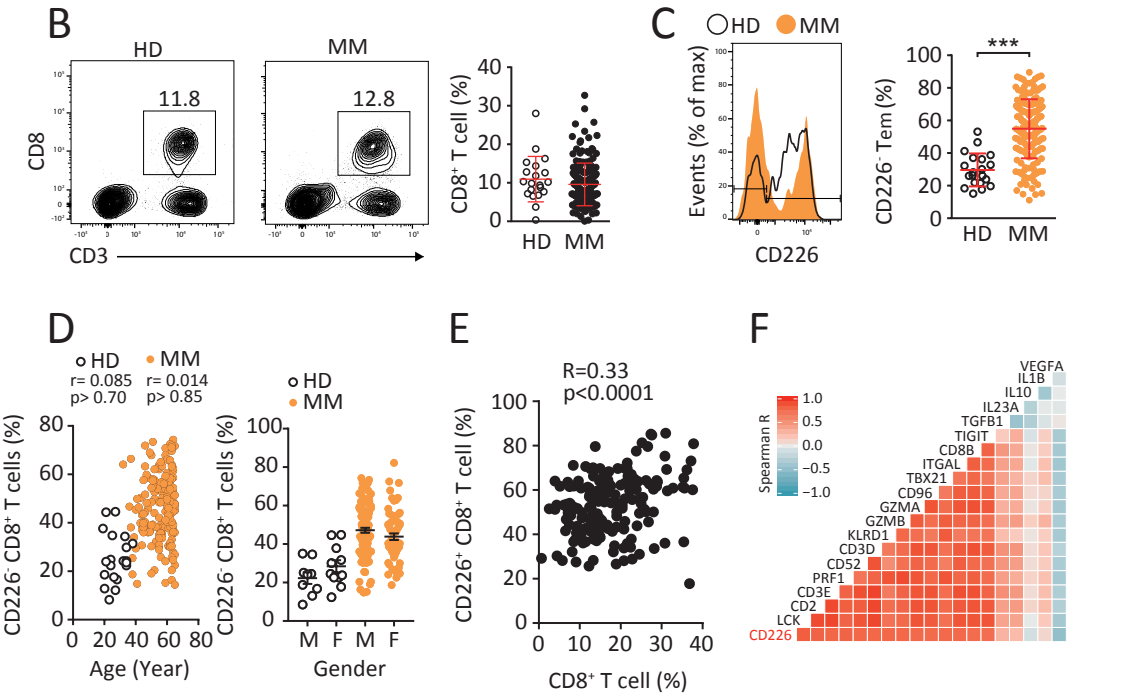

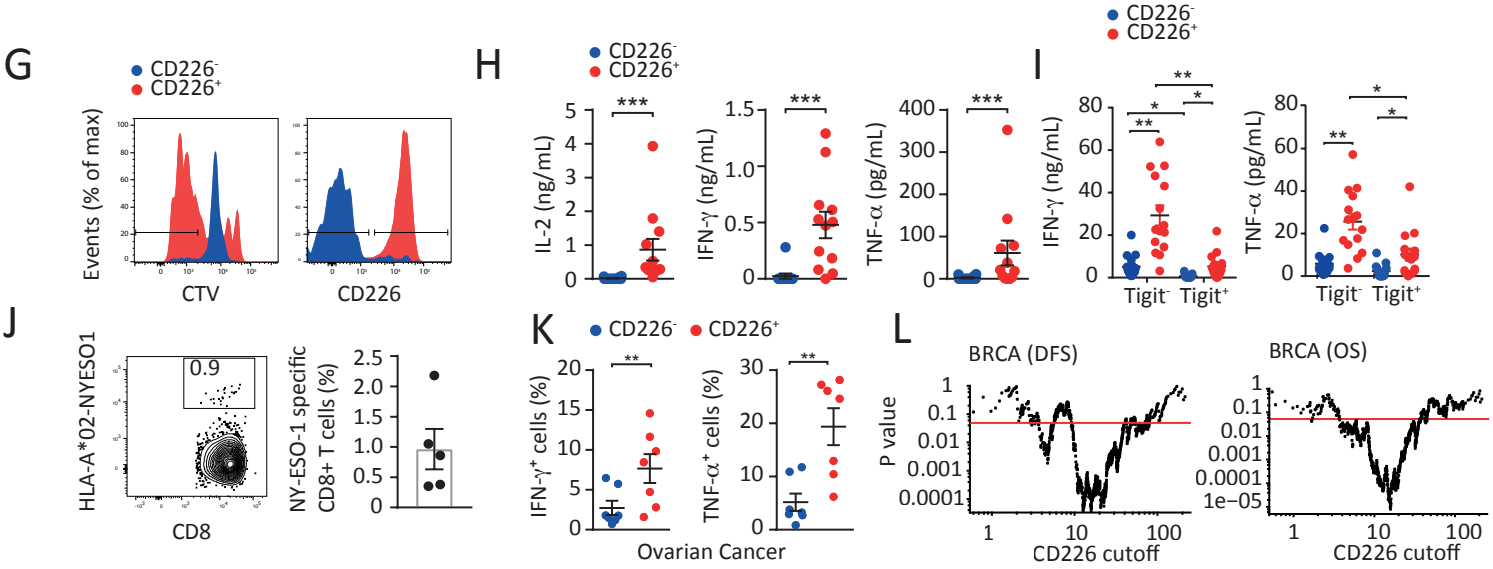

Figure S5 related to Figure 5

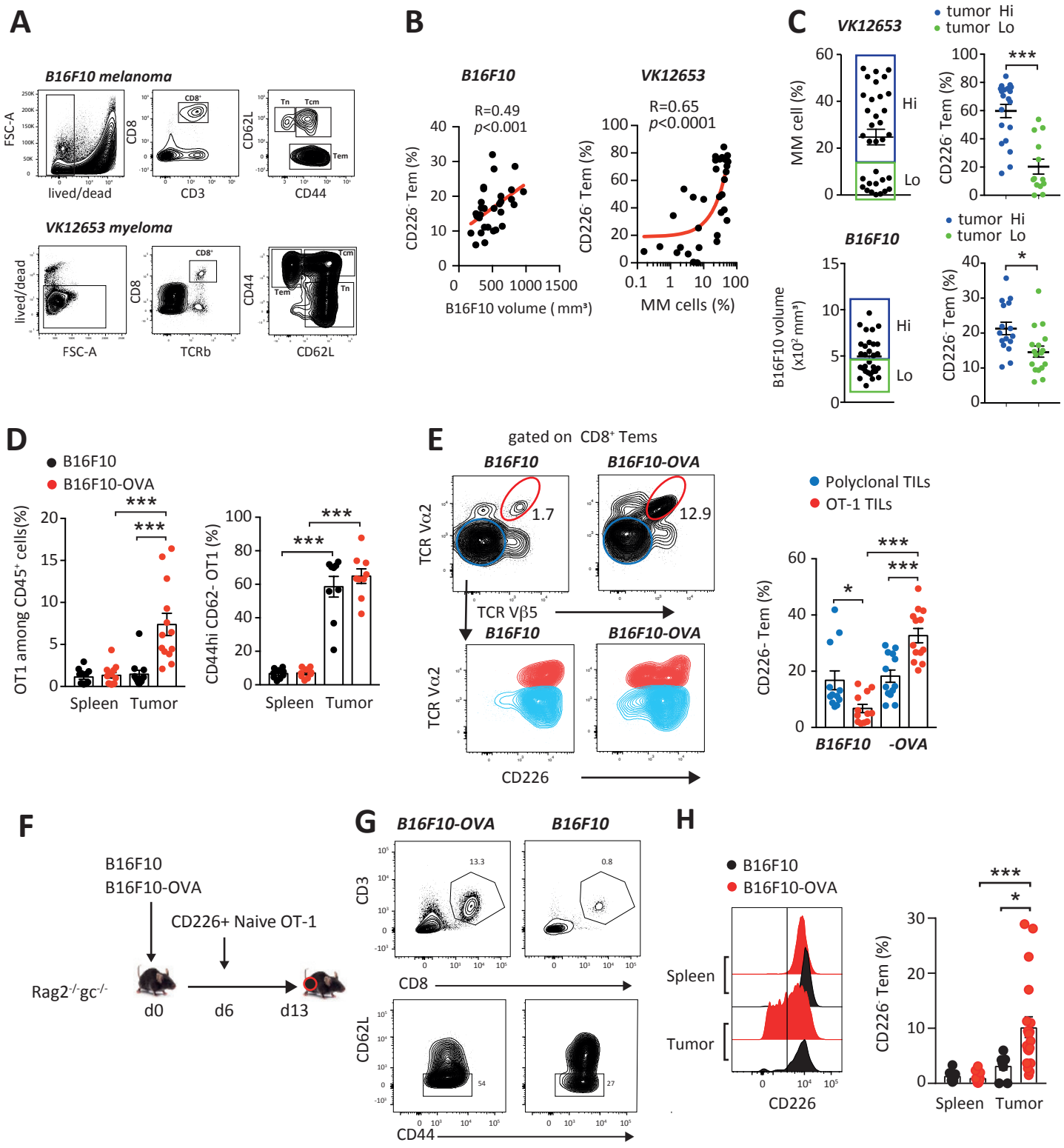

Figure S6 related to Figure 6

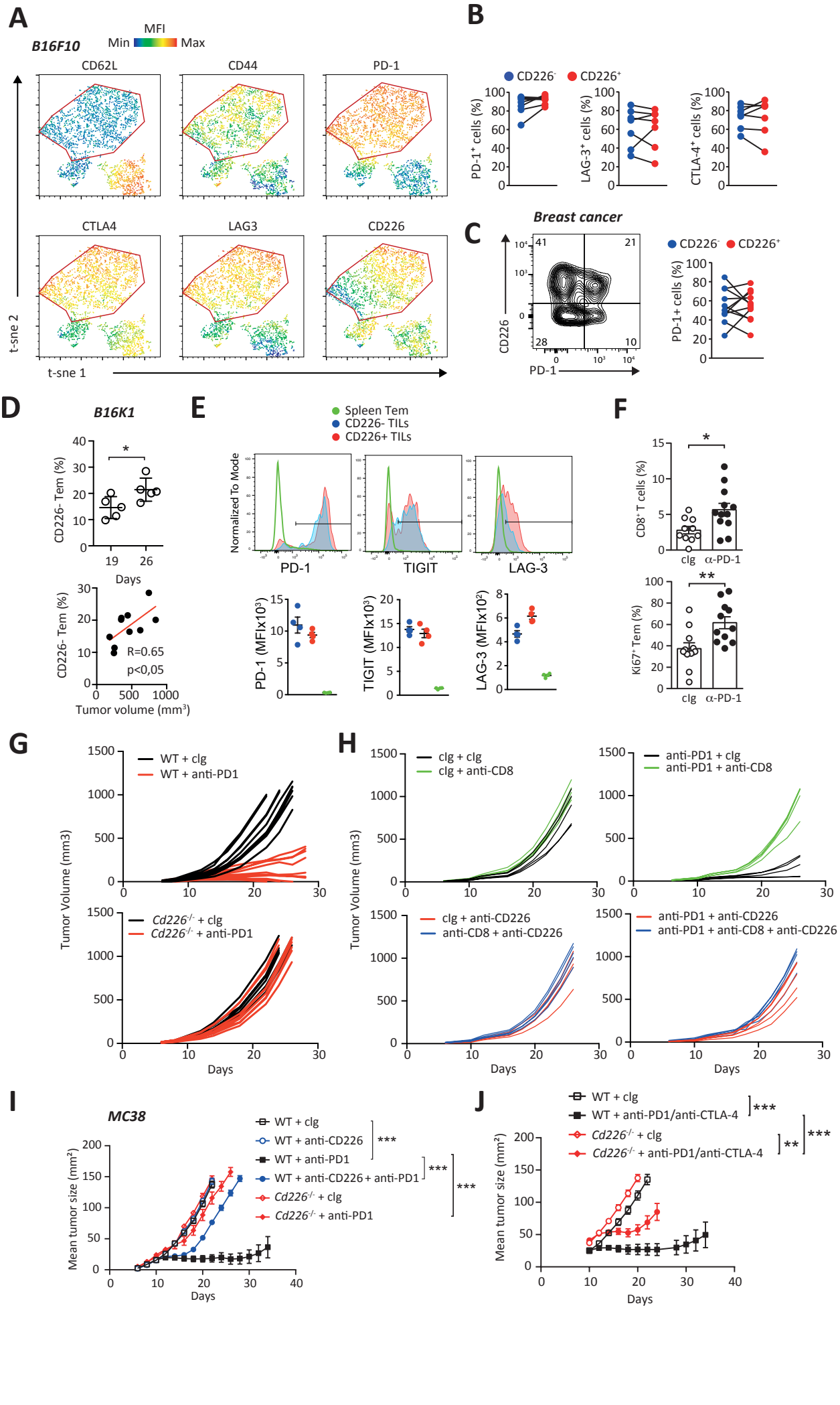

Figure S7 related to Figure 7

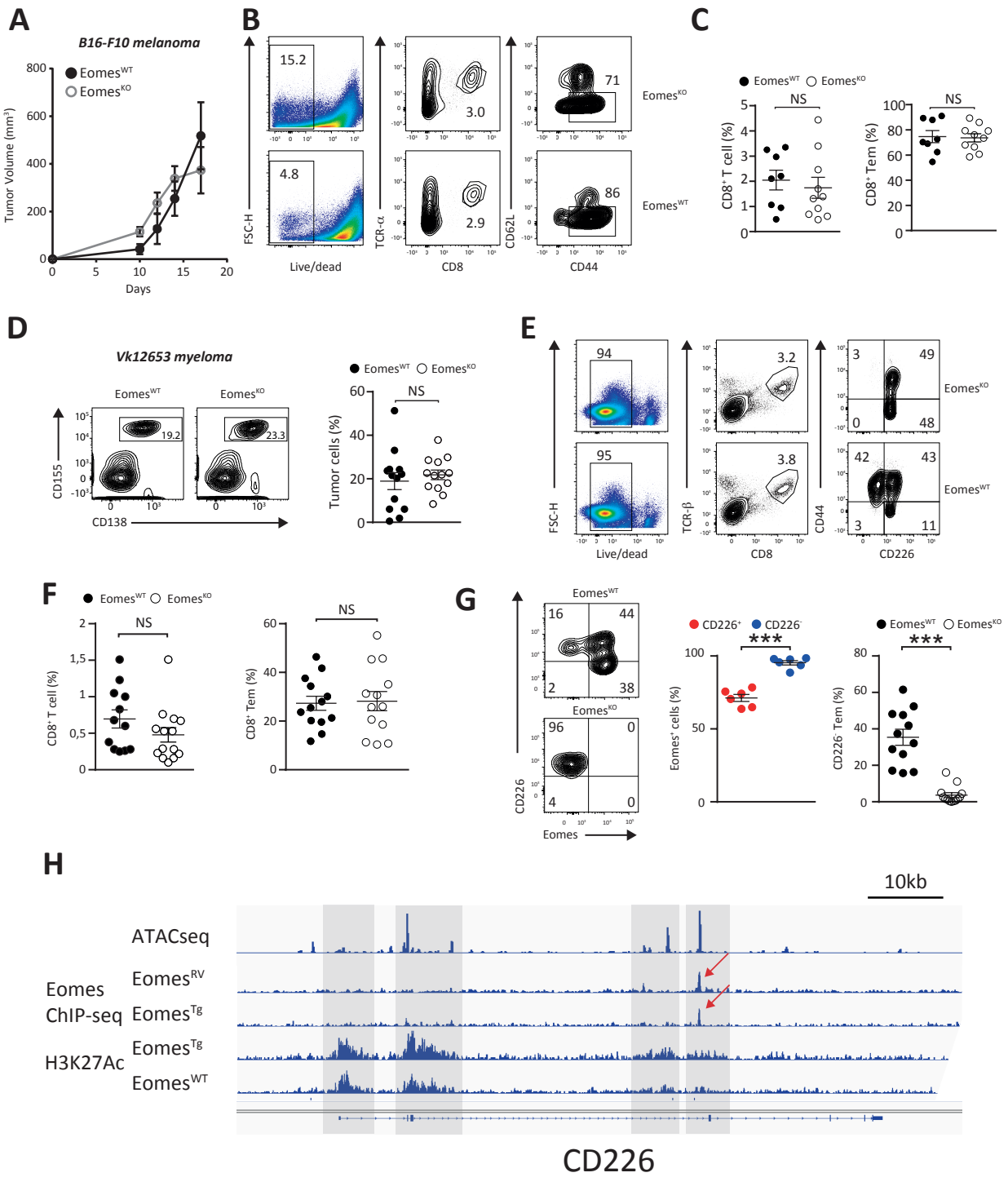

Figure S8 related to Figure 8